

A NOVEL IN-SITU GENERATED ACID SYSTEM ON CARBONATE
MINERAL DISSOLUTION IN SANDSTONE RESERVOIRS

A Thesis

by

CHRISTINE IKRAM NOSHI

Submitted to the Office of Graduate and Professional Studies of
Texas A&M University
in partial fulfillment of the requirements for the degree of

MASTER OF SCIENCE

Chair of Committee,	Hisham A. Nasr-El-Din
Committee Members,	Jerome J. Schubert
	Mahmoud El-Halwagi
Head of Department,	A. Daniel Hill

December 2015

Major Subject: Petroleum Engineering

Copyright 2015 Christine I. Noshi

ABSTRACT

Matrix acidizing has been used in oil and gas well stimulation for permeability and productivity enhancement purposes. HCl has been repeatedly used as a stand-alone stimulating fluid to decrease skin damage, create highly conductive wormholes in carbonate reservoirs, and stimulate sandstone reservoirs as a part of mud acid treatment. However, HCl in high-pressure/high-temperature (HP/HT) wells is a concern because of its rapid reactivity resulting in face dissolution, corrosion, and associated increased inhibition costs. This study investigates the effectiveness of a novel insitu-generated acid formulation with slower reaction and corrosion rates in stimulation operations in high temperature reservoirs.

The new insitu-generated acid treatment was applied to stimulate two types of sandstone cores (Grey Berea and Bandera). X-Ray Diffraction (XRD) was performed on the sandstone cores to analyze their carbonate and clay content. Coreflood studies were conducted to investigate the impact of the treatment fluid on the permeability of outcrop and reservoir cores. Different flow rates of acid injection were set at 1 and 5 cm³/min.

The influence of temperature of 250 and 300°F (121-148°C) was investigated using the resulting effluent samples. These samples were analyzed using Inductively Coupled Plasma (ICP) for elemental analysis of key cations. Porosity profiles were determined before and after treatment using CT scans.

Experiments were conducted on both the regular HCl acid system and the insitu-generated acid system for comparative purposes. Superior stimulation results were achieved at 121°C (250°F) with the insitu-generated acid system. Although plugging

problems caused by clay instability in reaction with HCl remains a major concern, positive stimulation results occurred in both Grey Berea and Bandera sandstone cores. This insitu-generated acid system efficiently removes carbonate and oxide minerals in HPHT sandstone reservoirs. No fines migration was observed with Grey Berea. A stimulation K_f/K_i (% increase) ranging from 10 to 30% was achieved with Grey Berea sandstone.

The outcomes of this study will assist in a more cost-effective and efficient design of acid treatments with minimal jeopardy to the formation integrity.

DEDICATION

I dedicate this thesis to my parents for their continuous support and encouragement.

ACKNOWLEDGEMENTS

I would like to express my sincere appreciation to my supervisor, professor Dr. Hisham A. Nasr-El-Din. I am grateful for his assistance and guidance throughout my studies and research. I am heartily thankful to him, whose encouragement, management, and support from the preliminary to the concluding level enabled me to develop an understanding of this subject.

I would like to thank Khatere Sokhanvarian for her help and guidance throughout the project.

I wish to extend my appreciation to Dr. Schubert and Dr. El-Halwagi for devoting their invaluable time to review my research work and evaluate its results. Their comments during the course of my studies are highly appreciated.

I would like to thank the technical staff at Lubrizol Company for their help in providing chemicals and knowledge in this project.

I wish to express my love and gratitude to my beloved parents for their understanding and endless support shown throughout the duration of my study.

NOMENCLATURE

BHT	Bottom-hole Temperature
CI	Corrosion Inhibitor
CT _{wr}	CT number of the water-saturated rock
CT _{ar}	CT number of the air-saturated rock
CT _w	CT number of water = 0
CT _a	CT number of air = -1,000
FA	Fixing Agent
GCMS	Gas Chromatography-Mass Spectrometry
HPHT	High-Pressure High-Temperature
HPLC	High-Performance Liquid Chromatography
ICP-OES	Inductively Coupled Plasma-Optical Emission Spectroscopy
K _i	Initial permeability
K _f	Final permeability
Psi	Pound per square inch
PV	Pore Volume
PVTB	Pore Volume to Breakthrough
RT	Room Temperature
SEM	Scanning Electron Microscope
TDS	Total Dissolved Solids
UKC	Urea Kaolinite Composite
XRD	X-ray Diffraction

TABLE OF CONTENTS

	Page
ABSTRACT	ii
DEDICATION	iv
ACKNOWLEDGEMENTS	v
NOMENCLATURE	vi
TABLE OF CONTENTS	vii
LIST OF FIGURES	ix
LIST OF TABLES	xiv
1. INTRODUCTION AND LITERATURE REVIEW	1
Reactions in Sandstone Reservoirs	4
Challenges Associated with Mud Acid Jobs	5
HCl Acidizing in Carbonate Reservoirs	6
Clay and Mineral Reactions	8
Clay Instability	10
Mud Acid Alternatives	15
Urea	18
Urea Hydrochloride	23
Applications	25
Advantages	25
Hydrolysis of Urea Hydrochloride	26
The Intercalation of Urea in the Interlamellar Spaces of Kaolinite	31
2. EXPERIMENTAL METHODS	35
Materials	35
Core Preparation	37
Solution Preparation	38
Equipment	39
Coreflood	39
CT Scan	40
Hot Rolling Oven	41
X-Ray Diffraction (XRD)	42

	Page
Inductively Coupled Plasma Optical Emission Spectrometry (ICP-OES) Titrator.....	43
Dean Stark	45
Gas Chromatography-Mass Spectrometry	46
3. RESULTS AND DISCUSSION.....	49
XRD Results.....	50
CT Scan	53
Gas Chromatography- Mass Spectrometry (GCMS) Results.....	53
Viscosity and Density Measurements	55
Coreflood Studies.....	58
List of Experiments	60
Grey Berea Experiments	60
Bandera Experiments.....	63
Coreflood Experiments	64
Section-A: 15 wt % HCl - All of the Additives Included-250°F @ 5 cm ³ /min -Berea Sandstone.....	64
Section-B: 30 wt% Urea-HCl - All of the Additives Included @ 5 cm ³ /min-Berea Sandstone.....	74
Section-C: 30 wt% Urea-HCl - Only CI and Intensifier Included -250°F @ 5 cm ³ /min- Berea Sandstone	91
Section-D: 30 wt% Urea-HCl - Only CI and Intensifier Included -250°F @ 2 and 5 cm ³ /min- Bandera Sandstone.....	96
Section-E: 30 wt% Urea-HCl - 250°F @ 1cm ³ /min- Berea Sandstone with Different Mineralogy.....	102
4. CONCLUSIONS AND RECOMMENDATIONS.....	111
REFERENCES.....	113

LIST OF FIGURES

	Page
Fig. 1—1 Structure of the tetrahedral layer (geology.uprm.edu 2013).....	8
Fig. 1—2 Structure of the octahedral layer (Averill and Eldredge 2012).....	8
Fig. 1—3 SEM picture of different clays showing the variations in morphology (Wilson 1982).....	10
Fig. 1—4 Percent chloride destroyed by acid at 180°F.....	12
Fig. 1—5 Size of different sandstone minerals	15
Fig. 1—6 Structures of urea	19
Fig. 1—7 Appearance of urea	19
Fig. 1—8 Thermogravimetric analysis of urea pyrolysis. Mass losses (-) and 1st derivative (--). Adapted from Schaber et al.2004.....	22
Fig. 1—9 HPLC Mass Plot: urea pyrolysis reaction (100.0 g of urea initially).....	23
Fig. 1—10 Structures of urea-HCl	24
Fig. 1—11 Appearance of urea-HCl	24
Fig. 1—12 Observed Retardation Factor with Urea	30
Fig. 1—13 Comparative PVTB between a typical retarded acid system vs. Urea hydrochloride system at 300°F (Patent no. 955394)	31
Fig. 1—14 Kaolinite-urea system after reaching equilibrium. A, B and C represent the three distribution structures of intercalated urea molecules	32
Fig. 1—15 Infrared absorption spectra of (a) raw kaolinite and (b) kaolinite-urea intercalation composite	33
Fig. 1—16 XRD patterns of (a) raw kaolinite and (b) kaolinite-urea intercalation composite	34
Fig. 2—1 A schematic diagram of the Coreflood Apparatus.....	40

	Page
Fig. 2—2 CT- scan device.....	41
Fig. 2—3 X-ray diffraction	42
Fig. 2—4 An illustration of ICP theory.....	43
Fig. 2—5 Optima 7000 ICP-OES Spectrometer	44
Fig. 2—6 Thermo Scientific Orion 950 Titrator	46
Fig. 2—7 Dean Stark Apparatus	47
Fig. 2—8 Circulation system	47
Fig. 2—9 GC-MS Instrument.....	48
Fig. 3—1 Bandera Sandstone XRD Results.....	51
Fig. 3—2 Grey Berea Sandstone XRD Results.....	52
Fig. 3—3 Grey Berea Sandstone with Different Mineralogy XRD Results	52
Fig. 3—4 Untreated urea-HCl graph.....	55
Fig. 3—5 Heated Urea-HCl at 250°F graph	55
Fig. 3—6 Temperature vs kinematic viscosity measurements from RT to 250°F(121.11°C)	57
Fig. 3—7 Initial permeability of Berea-05 core at 75 °F	68
Fig. 3—8 Pressure drop profile of Berea-05 during HCl injection at 250° F	69
Fig. 3—9 Final permeability of Berea-05 core at 75° F	69
Fig. 3—10 pH of effluent samples from Berea-05 core at 75°F	70
Fig. 3—11 ICP analysis for 30wt%Urea-HCl with Berea-05 core	71
Fig. 3—12 Initial permeability of Berea-06 core at 75°F	72
Fig. 3—13 Pressure drop profile during urea-HCl injection at 300 °F	72

	Page
Fig. 3—14 Final permeability of Berea-06 core at 75 °F	73
Fig. 3—15 ICP analysis for 15 wt% HCl with Berea-06 core	73
Fig. 3—16 Initial permeability of Berea-02 core at 75 °F	78
Fig. 3—17 Pressure drop curve of Berea-02 during urea-HCl injection at 250°F	78
Fig. 3—18 Final permeability of Berea-02 core at 75 °F	79
Fig. 3—19 pH of effluent samples from Berea-02 core.....	79
Fig. 3—20 Density of effluent samples from Berea-02 core at 75°F.....	80
Fig. 3—21 ICP analysis for 30 wt% urea-HCl with Berea-02 core	81
Fig. 3—22 Porosity profile before and after 30 wt% urea-HCl treatment for Berea-02	81
Fig. 3—23 Pressure drop profile during 30 wt% urea-HCl injection at 250 °F for Berea-09.....	82
Fig. 3—24 Final permeability of Berea core-09 at 75°F	83
Fig. 3—25 ICP analysis for 30 wt% urea-HCl with Berea-09 core	83
Fig. 3—26 Pressure drop profile during urea-HCl injection at 250 °F for Berea-10 core	84
Fig. 3—27 Porosity profile before and after 30wt% urea-HCl treatment for Berea-10	85
Fig. 3—28 Pressure drop profile during urea-HCl injection at 250°F for Berea-11	86
Fig. 3—29 Porosity profile before and after 30 wt% urea-HCl treatment for Berea-11	86
Fig. 3—30 Pressure drop curve of Berea-03 during urea-HCl injection at 250 °F	88
Fig. 3—31 Initial permeability of Berea-03 core at 75 °F	88
Fig. 3—32 Final permeability of Berea-03 core at 75 °F	89

	Page
Fig. 3—33 pH of effluent samples from Berea-03 core at 75°F	89
Fig. 3—34 Porosity profile for the before and after treatment for Berea-03 core	90
Fig. 3—35 ICP analysis for 30wt% Urea-HCl for Berea-03 core	90
Fig. 3—36 Pressure drop curve during urea-HCl injection at 250°F Berea-08	92
Fig. 3—37 Final permeability of Berea core-08 at 75°F.....	93
Fig. 3—38 ICP analysis for 30 wt %Urea-HCl with Berea-08 core	93
Fig. 3—39 Pressure drop curve during urea-HCl injection at 250 °F for Berea-13.....	94
Fig. 3—40 ICP analysis for 30 wt % urea-HCl with Berea-13 core.....	95
Fig. 3—41 Porosity profile before and after 30 wt% urea-HCl treatment-only CI and intensifier Included for Berea-13	95
Fig. 3—42 Initial permeability of Bandera-01 core at 75°F	97
Fig. 3—43 Pressure drop profile during urea-HCl injection at 250°F	98
Fig. 3—44 Final permeability of Bandera-01 core at 75°F.....	98
Fig. 3—45 ICP analysis for 30wt%Urea-HCl with Bandera-01 core.....	99
Fig. 3—46 pH of effluent samples from Bandera-01 core.....	99
Fig. 3—47 Initial permeability of Bandera-02 core at 75°F.....	100
Fig. 3—48 Pressure drop curve of Bandera-02 core during urea-HCl injection at 250°F	101
Fig. 3—49 Final permeability of Bandera-02 core at 75°F.....	101
Fig. 3—50 ICP analysis for 30 wt% urea-HCl with Bandera-02 core.....	102
Fig. 3—51 Initial permeability of Berea-G-14 core at 250°F	104
Fig. 3—52 Pressure drop profile of Berea-G-14 core during urea-HCl injection at 250°F	104

	Page
Fig. 3—53 Final permeability of Berea-G-14 core at 250°F.....	105
Fig. 3—54 ICP analysis for 30 wt% urea-HCl with Berea-G-14 core.....	105
Fig. 3—55 Initial permeability of Berea-G-15 core at 250°F	106
Fig. 3—56 Pressure drop curve of Berea-G-15 core during urea-HCl injection at 250 °F	107
Fig. 3—57 Final permeability of Berea-G-15 core at 75°F.....	107
Fig. 3—58 ICP analysis for 30 wt% Urea-HCl with Berea-G-15 core.....	108
Fig. 3—59 Density of 2 sets of effluent samples from Berea-G-15 and G-14 core at 75°F	109
Fig. 3—60 pH of 2 sets of effluent samples from Berea-G-15 and G-14 core at 75°F	110

LIST OF TABLES

	Page
Table 1—1 Ions leached from chlorite by various acids.....	12
Table 1—2 stability limit of clays in HCl.....	13
Table 1—3 Hibbeler and O’Driscoll guidelines	14
Table 1— 4 Relative surface area of sandstone minerals (McLeod and Norman 2000)	14
Table 1—5 Properties of Urea in the Urea-HCl solution including chemical formula, molecular weights, density, and solubility constants (Williams 2001; Godfrey et al. 1997)	20
Table 2—1 The characteristics of treatment fluid.....	35
Table 2—2 Mineralogy of Grey Berea Core.....	36
Table 2—3 Mineralogy of Bandera Core.....	36
Table 2—4 Types of acid additives used with HCl in this study	38
Table 2—5 the types of acid additives used for urea/ HCl in this study.....	39
Table 3—1 Quantitative XRD mineralogy for Grey Berea and Bandera sandstone.....	50
Table 3—2 Viscosity and density measurements at 75°F	57
Table 3—3 Berea sandstone experiments summary	61
Table 3—4 Bandera sandstone experiments summary	64
Table 3—5 Summarizing 15 wt% HCl experimental conditions.....	67
Table 3—6 Berea-05 rock, flow, and % stimulation/damage properties	67
Table 3—7 Berea-06 rock, flow, and % stimulation/damage properties	71
Table 3—8 Summarizing 30 wt% Urea/ HCl experimental conditions.....	77

	Page
Table 3—9 Berea-02 rock, flow, and % stimulation/damage properties (Urea-HCl plus additives)	77
Table 3—10 Berea-09 rock, flow, and % stimulation/damage properties	82
Table 3—11 Berea-10 rock, flow, and % stimulation/damage properties	84
Table 3—12 Berea-11 rock, flow, and % stimulation/damage properties	85
Table 3—13 Berea-03 rock, flow, and % stimulation/damage properties	87
Table 3—14 Berea-08 rock, flow, and % stimulation/damage properties	92
Table 3—15 Berea-13 rock, flow, and % stimulation/damage properties	94
Table 3—16 Bandera-01 rock, flow, and % stimulation/damage properties	97
Table 3—17 Bandera-02 rock, flow, and % stimulation/damage properties	100
Table 3—18 Berea-G-14 rock, flow, and % stimulation/damage properties	103
Table 3—19 Berea-G-15 rock, flow, and % stimulation/damage properties	106

1. INTRODUCTION AND LITERATURE REVIEW

According to Walker et al.1991, stimulating wells with acid was first reported in 1896.The chief aim of an acidizing job is to bypass the nearby wellbore damage to enhance the well productivity. In sandstone reservoirs, the key objective is to accomplish deep penetration into the formation region caused by completion and drilling operations. The goal is to bypass formation damage and/or restore the flow capacity in the near wellbore zone (a radius of 8 to 24 in. [20.3 to 61 cm]) without fracturing the producing regions. In carbonate acidizing, the chief purpose is to dissolve large amounts of alkaline-earth metals to form channels or effective wormholes to increase the productivity and injectivity index of the reservoir rock. However, the lack of good corrosion inhibitors prevented the widespread use of acid treatments. Not until the early 1930's did the acidizing industry flourish due to the introduction of arsenic inhibitors (Nitters et al. 2000).

Matrix acidizing is not capable of mitigating all formation damage; nevertheless, it is a valuable technique in removing acid-soluble damaging material. However, sulfate scales, paraffin, tar, water blocks, and the majority of emulsions are to a great extent unaffected by various types of mineral and organic acids. As a result, not all sources of permeability damage are acid-soluble. To mitigate these complexities, special treatments are required instead of (or in addition to) matrix acidizing. Successful matrix acidizing depends upon several factors including; but not limited to, good evaluation of candidate wells, proper design for the comprehensive coverage of all the plugged perforations, selection of compatible solvents, acids, and mineralogy to prevent or reduce fluid-fluid

and fluid-rock incompatibilities (McLeod 1989). Moreover, a crucial factor in the success of any matrix acidizing treatment is proper acid placement so that the target zones are sufficiently contacted by adequate acid volumes. In a heterogeneous reservoir, acid tends to flow through the path of least resistance flowing predominantly to higher permeability zones leaving lower permeability zones unacidized (Hill and Rossen 1994). Knowing how the formation will react to the acid designed and to anticipate the chemistry of the spent acid invading the lithology is crucial to acidizing success (McLeod 1984). Furthermore, the nature of the detrimental material and the knowledge of the depth at which the damage enters the formation are of vital importance to the success of the acid treatment. Well completion fluid systems design has always been a perplexing challenge to engineers and researchers. Cost considerations, material incompatibilities, undesired chemical interactions, and physical limitations present immense complexities in matrix acidizing treatments (Chiu et al.1993; Coulter and Jennings, 1999; McLeod 1984,1989; McLeod et al.1983; Shaughnessy and Kunze 1981).

A pressure-buildup test should be executed to determine the degree of skin (permeability) damage. However, a buildup test may not reveal the exact formation permeability damage. Overall formation damage calculated from the performed test will collectively appear as a result of inadequate or too few perforations. It is often more cost-effective to re-perforate than to acidize if the quality of the perforations are suspected. 15 to 200 gal/ft. (0.19 to 2.5 m³) of acid in the target zone is typical in matrix acidizing treatments. The acid is pumped at a lower pressure than the formation fracture pressure. Formation permeability is considered the main factor in the determination of

the acid pumping pressure into the formation. The lower the permeability, the higher the pumping pressure. Acid can be pumped into the formation at relatively low pumping pressures in high permeability formations.

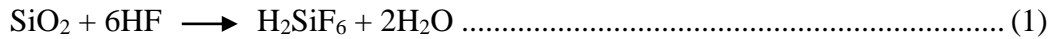
Mud acid was introduced into the petroleum industry in 1935 (Smith and Hendrickson 1965). Mud acid is a blend of both HF and HCl. Hydrofluoric acid (HF) has a unique ability to react with silica and silicates; making it an essential component in sandstone acidizing. Reaction products should be maintained in solution in order to accomplish successful acidizing treatments. HF by itself is a feeble acid; it is not capable of keeping the reaction products in solution. To date, mud acid has been extensively used since its discovery. However, the reactions and interactions of sandstone minerals with acids are different. The elaborate reactions of mud acid with aluminosilicates will be discussed in the next section. Unlike carbonate acidizing, sandstone acidizing can be complicated in many aspects. As yet, its reactions remain not fully comprehended. Each type of mineral is different with unique elements, structure, surface area, and acid sensitivity. This poses additional challenges in acid treatment design.

Sandstone reservoirs are composed of several minerals including sand, feldspars, clays, zeolites, carbonates, oxides, sulfates, and sulfides. Sandstone acidizing consists of three key phases: (1) a preflush, typically of a weak HCl solution, (2) a mud-acid stage of HCl and HF, and (3) a post-flush of HCl, ammonium chloride or diesel oil (Gidley 1996). However, Gidley et al. (1996) suggested that many complications may occur during sandstone acidizing with mud acid. Those problems include, but are not limited to, disintegration of clays in HCl,

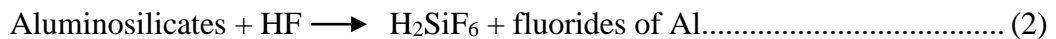
fluosilicates precipitation, carbonate presence in sandstone resulting in calcium fluorides precipitation, silica-gel formation and deposition.

Reactions in Sandstone Reservoirs

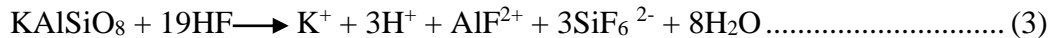
Primary Reactions: The primary reaction of HF with sand particles is:



The reaction of HF with aluminosilicates is

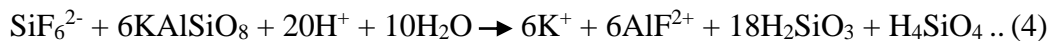


For example, the reaction of potassium feldspar with HF is (Li et al. 1998)

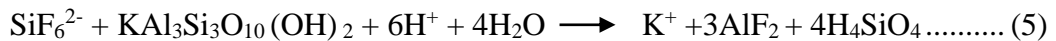


Secondary Reactions: These are the reactions of fluorosilicic acid, derived from the primary reaction, with aluminosilicates.

The reaction of fluorosilicic acid with potassium feldspar is



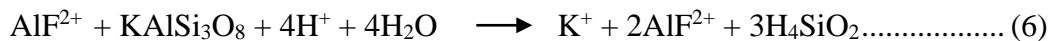
The reaction with fluorosilicic acid with illite is



Dissolution of aluminosilicates results in the formation of amorphous silica gel.

Tertiary Reactions: The tertiary reaction of aluminum fluorides with aluminosilicates in the presence of HCl involves further reduction of the fluorine (F)/ aluminum (Al) ratio in the dissolved aluminum fluoride species.

The reaction with K-feldspar will be:



The reaction will continue reducing F/Al ratio in the spent HF until the remaining HCl is consumed.

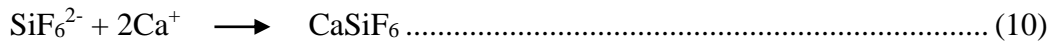
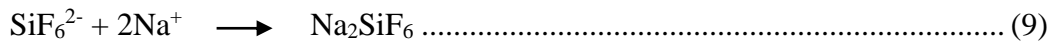
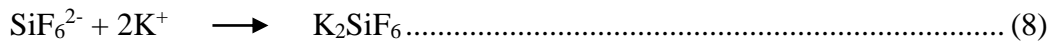
Challenges Associated with Mud Acid Jobs

Several problems could arise during mud acid treatments. The following reactions discuss the potential cause of precipitations. Quartz reacts comparatively slowly with HF, where aluminosilicates (clay minerals, feldspars, and mica) reacts fairly quickly (Li et al 1998). Mud acid cannot be used in sandstone with high calcite concentration. Calcite reacts very rapidly to completion with HCl but in the presence of HF, the reaction continues as follows:



CaF₂ has extremely limited solubility. Preflushing near the wellbore with HCl minimizes this problem. The reaction products of fluosilicic acid and fluoauric acid are typically water soluble, but their potassium, sodium, and calcium salts are partially unsolvable.

The salts form by the resulting reactions:



Spent or unspent HF should not come in contact with calcium, potassium, and sodium ions. Avoid formation water containing calcium chloride, potassium chloride, and sodium chloride. Ammonium chloride is considered the only compatible salt solution with HF. As soon as the acid spends and pH rises, ferric hydroxide forms. Ferric iron is produced from minerals such as chlorite, siderite, hematite, and tubing rust. HF

possesses the capability to dissolve carbonates, clays, feldspars, micas, and quartz. HF is primarily used to remove clays. Reaction rate of HF with sand and clays is dependent on the volume of acid used in sandstone reservoirs to the ratio of the surface area of the rock.

HCl Acidizing in Carbonate Reservoirs

In carbonate reservoirs, HCl has always been the “go-to solution”; it has been comprehensively used as a stand-alone stimulating fluid to decrease skin damage and create optimized wormholes in carbonate reservoirs. Also, carbonate and iron scales are typically removed by using HCl in strengths of 5 to 15%. HCl is also used as a pre-flush for HCl/HF (mud) acid to remove drilling mud and to mitigate clay damage. HCl is used with HF at a strength of 1.5 to 3% (King 1986). HCl systems have been looked upon favorably due to their affordable cost and high rock-dissolving power, with the added benefit of soluble reaction products (Coulter and Jennings 1999). However, HCl in high-pressure high-temperature (HP/HT) wells is a major challenge because of its rapid and uncontrolled reaction rate. HCl and its based fluids have major drawbacks. First, in stimulating shallow formations as they may cause face dissolution if injected at low rates and may potentially collapse weakly consolidated formations. Second, the associated high cost of inhibition, third, the HCl sensitivity of clay minerals and zeolites, and sludging tendencies in asphaltene rich crudes. Chrome-based tubulars (Cr-13) and duplex steel corrosion is another major concern. According to Tuttle (1987), the corrosion rate largely depends on “the susceptibility of the material under the environmental conditions to which it is exposed”. Corrosion problems become more

intensified at elevated temperatures, and special pricey additives such as intensifiers are necessary to compensate for the corrosion inhibition loss at elevated bottom-hole temperatures (BHT) temperatures. Therefore, corrosion inhibitors and intensifiers must be supplemented to the acid solution before the treatment is injected to minimize the rates of corrosion. The most efficient category of corrosion inhibitors are typically film-forming amines and their salts. However, they begin to decompose at 482°F (Schauhoff and Kissel 2000).

Unfortunately, the cost of these additives exceeds 5% of the total treatment cost (Nitters et al. 2000). Furthermore, the excessive addition of corrosion inhibitors may induce other problems, such as the adsorption of the corrosion inhibitor on the surface of the pay zone; changing its wettability or causing severe emulsion problems, particularly in low permeability reservoirs (Schechter 1992). In more extreme environments or less corrosion-resistant metallurgy, a higher loading of corrosion inhibitor intensifiers become necessary. Fluid incompatibility issues can occur when these inhibitors are combined with other additives present in the treatment fluid. Not to mention, with regards to illitic-sandstone reservoirs, HCl-based fluids are not a viable option as when HCl directly contacts illite, it breaks down inducing fines migration resulting in a sharp decrease of permeability due to clogged formation pores (Mahmoud et al. 2011). Literature repeatedly proved that the majority of the clay minerals are basically unstable in HCl at temperatures larger than 300°F.

Clay and Mineral Reactions

Clays are layered silicates formed by the erosion and/or disintegration of rocks, caused by the chemical reactions of other rock-forming silicate minerals. The layers are composed of various combinations of two fundamental units:

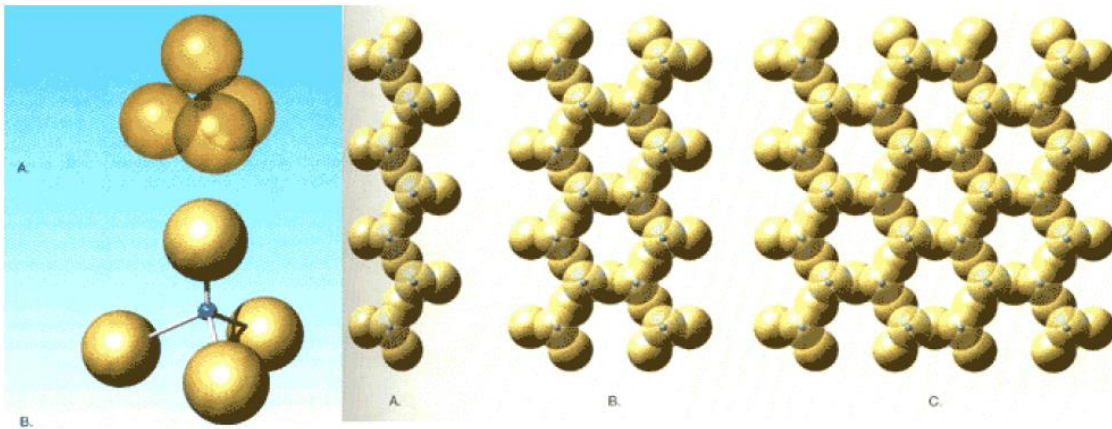


Fig. 1—1 Structure of the tetrahedral layer (Reprinted from geology.uprm.edu 2013)

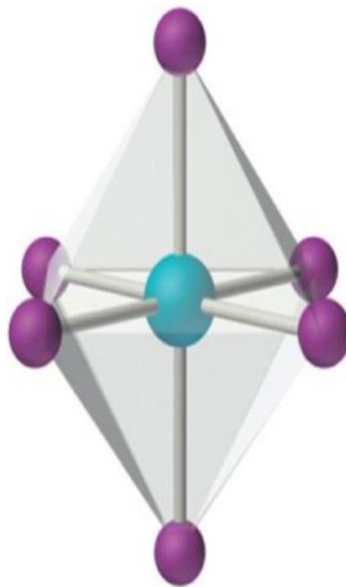


Fig. 1—2 Structure of the octahedral layer (Reprinted from Averill and Eldredge 2012)

1. Tetrahedral layers consisting of linked silicon-oxygen tetrahedra **Fig. 1—1.**
2. Octahedral layers in which hydroxyl ions fall in two planes, above and below a plane of magnesium or aluminum ions **Fig. 1—2.**

Sedimentary rocks are formed of clay minerals in the form of crystal packs. They are particularly tiny materials with a maximum dimension of a normal clay particle is less than 0.005 mm. There are three main clay minerals in Berea and Bandera sandstone cores: kaolinite, illite, and chlorite. Kaolinite is composed of a two-layer structure, K^+ exchange cation with a negligible base exchange capacity. Kaolinite is a non-swelling clay, but will readily disperse and migrate. Formation damage from fines is situated in the vicinity of the wellbore region within approximately 3-55 ft radius. Kaolinite has the ability to adsorb water; which is held tightly to the clay surfaces. Conversely, illites are interlayered, thus, possess the poorest characteristics of the dispersible and swellable clays. Moreover, illites are the most problematic to stabilize. Also, this type of clay can adsorb water, due to concentration imbalances between the ions found at the interchange locations on the clays and the solute content of the fluid in clay contact. Chlorite with HCl, becomes unstable and Al and Fe are leached from clays, leaving the amorphous silica gel which causes damage **Fig. 1—3** shows the SEM picture of the various clays showing the variations in morphology (Wilson 1982).

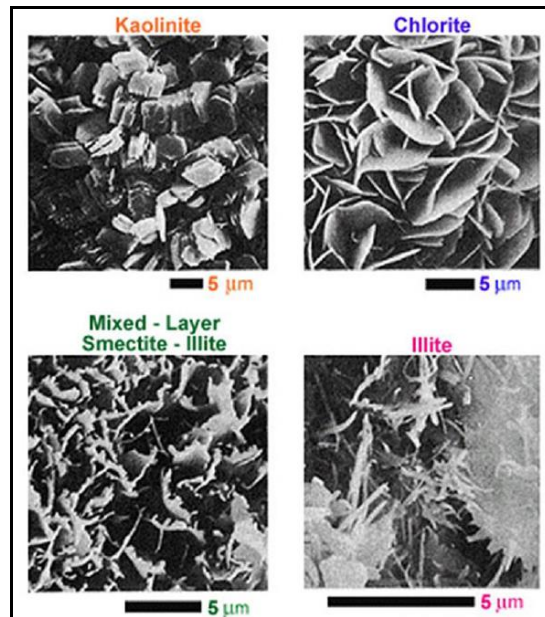


Fig. 1—3 SEM picture of different clays showing the variations in morphology (Reprinted from Wilson 1982)

Clay Instability

Simon and Anderson (1990) studied the stability of clays in HCl and their temperature limitations. Kalfayan and Metcalf (2000) modified McLeod's work to consider the effect of certain mineral sensitivities such as zeolites and the importance of using higher HCl:HF ratios to avoid precipitations, and Economides and Nolte (2000) modified the guidelines to account for chlorites and zeolites. Since then, widespread research has been devoted to the subject of mineral sensitivity to acids. Hibbeler and O'driscoll (1996) presented the guidelines to designing the acid treatment at different temperatures. Walsh et al. (1982) presented guidelines to the minimum HCl requirement to prevent precipitations based on the concentration of HF and the amount of remaining carbonates after the pre-flush. Gdanski (1999, 1998) defined the secondary and tertiary reactions in sandstone reservoirs and the

effect of both temperature and HF concentration on these reactions. Thomas et al. (2002) highlighted the effect of HCl: HF ratio on the formation of hydrated silica.

Amaefule et al. (1988) stated that rock-fluid interactions in illite and smectite-rich sandstone reservoirs, can be classified in two main categories: (a) chemical interactions caused by the rock minerals contact with incompatible fluids, and (b) excessive flow and pressure rates.

Thomas et al. (2001) described that HCl has destabilized illite and chlorite in the investigated cores from producing sandstone formations. The degradation of illite and chlorite contributed to significant core damage.

Decomposition of clay minerals readily consume HCl at elevated BHT. To avoid Fe precipitation, HCl acid should be avoided with chlorite content ranging from 0.5-2%. This is explained by the fact that when chlorite contacts HCl, it discharges iron and other clays and feldspars releases sodium or potassium. Silica gel forms, polymerizes, and creates colloidal particles inducing plugging problems. Literature shows that clays react to acetic acid in the same manner it reacts to fresh water, however, it does not decompose clays. In numerous reports, acetic acid encouraged smectite and illite clays to swell. Fortunately, this issue can be alleviated by the addition of 5% NH₄Cl. This process helps prevent the disintegration and clay swelling after clay ion exchange completion. **Fig. 1—4** shows the percentage of chlorite destroyed by acid at 180°F while **Table 1-1** shows the different cations leached from chlorite by various acids.

Fluid	Ionic Concentration (mg/l)					Amorphous Material	Percent Chloride Destroyed
	Mg	Al	Si	Ca	Fe		
DI Water							
10% Acetic	1	1	7	6	1	0%	0%
Acetic	27	11	26	35	53	4%	30%
10% Formic	158	214	110	73	460	35%	92%
Formic	158	265	125	65	565	55%	100%
3% HCl Acid							

Table 1—1 Ions leached from chlorite by various acids.

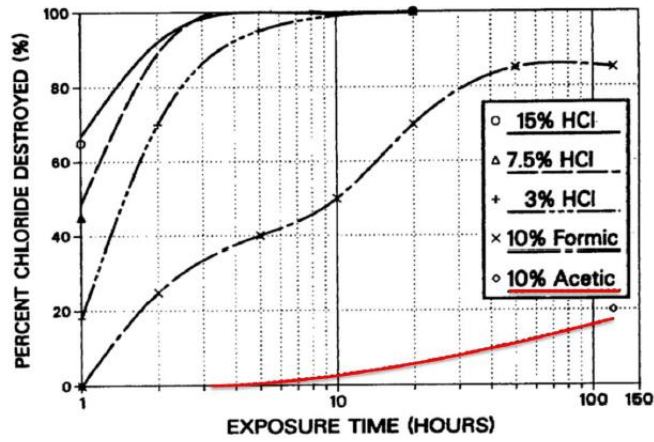


Fig. 1—4 Percent chloride destroyed by acid at 180°F.

Mineral Type	Temperature, °F
Zeolites	75-150
Chlorite	150-175
Illite	190
Smectite	200
Kaolinite	225

Table 1—2 stability limit of clays in HCl (Reprinted from Coulter and Jennings 1999).

Coulter and Jennings (1999) summarized the efforts done in the subject of mineral sensitivity with HCl. General consensus in literature have proven that all clays become unstable in HCl at different temperatures (Coulter and Jennings 1999).

The stability of temperatures of the different clay minerals with HCl are displayed above in **Table 1—2**.

Hibbeler and O'Driscoll (1996) published their recommendations for the maximum mud acid concentrations based on different temperatures. Their recommendations are summarized in **Table 1—3**.

Temperature	Maximum HCl Concentration, wt%	Maximum Mud Acid strength, wt%
<180°F	15	12-3%
180-220 °F	10	9-3%
>220 °F	7.5	7.5-1.5%

Table 1—3 Hibbeler and O’Driscoll guidelines (Reprinted from Hibbeler and O’Driscoll 1996).

Clays have much higher surface areas compared to feldspars making them more reactive. Quartz on the other hand has a very small surface area which is why its reaction with acids could be completely ignored. Clay concentration is crucial to detect, as they affect the acid design greatly. **Table 1— 4** has a list of the surface areas of different sandstone minerals. This is also shown in **Fig. 1—5**.

Mineral	Surface Area
Quartz	<0.1 cm ² /g
Feldspar	few m ² /g
Kaolinite	15-30 m ² /g
Smectite	82 m ² /g
Illite	113 m ² /g

Table 1— 4 Relative surface area of sandstone minerals (Reprinted from McLeod and Norman 2000).

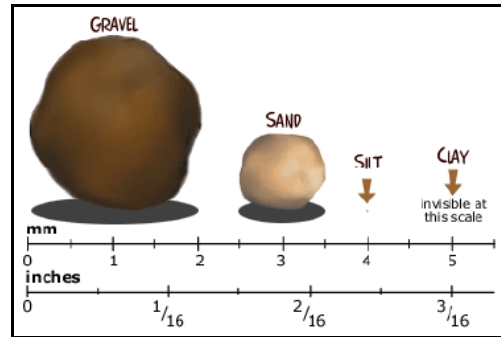


Fig. 1—5 Size of different sandstone minerals (Reprinted from McLeod and Norman 2000).

Mud Acid Alternatives

With the advancement of technology, alternative fluids to mud acids were introduced to stimulate sandstone reservoirs as several cases reported formation damage (Smith and Anderson 1990; Nasr-El-Din et al. 1998; Thomas et al. 2002). The following disappointing results were attributed to the shortcomings of the conventional mud acid system. Those problems include, but are not limited to, formation damage caused by HCl-sensitive clays (e.g., illite) decomposition, rapid rate of reaction and corrosion rates associated with high temperatures resulting in reaction products precipitation during secondary and tertiary reactions. Efforts have been made to overcome the problems associated with mud acid treatments. These attempts included the practice of retarded mud acid systems (Gdanski 1985, 1998; Gdanski and Shuchart 1996; Al-Dahlan et al. 2001). Nevertheless, at elevated temperatures, these systems proved to have similar problems as the conventional mud acid treatment. For instance, according to Dahlan et al. 2001, aluminum chloride retarded HF system is predisposed to aluminum fluoride precipitation. Fluoboric-based retarded mud acid might form a potassium-based precipitate (KBF_4) if it contacts clays such as illite or K-feldspars. In an

attempt to improve sandstone acidizing, organic acids such as acetic or formic acid were presented as alternatives to HCl owing the reason to their retarded reaction rate, lower corrosivity, easier inhibition, and a reduced tendency to form acid/oil sludge in asphaltene-rich crudes (Domelen and Jennings 1995). Organic acids provide more conductive length as it spends slower on the rock and penetrates deeper into the formation compared to regular HCl. A combination of 13/9% acetic/formic acid is utilized as it has similar overall acid strength as 15% HCl. However, the rock-dissolving capacity of 13/9% acetic/formic acid is noticeably lower than that of 15% HCl. (Harris, 1961; Smith et al., 1970; Chatelain et al. 1976; Fredd and Fogler; Huang et al. 2000; Nasr-El-Din et al.2001). Nevertheless, organic acids have many drawbacks. Several case studies showed that formic acid can help trigger fines flocculation (Chang et. al 2008). These acids cannot be used at high acid concentrations to prevent precipitation of their calcium salts (calcium acetate and formate). Organic acids possess a small dissociation constant. Their low dissolution capability may still hinder wormhole propagation leading to inadequate formation stimulation. The release of CO₂ from carbonate dissolution prevents organic acids from reacting to their full capacity. Moreover, the extent of hydrogen ion generation diminishes with elevating temperature, and, lastly, the cost of organic acid is considerably more expensive than that of HCl for a comparable mass of rock dissolved. Nasr-El-Din et al. 2007b observed that not all of the solid beads containing lactic acid hydrolyzed in the field and some of the lactic acid beads reacted with mill scales. Apelblat (1993) detected that an insoluble precipitate of calcium citrate formed from the reaction of carbonates with citric acid. To mitigate these problems,

many researchers proposed a blend of organic-HCl acids. However, there have been allegations that the organic acid spending amount will be additionally reduced when it is mixed with HCl due to the CO₂ release by the HCl-CaCO₃ reaction. In a study by Buijse et al. 2004, only 24% of the 10 wt% acetic acid was spent in a 15 wt% HCl/10 wt% acetic acid solution. In a further attempt to reduce the rate of acid-rock reactions, chelating agents such as EDTA (ethylene diamine tetra-acetic acid), HEDTA (hydroxyl ethylene diaminetriacetic acid), and GLDA (glutamic acid-N, N-diacetic acid) were evaluated. GLDA was found to be compatible with the sandstone mineralogy having up to 18 wt% illite (Mahmoud et al. 2011). At 300°F, GLDA, HEDTA, and EDTA showed decent compatibility with illitic-sandstone cores. Moreover, the optimum ratio of GLDA/HF concentration was 20 wt% GLDA/1 wt% HF giving a major increase in sandstone permeability. Nonetheless, Fernier et al. 2000 found out that an EDTA in an acid solution has inadequate solubility in the acid at pH < 4 and that EDTA is not typically biodegradable while NTA has a lower stability constant for Fe and Ca, it was also found to be an animal carcinogen (Fernier et al. 2000; 2001ab; 2003).

Despite the technological advancements in the area of acidizing, success rates are hardly consistent and fairly low (estimated 50%-70%) particularly in sandstones. In fact, Nitters et al. (2000) specified that major companies report treatment failures as high as 25 to 30%. Severe problems may arise when an acid job fails; further damage to the well may occur, not to mention the cost of the treatment is squandered. Nonetheless, with properly engineered matrix acidizing treatments, considerable production enhancements

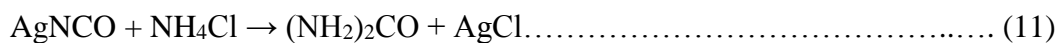
can be attained. The success of matrix stimulation can be enhanced if it is systematically implemented.

These findings fueled the desire to test a novel in-situ generated acid system that had similar dissolution power compared to regular HCl but with a lower reaction rate, more clay stabilization properties, and finally results in lower corrosion rates.

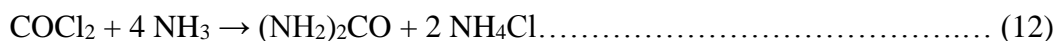
In the area of matrix acidizing, urea hydrochloride contribution has been a practically untouched subject. The aim of this work is to primarily investigate the performance of urea hydrochloride as an alternative to regular HCl in the dissolution of carbonate minerals in sandstone formations. Second, to identify the effect of mineralogy of the cores on the outcome of the urea hydrochloride treatment. Third, is to identify the effect of additives on the stimulation of Grey Berea and Bandera sandstone cores and, finally to evaluate the effect of temperature and flow rate on the outcome of the treatment.

Urea

According to Walker 1988 Urea, or carbamide, is an organic compound known with the chemical formula of $\text{CO}(\text{NH}_2)_2$. The urea molecule is composed of two amino ($-\text{NH}_2$) groups linked to a carbonyl ($\text{C}=\text{O}$) functional group. Urea has many distinctive characteristics; it is a white, odorless solid, with high water solubility, and typically non-toxic when used in minute quantities. It is slightly basic, which gives it the advantage of acting as a buffering medium for acid reactions. Urea has long been used since its synthetic discovery by Friedrich Wöhler in 1828 by treating silver cyanate with ammonium chloride using the following reaction:



Also, in the laboratory, urea is formed when phosgene reacts with ammonia as shown by the following reaction:



The appearance and structure of urea can be seen as follows in **Fig. 1—6** and **Fig. 1—7** respectively:



Fig. 1— 6 Appearance of urea.

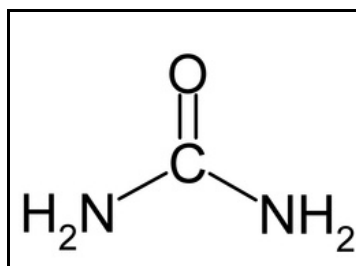


Fig. 1— 7 Structure of urea (Reprinted from Urea 2015).

Urea has many uses in a multitude of industries. In the oil and gas industry, it is used to help isolate straight chain and branched hydrocarbons in petroleum. Moreover, urea is extensively utilized in the production of many plastics and resins. Polyurea, on the other hand, is a unique product used to prevent corrosion and renew damaged

surfaces of pipes and pipelines, tanks, and compressors. For industrial purposes, urea is manufactured from synthetic ammonia and carbon dioxide. The properties of urea are shown in **Table 1—5**. Ever since the decomposition of urea was first presented by Wöhler (1829), the understanding of its products, by-products and reaction pathways have been the subject of several studies. Knowing which products, the scope of chemical reaction or when are they formed is obviously of practical interest when understanding its chemical kinetics and most recently its interactions with the reservoir rock formation. The main decomposition products of urea are ammonia (NH₃), isocyanic acid (HNCO), and carbon dioxide (CO₂).

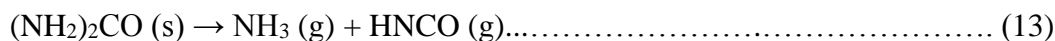
Chemical formula	CH ₄ N ₂ O
Molar mass	60.06 g·mol ⁻¹
Appearance	White solid
Density at 25 °C {77°F}, 100 kPa	1.32 g/cm ³
Melting point	133 to 135 °C (271 to 275 °F)
Solubility in water	107.9 g/100 ml (20 °C)
Solubility	500g/L glycerol, 50g/L ethanol
Basicity (pK _b)	PK _{BH⁺} = 0.18

Table 1—5 Properties of Urea in the Urea-HCl solution including chemical formula, molecular weights, density, and solubility constants (Reprinted from Williams 2001; Godfrey et al. 1997).

Urea is remarkably stable owing to its resonance stabilization. This diminishes the electrophilicity of the carbon atom (Wheland 1955).

Urea decomposes into ammonium cyanate (see reaction 3). Ammonium cyanate decomposes into ammonia and cyanic acid (see reaction 4) followed by a second reaction where HNCO is hydrolyzed into carbon dioxide and ammonia (see reaction 5).

For dry solid urea,



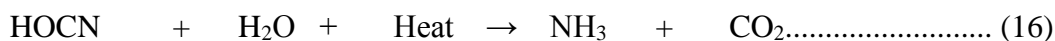
For urea-water solutions,



Urea ammonium cyanate



Ammonium cyanate ammonia Cyanic acid



Cyanic acid water ammonia carbon dioxide

The quest for trustworthy information is crucial as the decomposition reactions for urea are complex and are contingent on various conditions such as temperature, heating rate, pressure, open or closed vessel, and mass and heat transfer limitations are also thought to be essential (Schaber et al. 2004). The impact of each parameter is not yet completely understood. The following mechanisms are related with intramolecular and intermolecular proton-exchange interactions involving both amino groups or the amino and the carbonyl groups (Estiu and Merz 2004).

The thermolysis of solid urea studies two focal decomposition areas and involves thermogravimetric analysis of urea decomposition shown in **Fig. 1—8**. In the first region, above its melting point of 133 °C (271°F) and up to 250 °C (482°F), urea starts to slowly vaporize and then starts to decompose according to reaction pathway (see reaction 13). Other problems arise with temperature elevation as the production of biuret from urea and isocyanic acid or the formation of cyanuric acid, ammelide, ammeline or melamine. The decomposition of biuret back into HNCO is also believed to happen in this similar area.

After 250 °C (482°F), the high-performance liquid chromatography (HPLC) analysis showed that there is no noticeable quantities of urea, only some residual by-products that begin to decompose into HNCO in this second region; above 350 °C (662°F) and up to 500 °C (932°F).

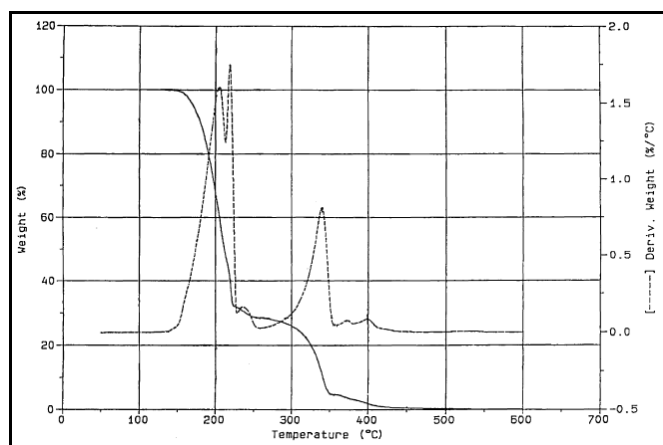


Fig. 1—8 Thermogravimetric analysis of urea pyrolysis. Mass losses (—) and 1st derivative (- -). Reprinted from Schaber et al.2004.

The HPLC plot shown in **Fig.1—9** shows the different distribution of urea pyrolysis products at a wide array of temperatures from 100-350 °C (212-662°F).

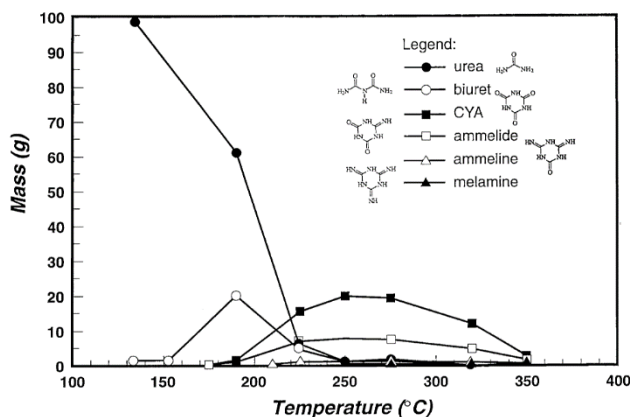


Fig. 1—9 HPLC Mass Plot: urea pyrolysis reaction (100.0 g of urea initially)(Reprinted from Schaber et. al 2004).

Urea Hydrochloride

Urea Hydrochloride is an organic salt that hydrolyses insitu bottomhole releasing H⁺ ions which reacts with earth-alkaline elements forming in-situ ammonium chloride (NH₄Cl) which acts as a clay stabilizer. Urea Hydrochloride is 71% as strong as HCl Acid and twice as strong as Phosphoric acid. With the constant need to search for the optimum acidizing solution, the aim of this work was done to determine the feasibility of using this novel in-situ generated acid as a potential stand-alone fluid for dissolving carbonates (Calcium and Magnesium) in sandstone reservoirs, especially, illite-rich sandstone and to investigate the formulation in corrosivity reduction and clay stabilization compared to regular HCl during stimulation operations at high temperature reservoirs. Urea-HCl is given by the following formula CH₅ClN₂O and has a molecular weight of 96.5162

g/mol. The structure and appearance of urea-HCl can be seen as follows in **Fig. 1—10** and **Fig. 1—11** respectively:

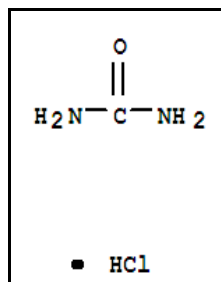


Fig. 1—10 Structure of urea-HCl (Reprinted from urea hydrochloride 2005).

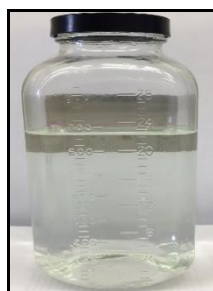


Fig. 1—11 Appearance of urea-HCl.

Urea hydrochloride can be produced with any desired ratio of urea and HCl. A combination of 1:4 and 4:1 moles of urea with HCl can be formed to fit the desired purpose. However, a typical ratio is between 0.5 moles of urea with 1 mole of HCl. A more ideal composition contains at least roughly 1 mole of urea to one mole of HCl. The mixing of both components results in a slight exothermic reaction (Sargent et al. 1997).

The molar ratio of the fixing agent (FA): HCl is provided to be 1.7. It is proposed that the adduction between HCl and urea via hydrogen bonding allowed for the dissolution of urea beyond the typical solubility limit. A proposed theory is that FA

complexes with the HCl molecules to keep them in solution having higher concentration than 37 wt% (Jiang et al. 2013).

Applications

- Urea-HCl helps eliminate the accumulation of water-insoluble metal salts on surfaces such as Ca, Mg, Ba, Al, Sr, and Be
- Urea hydrochloride also provides a method to reduce the solids content of industrial liquids containing water-insoluble metal salts
- Removal of carbonate scale from boilers
- Urea hydrochloride is an affordable and useful agent in the dissolution of metal salt dispersions or suspensions, especially, calcium carbonate
- Urea hydrochloride adjusts pH of dyeing baths and recreational waters, as well as, acting as a corrosion inhibitor and an anti-scaling agent
- Used in ore reduction, food processing, pickling, industrial acidizing, and general cleaning

Advantages

- Retarded reaction rate, greater ability to get the acid deeper into the formation before spending
- The acid is released insitu, this leads to the reduction of CI loading, and as a result a reduction in the overall cost of the acid job
- Urea hydrochloride is less corrosive to metal equipment, tubing, and smart completion
- NH_4Cl is generated insitu, thereby acting as a clay stabilizer

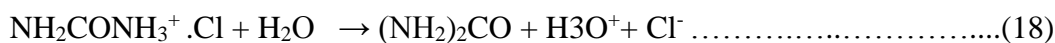
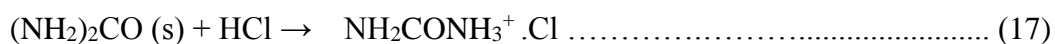
- The HCl in the formula forms soluble reaction products so there is a lower chance to form insoluble precipitations
- No need for Fe-control agents as the effluent pH is 0. The effluent samples generated contain live acid
- Urea-HCl has a significantly lesser tendency to discharge hydrogen chloride gas
- No fluoride into the formulation, therefore, no risk of damaging the formation and creating insoluble precipitates (CaF_2 , Na_2SiF_2 , and K_2SiF_6)
- The capacity to leave the formation water-wet and clean for optimum oil and gas production/injection
- Both urea and HCl are readily available and affordable
- Environmentally friendly as urea is biodegradable (93-98%) in a 24-hour cycle
- The formulation has a pH reduction capability
- The urea-HCl can act as a pre-flush before the mud acid treatment

Hydrolysis of Urea Hydrochloride

In this section two proposed methodologies for the study of urea-HCl hydrolysis is presented. The first suggested mechanism is based not only on other studies available from the literature, but also on the conditions detailed below.

According to Walker and wood (1903), the salts of weak bases (urea in this study) are incompletely disintegrated in aqueous solution into free acid and base, with a greater extent of hydrolysis as the base is weaker. Moreover, the concentration of the free mineral acid in the aqueous solution is roughly proportional to the rate at which methyl acetate is transformed into methyl alcohol and acetic acid. It is therefore

plausible to approximate the hydrolysis magnitude of the hydrochloride of the weak base by matching the rate at which a certain solution of methyl acetate is catalyzed under its impact with the rate at which the methyl acetate is catalyzed by a comparable solution of pure HCl. The rate of catalysis of methyl acetate by regular HCl was 0.00315; the rate of catalysis by regular urea hydrochloride under similar conditions was 0.00174. A normal solution of urea hydrochloride comprises less than half the quantity of urea hydrochloride. Consequently, about 55% of the whole formulation is decomposed by water into free urea and HCl. The range of 77 to 104°F (20 - 40°C), has no effect on the hydrolysis of urea Hydrochloride. Moreover, the addition of NaCl slightly decreased the hydrolysis rate. The following equations propose the possible hydrolysis of urea-HCl in water.

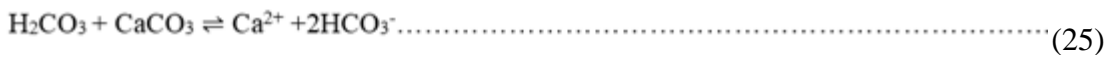
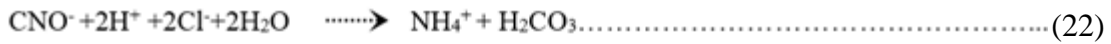


The second suggested mechanism is advocated by Shaw and Bordeaux (1995) by employing the method of initial rates. Earlier works presented by Walker and Hambley 1895; Fawsitt 1902; Werner 1918, 1920; Price 1919; and Warner 1942 have studied the reaction of urea decomposition in the presence of acids and bases. The reaction of HCl with urea hydrochloride was found not to be catalyzed by the acid. Several of the above-mentioned works collectively agreed that ammonium cyanate is an intermediate in the decomposition of urea in aqueous solution.

Nessler technique allowed the measurement of ammonium ion concentrations that corresponded to urea conversion to reaction products. The technique of initial rates was

applied (i.e., $\Delta u / \Delta t$ can be set equal to du/dt , where u is the urea concentration and t is time). Product-time curves were generated and were found linear for all temperatures. In the reaction of water only, however, the curves displayed some departure from linearity. The effect was amplified with increasing urea conversion.

In acid, a rapid quantitative conversion of the cyanate ion to ammonium ion occurs and is shown in (see reaction 22). If insufficient acid is available (see reaction 22) it does not go to completion. However, if adequate acid is existent all the cyanate ion is quantitatively converted to ammonium ion. Cyanate forms ammonium ions which in turn dissociates releasing H^+ ions shown by (see reaction 23). This closed loop retards the rate of reaction as H^+ ions circulates between both reactions, allowing less available ions at any given time to attack the carbonate surface. This reaction, on the other hand, might not go to completion under certain conditions. But, the reaction is complete at room temperature in sufficiently concentrated acid solution. At RT, the reaction is extremely slow. At pH of 1.4, the E_o for the reaction in the presence of acid is the same as in water alone which is equivalent to 30.9 Kcal, the frequency factor corresponds to $5 \cdot 10^{13} \text{ sec}^{-1}$. According to Warner 1942, the constant in acid has a slight tendency to be higher than that in water. Werner (1918, 1920) established the structure of urea in aqueous solution as **I** shown in (see reaction 19).



The reaction was observed to be a first order reaction with respect to urea over a wide range of concentration. This is displayed by (see equation 1):

$$\text{Rate} = - \frac{du}{dt} = k_1 \cdot [u]^1 \quad \text{.....(1)}$$

$$k_1 = k_0 e^{-E_a/RT} \quad \text{.....(2)}$$

$$E_0 = 30.9 \text{ Kcal}$$

$$R = 1.986 \text{ Cal mol}^{-1}\text{K}^{-1}$$

$$K_0 = 5 \cdot 10^{13} @ 80^\circ\text{C} = 176^\circ\text{F} = 353 \text{ K}$$

$$K = 5 \cdot 10^{13} \cdot \exp \left[\frac{-30.9 \cdot 1000}{1.98 \cdot 353} \right]$$

The first order rate constant was calculated based on data gathered by Warner 1942 using the Arrhenius (see equation 2) and was found to be $K = 3.15 \cdot 10^{-16} \text{ sec}^{-1}$.

Fig. 1–12 references the observed retardation factor for an aqueous solution with HCl and the FA (urea in our study) at 68 °F (20 °C). Retardation factor signifies the time it took for the retarded HCl of an equal effective concentration to consume a calcite sample, compared to regular HCl (HCl amounts being between 15 and 28 wt%). The

percentage of effective HCl is directly proportional to the retardation factor provided by urea but no further increase in retardation was observed from 23 to 28 wt% HCl.

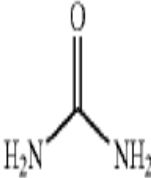
Observed retardation factors with certain Fixing Agents				
FA	Mol. Wt.	Structure	Effective HCl %	Retardation factor
Urea	60		17	14
			23	16
			28	16

Fig. 1—12 Observed Retardation Factor with Urea (Reprinted from patent no. 20150037234).

Fig. 1—13 depicts two retarded acid systems. The data displayed indicates the pore-volume to breakthrough (PVBT) for two fluids at various injection rates, which is the number of PV of acid that is pumped into a core before breakthrough is observed on the opposite end of the core sample. An indication of retarded acid reaction rates can be seen where a lower pumping rate provides the lowest PVBT. The treatment fluid (square points 104) having HCl and FA (urea or a urea derivative) showed significant retarded reaction rates relative to the typical retarded acid system (square points 102) at a temperature of 300°F. A proposition can be made that urea acts as an inhibitor/retarder, urea molecules and CaCO₃ compete for H⁺ ions causing a retarded reaction rate.

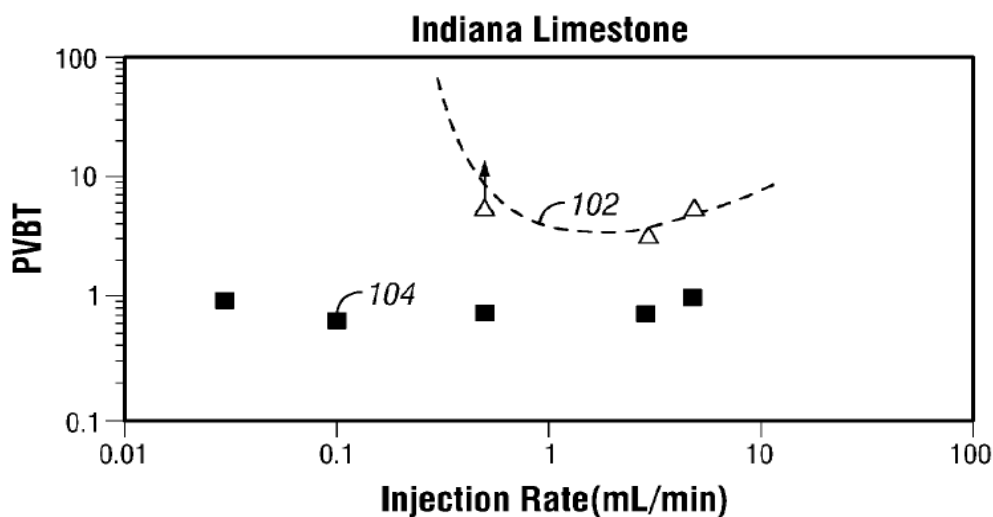


Fig. 1—13 Comparative PVTB between a typical retarded acid system vs. Urea hydrochloride system at 300°F

(Reprinted from Patent no. 955394).

The Intercalation of Urea in the Interlamellar Spaces of Kaolinite

One of the suggested modes of action of the novel insitu-generated system is the contact of urea present in the urea-HCl solution after hydrolysis with the kaolinite mineral present in the sandstone core mimicking the dynamic intercalation technique. In other words, it is possible that some of the urea in the urea-HCl formulation binds with the kaolinite present in sandstones for a sufficient time period. Literature showed that 90% intercalation occurred in 15 minutes (Yan et al. 2005) at 90°C. Therefore, it is plausible that the timing of the experiment (the time it takes to inject 5 PV of acid into the core) provided enough contact time between urea and kaolinite. The following proposition mimics the static/dynamic intercalation technique where urea molecules diffuse into the kaolinite crystal layers and delaminates it forming urea-kaolinite complex (UKC) displayed by the XRD patterns in **Fig. 1—14**.

During the intercalation process, the water amount present in the kaolinite is vital, as the catalysis action of the percentage of water present in kaolinite permits urea to form single molecules containing adsorbed water on its surface. This phenomenon allows the single urea molecules to effortlessly penetrate the kaolinite interlayers (Yan et al.2005). **Fig. 1—14**, below, shows the UKC after reaching equilibrium, where A, B, and C represents the three distribution structures of intercalated urea molecules.

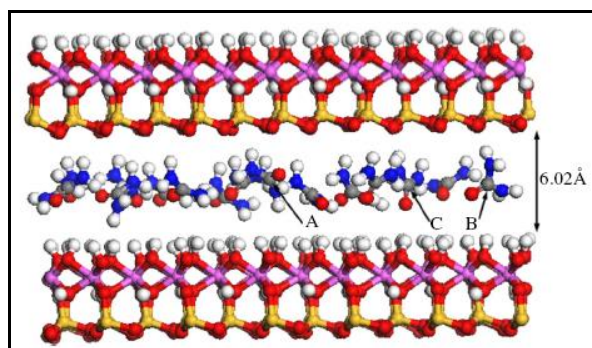


Fig. 1—14 Kaolinite-urea system after reaching equilibrium. A, B and C represent the three distribution structures of intercalated urea molecules (Reprinted from Yan et. al 2005).

In the kaolin group, kaolinite is the most profuse mineral, they are characterized by a 1:1 dioctahedral structure with the chemical configuration of $Al_2Si_2O_5(OH)_4$. Kaolinite possesses a unique asymmetric layered assembly with $(SiO)_6$ macrorings on one side and aluminol groups on the opposite side.

Infrared spectra of the raw kaolinite and the UKC have been collected displayed in **Fig. 1—15**. The raw kaolinite demonstrates four OH-stretching bands **Fig. 1—15a**. at 3695, 3668, 3653 and 3619 cm^{-1} . These four peaks occur for UKC as well, but the absorption band located at 3695 cm^{-1} , initiated by the inner surface hydroxyl of kaolinite,

is feeble. The two absorption bands situated at 3668 and 3653 cm^{-1} almost vanish, which is attributed to the inner surface hydroxyls of kaolinite. The band located at 3619 cm^{-1} , triggered by the inner hydroxyl of kaolinite, shows negligible change. This phenomenon confirms that urea molecules are bonded with the inner surface hydroxyls of kaolinite, but not with the inner hydroxyls. The UKC is not stable. According to Yan et al. 2005, during UKC heating, the gas generated by the decomposed urea in the composite caused the kaolinite in the composite to delaminate forming a number of perfect and thin crystal pieces. **Fig. 1—16** shows the XRD patterns of (a) raw kaolinite and (b) kaolinite–urea intercalation composite.

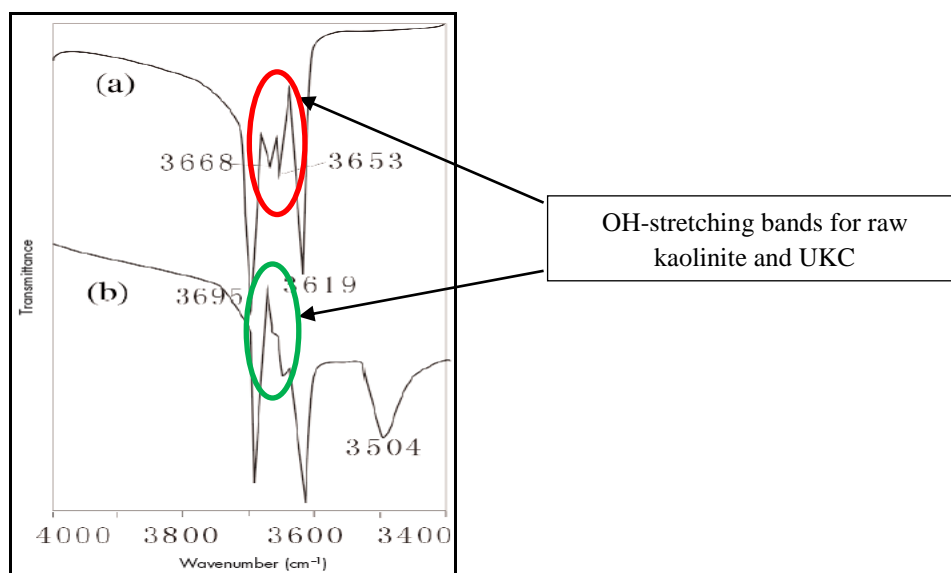


Fig. 1—15 Infrared absorption spectra of (a) raw kaolinite and (b) kaolinite–urea intercalation composite (Reprinted from Yan et. al 2005).

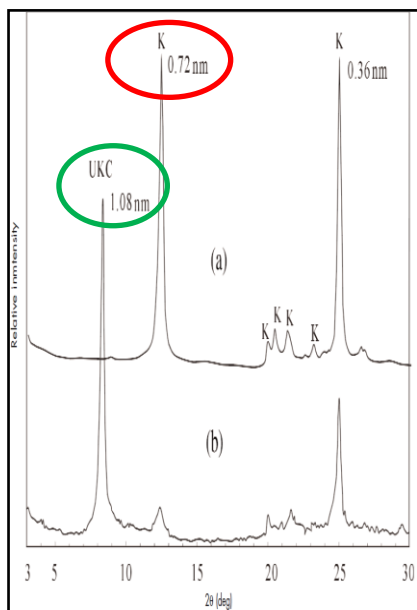


Fig. 1—16 XRD patterns of (a) raw kaolinite and (b) kaolinite–urea intercalation composite (Reprinted from Yan et. al 2005).

2. EXPERIMENTAL METHODS

Materials

Materials used for this study include the following:

- 30 wt% urea-Hydrochloric acid (HCl) was provided by a local service company
- Additives obtained from a local service company: such as corrosion inhibitor, intensifier, acid dispersant, anti-sludge, non-emulsifier, iron control were used
- Deionized water (TDS = 20 ppm) was used to prepare 2 and 5 wt% KCl solution

The characteristics of the treatment fluid are listed in **Table 2—1**. The core composition of Grey Berea and Bandera cores were determined using XRD techniques shown in **Table 2—2** and **2—3**.

Density, g/cc	Viscosity, cp	Concentration of HCl, %	pH
1.1128	1.656	16.3	0

Table 2—1 Characteristics of the treatment fluid.

Two types of Grey Berea cores with different mineralogy and a type of Bandera outcrop core with dimensions of 1.5 in. diameter and 6 in. length were used. The coreflood experiments were run at various flow rates of (1, 2, and 5 cm³/min) and different temperatures (250 and 300°F) to determine the optimum flow rate with which urea-HCl can dissolve the cementing material (Calcium and Magnesium) in sandstone.

Complete fluid analysis, including pH, density, and viscosity measurements, were measured for the coreflood effluent samples to investigate the reaction of urea-HCl with Grey Berea and Bandera sandstone cores.

Mineral Compositions	wt%
Quartz	86
K-Feldspar	3
Illite	1
Chlorite	2
Kaolinite	5
Calcite	2
Dolomite	1

Table 2—2 Mineralogy of Grey Berea Core.

Mineral Compositions	wt%
Quartz	57
Plagioclase	12
Dolomite	16
Chlorite	1
Illite	10
Kaolinite	3

Table 2—3 Mineralogy of Bandera Core.

Core Preparation

All types of sandstone cores were oven-dried at 250°F for 12 hours and the dry weight of the cores was measured. The cores were then saturated with 5 wt% KCl under a vacuum pump. The deionized water, used throughout the experiments, was attained from a purification water system having a resistivity of 18.2 MΩ.cm at RT. The weight of the saturated core was obtained after the measurement of the initial permeability to ensure that the core was completely saturated. The difference between the dry weight and the weight of the saturated cores divided by the density of the brine used in the experiments, was used to calculate the porosity of the cores (see equation 3).

$$V_p = \frac{W_{wet} - W_{dry}}{\rho} \dots\dots\dots (3)$$

Where:

V_p : pore volume, cm³; ρ : brine density, g/cm³

Initial and final permeability measurements were performed separately from the acid injection. Permeability was measured both at room and high temperature (250°F) by injecting a 2 or a 5 wt % KCl brine. Darcy's equation for laminar flow was used for the permeability calculation (see equation 4)

$$k = 122.8 \frac{qL\mu}{\Delta p d^2} \dots\dots\dots (4)$$

k : permeability, md; L : core length, inch; d : core diameter, inch; q : flow rate, cm³/min;
 μ : dynamic viscosity, cp; Δp : psia.

Solution Preparation

1. An example of solution preparation of 15 wt% HCl solution

To prepare 100 g of the solution:

$$\text{HCl acid weight} = \frac{15}{36.5} \times 100 = 41.1 \text{ g}$$

Plus the following additives were added in shown in **Table 2—4**.

Type of additive	Loading
Acid inhibitor	0.6 vol %
Anti-sludge	5 gpt
Non-emulsifier	1 gpt
Iron control	7.5 gpt

Table 2—4 Types of acid additives used with HCl in this study.

Finally, deionized water was added.

$$\text{DI H}_2\text{O weight} = 100 - (\text{weight of HCl acid} + \text{additives})$$

2. An example of solution preparation of 30 wt% urea-HCl solution

To prepare 250 ml of the solution:

The base fluid of 30 wt% urea-HCl solution was provided by a local service company plus the addition of the subsequent additives in a sequential order with the following loading amounts shown in **Table 2—5**.

Type of additive	Loading
Acid inhibitor	0.6 vol %
Acid dispersant	5 gpt
Anti-sludge	2 gpt
Non-emulsifier	2 gpt
Iron control	5 gpt
Intensifier	4 vol %

Table 2—5 The types of acid additives used for urea/ HCl in this study.

Equipment

Coreflood

The coreflood setup used in the experiments is shown in **Fig. 2—1**. A back pressure of 1200 psi was applied to all experiments to keep the CO₂, resulting from carbonate dissolution, in solution. The overburden pressure applied was approximately 1700 psi. A low-pressure transducer of the range 0-300 psi was used for all experiments. A pressure transducer was linked to a computer to measure the pressure drop across the core during the whole set of experiments. A Teledyne ISCO D500 precision syringe pump, having a maximum allowable pressure of 2000 psi, was utilized to inject the acid treatment into the core. The pressure drop across the samples was automatically recorded with time, while injecting the treatment.

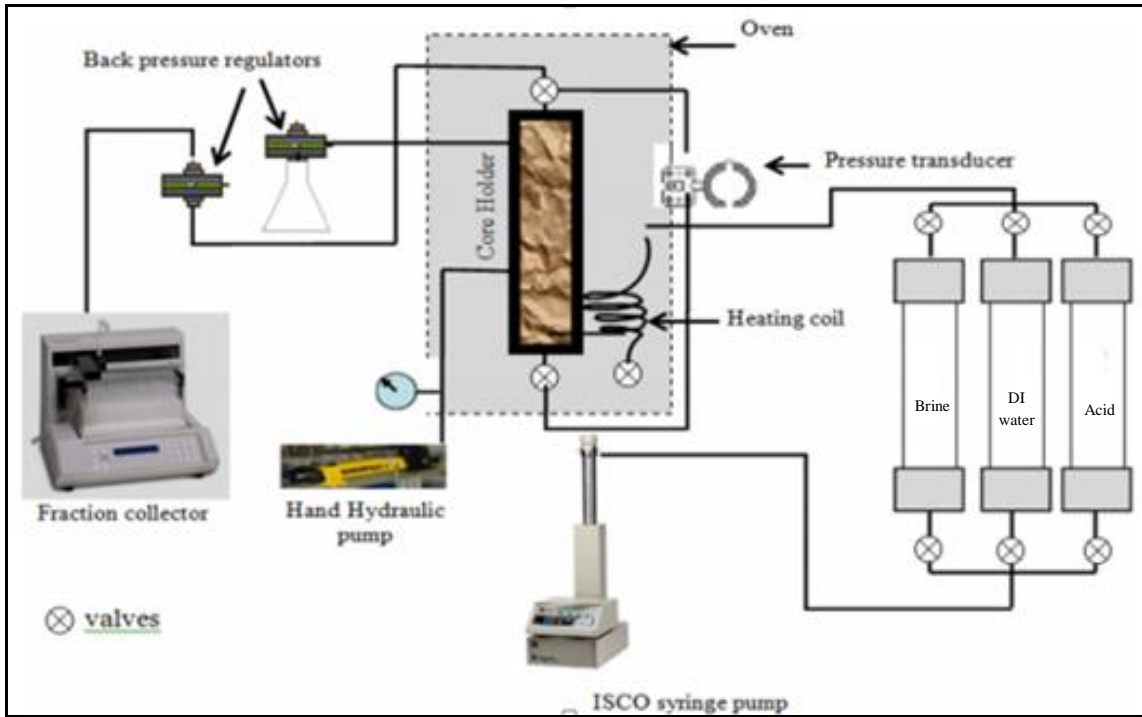


Fig. 2—1 A schematic diagram of the Coreflood Apparatus (Reprinted from Mahmoud et. al 2011).

CT Scan

Computed-tomography (CT) scanning is considered one of the best tools to pinpoint the damage in sandstone cores with high precision (Bartko et al.1995).

CT scans were conducted on the cores before and after the treatment to monitor changes in core porosity. The relationship between the CT number and the porosity can be described as follows (see equation 5, Izgec et al. 2005):

$$\text{Porosity} = \frac{CT_{wt} - CT_{ar}}{CT_w - CT_a} \dots\dots\dots (5)$$

Where CT_{wt} is the CT number of the water-saturated rock, CT_{ar} is the CT number of the air-saturated rock, CT_w is the CT number of water = 0, and CT_a is the CT number of air = -1,000.

The CT scanner shown in **Fig. 2—2** was used to get CT numbers and generate porosity profiles for the cores used in the coreflood experiments. The cores were CT-scanned dried and then saturated with its inlet direction facing the entrance of the scanner.

The CT number is correlated to bulk density as displayed in (see equation 6) (Izgec 2009).

$$\rho_{bulk} = aCTN + b \dots\dots\dots (6)$$

Where is ρ_{bulk} the bulk density, CTN signifies the CT number, a is the slope, b is the intercept of the linear relation between CTN and the bulk density.



Fig. 2—2 CT-scan device.

Hot Rolling Oven

All the sandstone cores used were dried at 220°F in the oven for 4 hours to a maximum of 12 hours to ensure the evaporation of any insitu water initially present in the core.

X-Ray Diffraction (XRD)

D8 DISCOVER displayed in **Fig. 2—3** is an analytical technique used to determine the atomic and molecular crystal structure, in which the crystalline atoms cause a beam of incident X-rays to diffract into various specific directions. A crystallographer can emit a 3D image of the electron density within the crystal by measuring the angles and intensities of these diffracted beams. XRD specimens mechanically crushed to fine powder and put in a concave sample base. Clay-size portion samples are separated from the bulk sample on a glass slide. XRD provides semi-quantitative information on the relative abundance of bulk and clay minerals present in the samples examined. These percentages are crucial to effective stimulation treatment design.

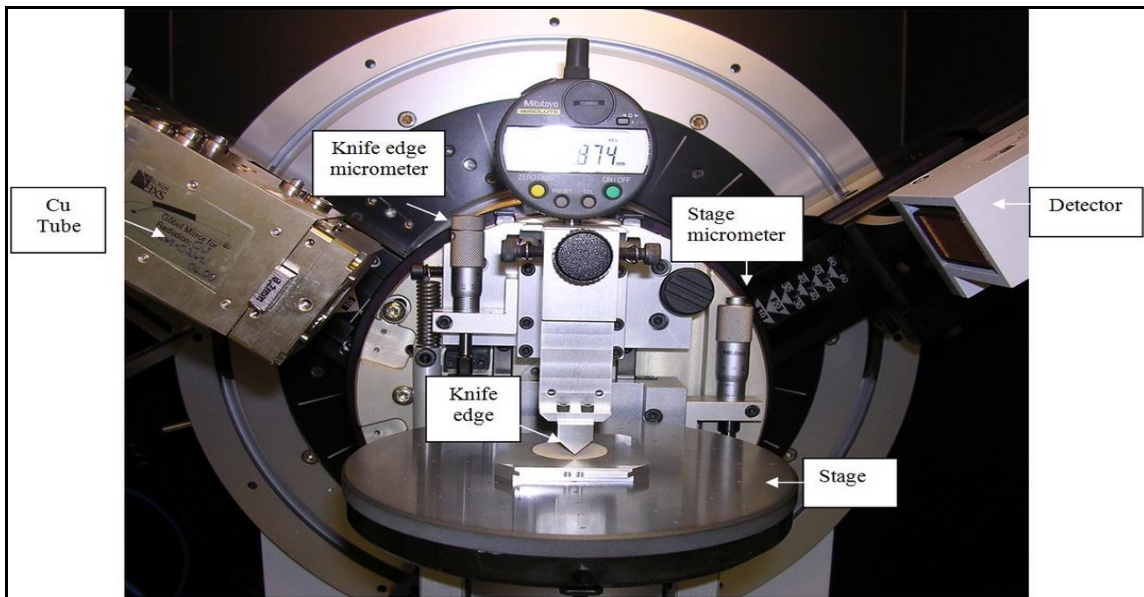


Fig. 2—3 X-ray diffraction (Reprinted from ammr.org.au/my scope/ xrd 2014)

Inductively Coupled Plasma Optical Emission Spectrometry (ICP-OES)

Optical emission spectroscopy (OES) utilizes quantifiable measurement of the optical emission from excited atoms to measure cation concentration. Those atoms dissolved in solution are aspirated into the excitation region where they are dissolved and atomised by a plasma. Electrons can either be in their stable state or excited when they are given energy. This is the excited state. A photon of light is emitted when an electron falls from its excited state to its ground state. Each element has a distinctive set of wavelengths that it can emit. A schematic is given in **Fig. 2—4**.

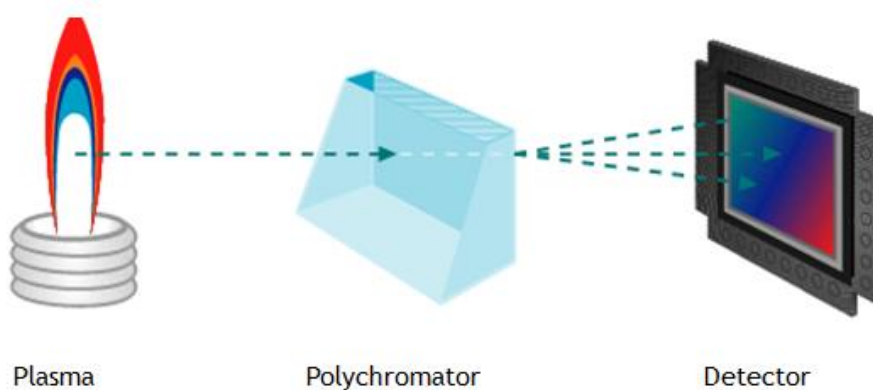


Fig. 2—4 An illustration of ICP theory.

An Optima 7000 ICP-OES Spectrometer was utilized in this research, **Fig. 2—5**, to investigate the core effluent samples collected for the iron, magnesium, silicon, aluminum, and calcium concentrations.

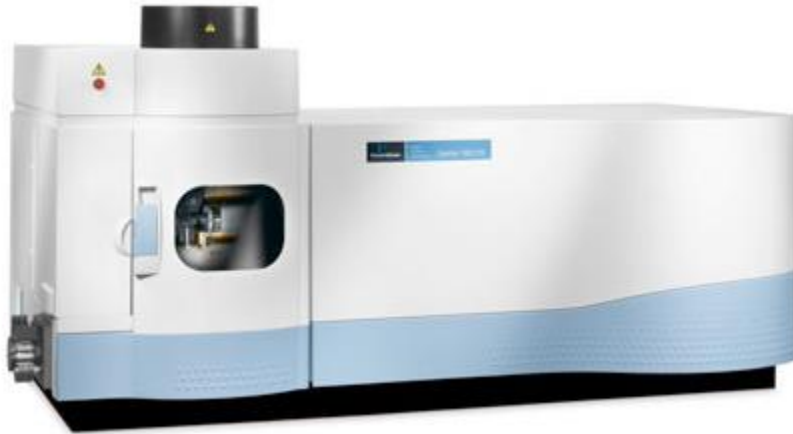


Fig. 2—5 Optima 7000 ICP-OES Spectrometer (Reprinted from .sisc.com.vn).

Steps for Using ICP-OES

1. Ventilation must be working.
2. Open the air and argon tanks and modify their pressures.
3. Switch the machine on.
4. Select the appropriate method from the computer attached to the ICP.
5. Light the lamp and leave it for 30 minutes to warm up.
6. Aspirate deionized water and select auto zero.
7. Aspirate the calibration blank (2% HNO₃) and select auto zero.
8. Calibrate using standards (5, 15, and 30) ppm and check the linearity of the standard and the correlation coefficient value.
9. Analyze samples.
10. Close the Winlab program window after closing the air and argon and bleeding them from the pipes. The results will be shown in ppm.

11. If any samples are deviated from the range of the standard curve (0-30 ppm), make the appropriate dilution and reanalyze them again.

Titrator

The acid titration is based on the volumetric method for determining the acid concentration. The Thermo Scientific Orion 950 Titrator utilized in this study is shown in **Fig. 2—6**. An auxiliary reagent (NaOH) of an identified concentration (1M) is applied to the pre-dose volume of titrant (acid solution). A dispenser is used to add the auxiliary reagent, until a pH electrode measures a pre-set pH value of 7. Then the volume of the reagent of a known molarity will be used for molarity calculations. The effluent sample acid concentrations is calculated using the flowing equation:

$$M_{\text{acid}} \times V_{\text{acid}} = M_{\text{base}} \times V_{\text{base}} \dots \dots \dots (7)$$

Where M_{acid} is the acid molarity, V_{acid} is the acid volume, M_{base} is the base molarity, and V_{base} is the base volume.

The titration is used to measure the equivalence of HCl in the 30 wt% urea-HCl solution.



Fig. 2—6 Thermo Scientific Orion 950 Titrator (Reprinted from .coleparmer.com 2015).

Dean Stark

The Dean-Stark tool is a piece of glassware used for water accumulation or other liquids from a reactor displayed in **Fig. 2—7**. The apparatus is used in an arrangement with a reflux condenser and a batch reactor for water continuous removal (Circulation system), shown in **Fig. 2—8**, produced during the chemical interactions performed at a specified temperature. It was invented by E. W. Dean and D. D. Stark in 1920 for the determination of the water content in petroleum. The apparatus usually consists of vertical cylindrical piece of glass with a full length volumetric graduation and a precision tap on its bottom. The topmost of the cylinder fits with the bottom of the condenser and the fluid collected drips into the distilling trap (Dean and Stark 1920). The following de-contamination method aims to de-contaminate the outcrop cores from any water remains. Throughout the reaction, the reaction solvent vapors (toluene) dissolves any solvents present in the core and is condensed by the cooling water circulating around the lines.



Fig. 2—7 Dean Stark Apparatus.



Fig. 2—8 Circulation system.

Gas Chromatography-Mass Spectrometry

Gas chromatography–mass spectrometry (GC-MS) shown in **Fig. 2—9** is an analytical technique combining both the characteristics of gas-chromatography and mass spectrometry to classify various compounds within a given sample. GC-MS is used to implement a particular test where it positively detects the physical presence of a specific substance in any given sample. The GC-MS consists of two central equipments: the gas chromatograph and the mass spectrometer. The relative affinity and the variance in the chemical characteristics between different molecules in a mixture, for the static phase of the column, will encourage molecule separation as the sample travels throughout the column. The molecules are reserved by the column and are eluted at different (retention times). This practice allows the mass spectrometer to capture, ionize, accelerate, deflect, and detect the ionized molecules independently. The mass spectrometer ensures this by breaking every molecule into ionized fragments and

detecting their fragments. Both of the two components, used together, permit a greater extent of compound identification than either unit used individually.

Precise identification of a certain molecule by gas chromatography or mass spectrometry alone is not reliable nor possible. The mass spectrometry process normally necessitates a pure specimen while gas chromatography uses a flame ionization detector were it cannot distinguish between compound molecules having equivalent retention times, resulting in two or more molecules that co-elute. In this study, GCMS tests were run on both unheated and treated 30 wt% urea-HCl at 250 °F to detect any possible decomposition products which might potentially contribute to some of the damage observed in Grey Berea sandstone cores.



Fig. 2—9 GC/MS Instrument (Reprinted from gcms confirmation 2010).

3. RESULTS AND DISCUSSION

In an attempt to counteract some of the major issues encountered by the use of regular HCl, urea-HCl with its retarded reaction rate capacity, lower corrosivity, and clay stabilization properties is experimented and evaluated as an acidizing alternative in the stimulation of Grey Berea and Bandera sandstone cores.

For this reason, three flow rates (1, 2, and 5 cm³/min) and two temperatures (250 and 300°F) were tested on different sandstone mineralogy. The coreflood outcomes were compared based on the ratio of final to initial permeability. After the injection of 5 PV of acid, the flow switched back to brine and collecting the effluent samples was started at every quarter of PV. The injection of brine and the collection of samples were stopped based on two scenarios:

- 1) The effluent sample became colorless.
- 2) The pressure drop stabilized, which means that the acid was pushed out by the brine.

The cores were scanned after treatments using a CT scanner to determine their porosity profile before and after treatment. The effluent samples were diluted a 1,000 times for Berea sandstone and 2,000 times for Bandera sandstone to make sure that the concentration of each of the cations was below 30 mg/l. These samples were analyzed using inductively coupled plasma (ICP) analysis using Optima 7000 DV ICP-OES system and WinLab 32™ software for the following elements: Ca, Mg, Al, Fe, and Si.

XRD was performed on the different sandstone cores to analyze their carbonate and clay content while GCMS detected the decomposition products on the treated and

unheated treatment fluid at 250 °F. Complete fluid analysis such as density and pH measurements for the resultant effluent samples was done to study the reaction of urea-HCl with Grey Berea and Bandera sandstone.

XRD Results

The following **Table 3—1** shows the quantitative mineralogy compositions of both Grey Berea and Bandera rock samples.

Mineral	Composition	Bandera (%)	Berea (%)
Quartz	SiO ₂	57	86
K-feldspar	KAlSi ₃ O ₈	-	3
Calcite	CaCO ₃	-	2
Dolomite	CaMg(CO ₃) ₂	16	0
Illite	(K,H ₃ O)(Al,Mg,Fe) ₂ (Si,Al) ₄ O ₁₀ [(OH) ₂ ,(H ₂ O)]	10	1
Kaolinite	Al ₂ Si ₂ O ₅ (OH) ₄	3	5
Chlorite	(Mg, Fe) ₅ Al(AlSi) ₃ O ₁₀ (OH) ₈	1	2
Plagioclase	NaAlSi ₃ O ₈	12	-

Table 3—1 Quantitative XRD mineralogy for Grey Berea and Bandera sandstone.

Qualitative XRD was performed on 3 different types of sandstone cores with different mineralogy. Bandera sandstone consisted of dolomite, albite, some kaolinite, illite, and chlorite shown in **Fig. 3—1**. Moreover, the G-14 and G-15 cores (a different type of Grey Berea core having different mineralogy) shown in **Fig. 3—3** had no calcite at all in their mineralogy. Dolomite and clay minerals such as Kaolinite, chlorite, and illite were present in abundance. Whereas the previous type of Grey Berea outcrop exhibited different mineralogy shown in **Fig. 3—2**. No dolomite was found but had calcite and kaolinite present with chlorite, illite, and albite.

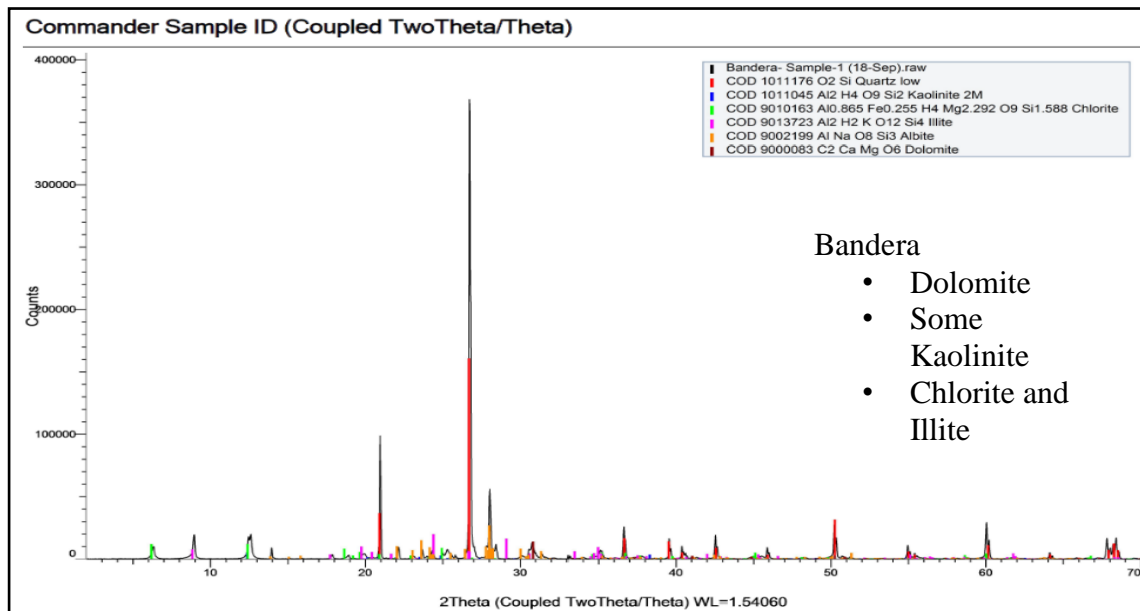


Fig. 3—1 Bandera Sandstone XRD Results

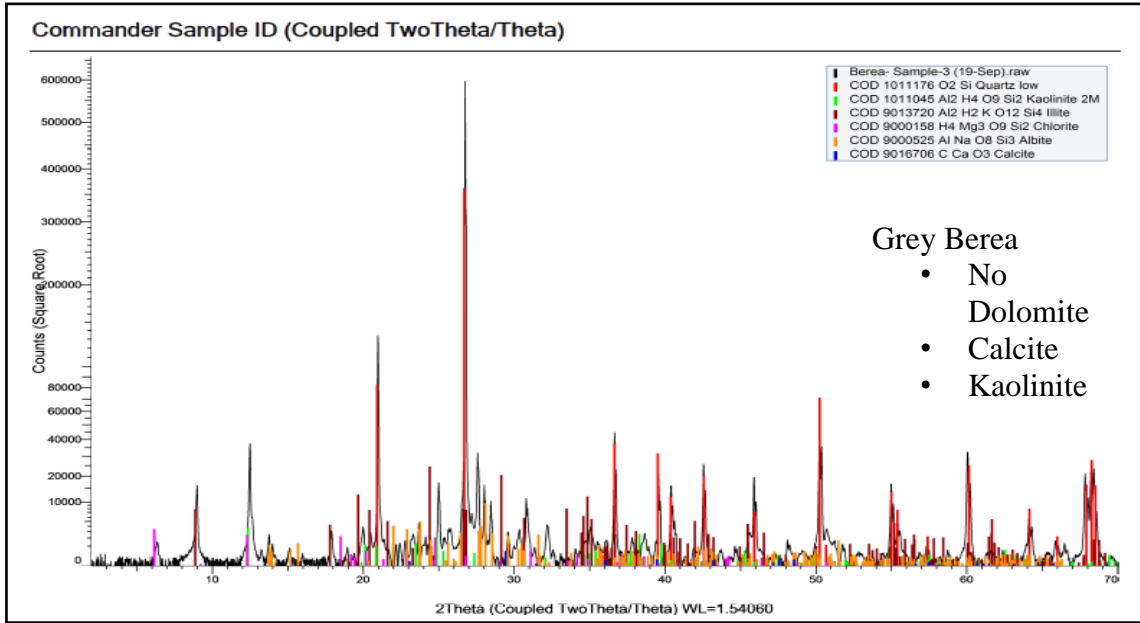


Fig. 3—2 Grey Berea Sandstone XRD Results.

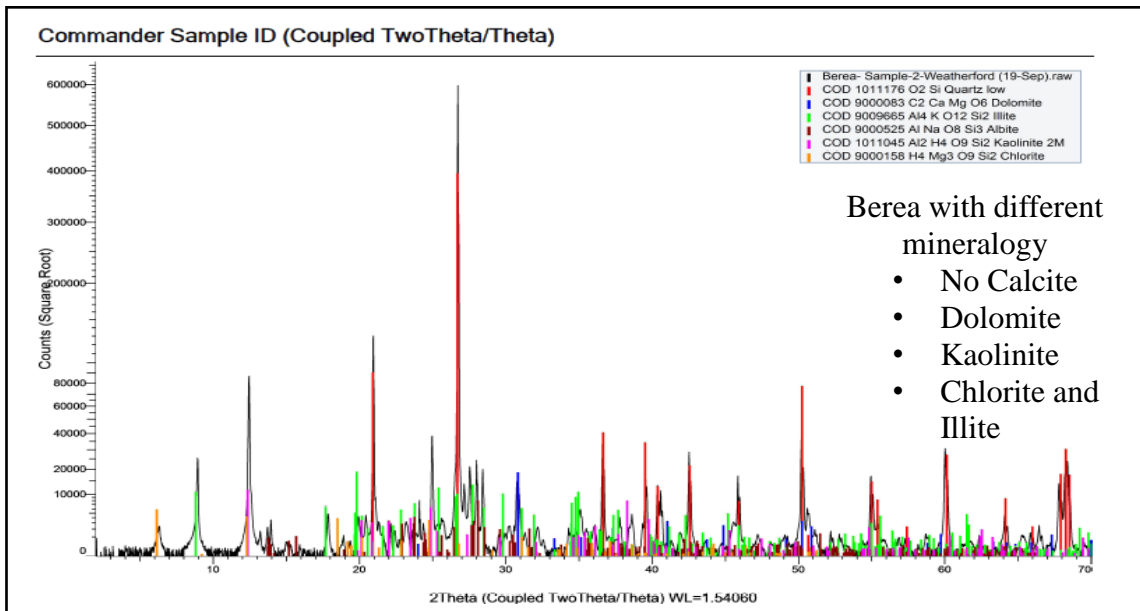


Fig. 3—3 Grey Berea Sandstone with Different Mineralogy XRD Results.

CT Scan

Cores were scanned using a CT scanner for better understanding of the porosity profile of the core **Fig. 3-22, 27, 29, 34, and 3-41** show porosity profiles for the 6 in. long, cores treated by the novel urea-HCl solutions at flow rates of (1-5) cm³/min, and at a temperature of (250 - 300) °F.

The decrease in the CT number typically suggests a lower density. This was observed in Be-13 coreflood experiment shown by **Fig 3-41**. This might indicate an increase in the core porosity after the treatment (i.e. the core was stimulated) or through the dissolution of a heavy material.

CT number increases were observed in four coreflood experiments (Be-02, 03, 10, and 11). The increase in CT number suggests a precipitation of a high density material compared to sandstone. This indicates a reduction in the core porosity (i.e., the core was damaged). The scans were taken before and after the coreflood experiments throughout the length of the core. The cores were saturated with the same type of brine used before scanning. As a result, changes in the CT number were caused by changes in the core porosity only. These changes might have occurred because of the precipitation of reaction products due to the development of secondary and tertiary reactions. Another cause could be due to the precipitation of urea and iron oxides or colloidal silica gel deposition.

Gas Chromatography- Mass Spectrometry (GCMS) Results

The following two graphs **Figs. 3-4 and 3-5** show GCMS results for both heated and unheated urea-HCl solution. The objective of the test was done to determine the thermal

stability of the formulation i.e. whether or not there is urea-HCl decomposition at a temperature of 250°F. The x-axis is the retention time for different components in the sample and in this case, the urea, which is the amount of time the sample spent interacting with the column and the y-axis is the relative abundance, which is the signal intensity normalized to the peak that gave the highest amount of signal. In Fig. 3–4, the unheated urea appears lower because the borate signal is much higher in the (untreated urea-HCl) graph than it is in the bottom graph (treated urea-HCl), so it is normalized to the borate peak instead of the urea peak like it is in the treated one.

In the top graph, the untreated formulation, the 3.45E9 corresponds to the signal intensity for the borate signal and since the urea is ~20% of the relative abundance of this signal, it is normalized to the 3.45E9 that means that the urea signal is ~ 6.40E8 counts. This actually means that in comparison to the heated urea-HCl sample shown by Fig. 3—5, which is 4.88E8, there is a higher amount of urea in the untreated sample.

In the heated urea-HCl graph at 250°F, the unidentified peak region shows more peaks compared to the untreated sample. The following signifies the occurrence of secondary and tertiary reactions within the formulation itself.

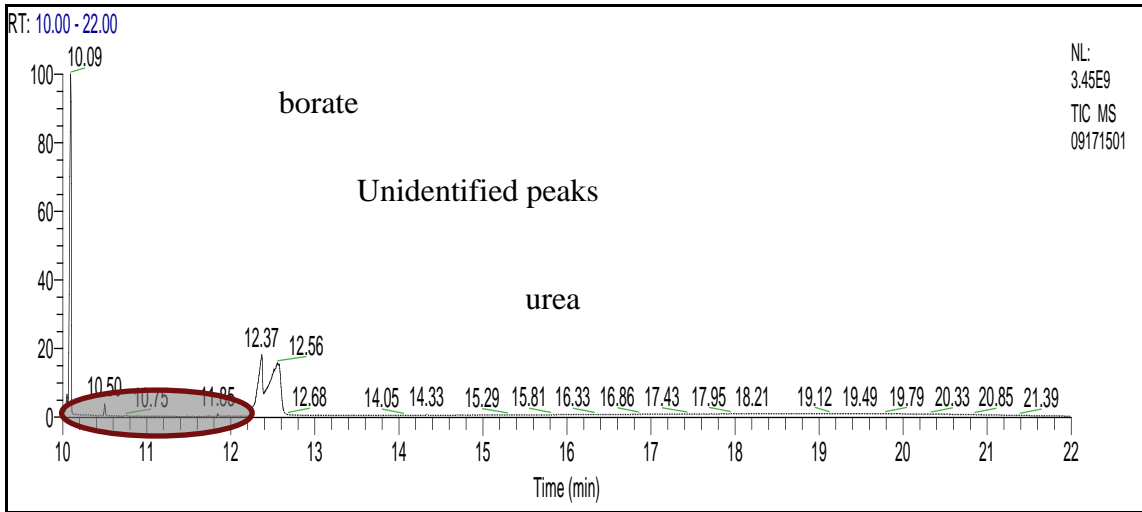


Fig. 3—4 Untreated urea-HCl graph.

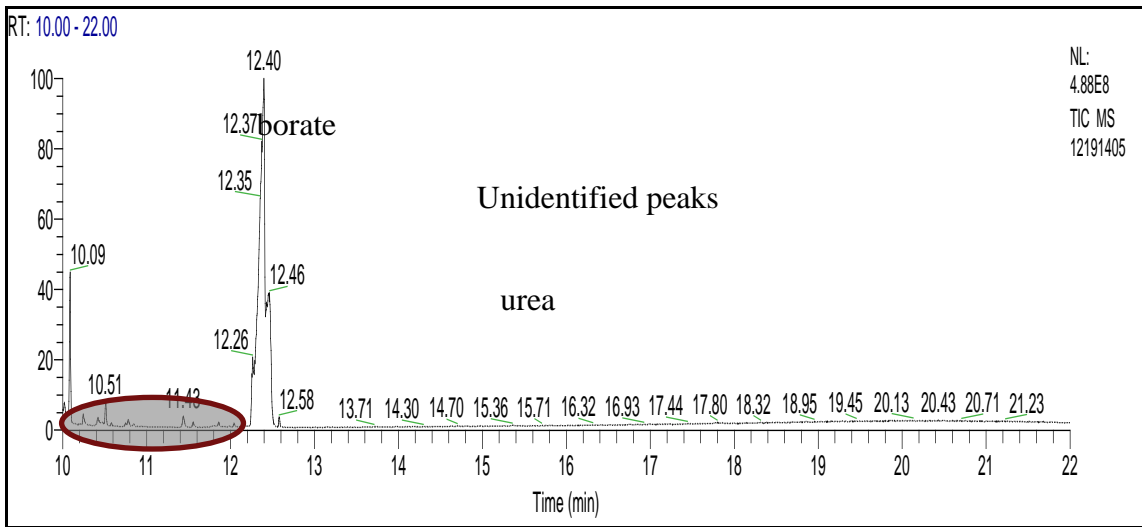


Fig. 3—5 Heated Urea-HCl at 250°F graph.

Viscosity and Density Measurements

The dynamic viscosity was first measured at RT using an Ubbelohde capillary viscometer. The viscosity was then measured at high temperature using an oil bath. Increments of 10°C (50°F) was added until a temperature of 90°C (194°F) was reached.

The treatment fluid was poured into the capillary tube of the 0C type viscometer. Three viscosity timings were recorded with a stopwatch and the averages were taken. The viscosity was calculated by multiplying the timing in seconds with the constant value, C, of 0.003. The viscosity measured was then divided by the density of the treatment fluid at high temperature and was extrapolated to 121.1°C (250 °F).

The faster it takes for the fluid to pass between the two marks on the capillary tube, the lower the viscosity of the fluid. The higher the temperature, the lower the viscosity. The **Fig. 3—6** below shows the temperature in celsius versus kinematic viscosity in centipoise. At our desired temperature of 250°F, the viscosity reached 0.2 cp. The kinematic viscosity is the proportion of the dynamic viscosity μ to the density of the fluid ρ . Kinematic viscosity was calculated using (see equation 8):

$$v = \frac{\mu}{\rho} \dots\dots\dots (8)$$

The density of both HCl and urea-HCl was measured both at RT using the DMA 35 portable density meter and at high temperature using the DMA 4100 high temperature density meter. Increments of 10°C (50°F) was added from RT till 90°C (194°F) then the density was extrapolated to 121.1°C (250°F). The higher the temperature, the lower the density of the fluid.

The viscosity and density of urea-HCl is shown in **Table 3—2** below, with the addition of all six types of additives, was found to be higher than regular HCl with its additives included. While the pH of both solutions were of similar acidity of 0. The HCl equivalence was almost the same in both acid systems.

Acid Type	Viscosity timings	Viscosity, cp	Density average	Density, g/cc	Concentration of HCl,%	pH
HCl+ additives	7min:7 sec		1.0771		15	0
	7min:11 sec	1.22	1.0774	1.0773		
	7min:13 sec		1.0775			
Urea-HCl +additives	9:00		1.102		16.7	0
	9:04	1.596	1.1025	1.1023		
	9:11		1.1023			

Table 3—2 Viscosity and density measurements at 75°F.

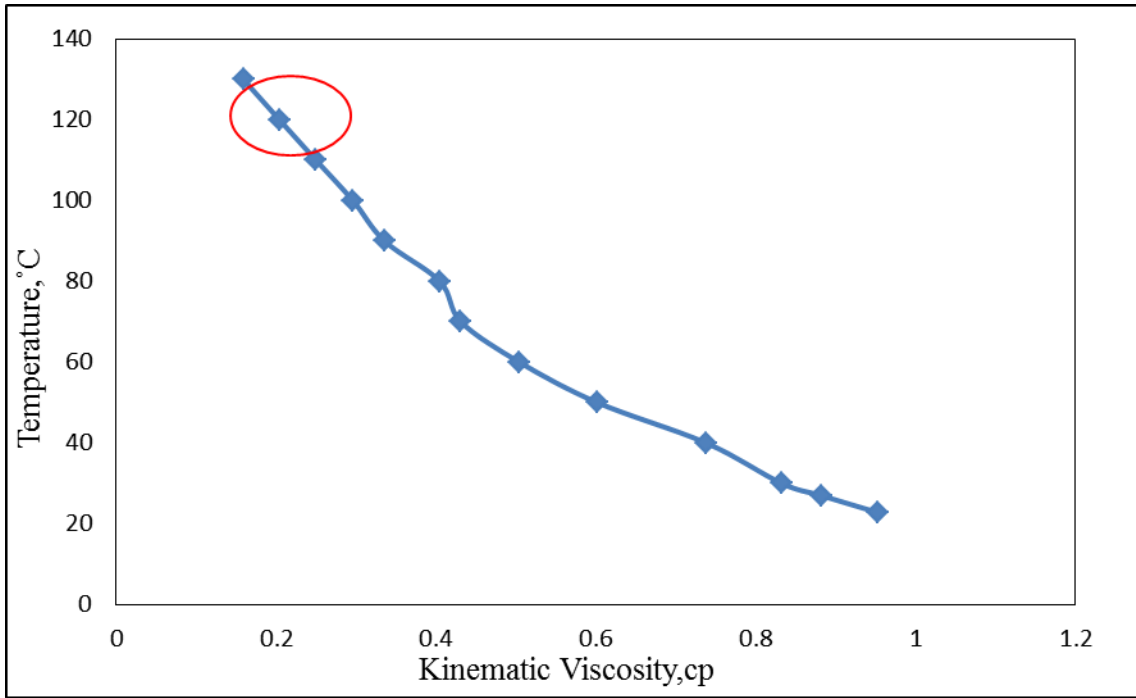


Fig. 3—6 Temperature vs kinematic viscosity measurements from RT to 250°F (121.11 °C).

Coreflood Studies

Coreflood experiments were run using the coreflood setup shown in the previous section. This methodology was designed to provide further insight into the complex action of urea-HCl and, with equal importance, achieve a coherent experimental approach for future work. As such, the equipment was chosen to cover a range of experimental conditions, including the operating temperatures of the coreflood system and the temperature range for urea's decomposition. To ensure inert conditions, argon and nitrogen were used.

In this section, the effect of temperature and flow rates in the acidizing treatments is studied. Five sets of coreflood experiments were conducted on 6 and 4 in. Grey Berea and Bandera sandstone of a wide range of permeabilities (4-163 md) up to 300°F. The first set of experiments was performed with 15 wt% HCl as a control for comparative reasons against the 30 wt% urea-HCl treatment. In the second set of experiments, 30 wt% urea-HCl solutions (17.6 wt % HCl) with the addition of the 6 types of additives were used. The experiments were performed at temperatures up to 300°F. The third set of experiments was performed with 30 wt% urea-HCl acid solution adding only a corrosion inhibitor and a corrosion inhibitor intensifier to study the effect of the insitu-generated acid (17.6 wt % HCl) on the dissolution of carbonate minerals in sandstone cores. In the fourth set of experiments, 30 wt% urea-HCl solutions (17.6 wt % HCl equivalence) with the addition of the 6 types of additives were used to stimulate Bandera sandstone. In the fifth and final set of experiments, 30 wt% urea-HCl solutions

(17.6 wt % HCl) with all of the 6 types of additives were used on a different type of Grey Berea core having different mineralogy (G-14 and 15).

Prior to the acid treatment, the cores were saturated utilizing 5 wt% KCl brine, the initial permeability was measured when the pressure stabilized. During the coreflood runs, 5 wt% KCl brine was injected while the core was heated to the desired temperature. Followed by that, 5 PV of the acid treatment was injected. Subsequently, the cores were flushed again with 5 wt% KCl brine. Finally, the cores were left to cool down and 5 wt% KCl brine was pumped at a steady rate until the pressure drop re-stabilized and the final permeability was measured. This procedure was repeatedly done for all of the first 4 sets of experiments. In the final set of experiments (section-E), however, 2 wt% KCl brine was pumped instead.

These runs were implemented to evaluate the success of the acid as a stand-alone stimulation fluid. For each coreflood experiment, the pressure drop across the core was plotted using Lab-View software.

Some results showed a significant amount of iron dissolved and precipitated on the injection face of the cores, i.e. where the contact occurs between the acid and the rock, producing a decrease in final permeability, which indicated severe formation damage. The damage increased with the increase of the amount of iron in the solution. At higher temperatures and lower flow rates, the damage was significant. Core length did not affect the degree of damage.

List of Experiments

The entire experiments composed of 30 wt% urea-HCl solutions with all of the additives included performed at a temperature of 250°F resulted in core sample damage from a range of (13-35%) on Grey Berea sandstone composed of calcite with no dolomite content available. Conversely, all of the 30 wt% urea-HCl with the addition of only the CI and the intensifier resulted in a range of stimulation (3-30%). The Grey Berea sandstone (G-14 and 15) with different mineralogy containing dolomite with no calcite showed a permeability enhancement of up to 30%. Specifically, The G-15 with all of the 6 types of additives included showed the most enhancement (30%), while, the G-14 core sample with the addition of only CI and intensifier showed only a slight enhancement of around 3%.

Grey Berea Experiments

Table 3—3 below shows the initial and final brine permeability measurements for 11 Grey Berea sandstone cores and their respective percent regain permeability values were obtained for each test. The treatment outcome and description is also mentioned below. In the following table, S: signifies stimulation, SD: signifies severe damage, and D: signifies damage.

Core ID	Test ID	Formation	Permeability				Treatment outcome	Test Description
			Initial K	Final K	K_f/K_i	% Regain		
Be-02	Test 1	GB	73.3	55.5	0.757	24.28	D	30 wt% Urea-HCl at 250 °F with all additives Included
Be-03	Test 2	GB	80.2	No stabilization	-	-	SD	30 wt% Urea-HCl at 300 °F with all additives Included
Be-05	Test 3	GB	85.2	99.4	1.666	17	S	15 wt% HCl at 250 °F
Be-06	Test 4	GB	93.2	112.1	1.203	20.27	S	15wt % HCl at 300 °F
Be-08	Test 5	GB	49.4	54.6	1.105	10.53	S	30wt% Urea-HCl at 250°F- Only CI and Intensifier Included-
Be-09	Test 6	GB	34.7	24.8	0.714	28.53	D	30wt% Urea-HCl at 250 °F with all additives Included

Table 3—3 Berea sandstone experiments summary.

Core ID	Test ID	Formation	Permeability				Treatment outcome	Test Description
			Initial K	Final K	K_f/K_i	% Regain		
Be-10	Test 7	GB	49.1	31.9	0.649	35.03	D	30wt% Urea-HCl at 250 °F with all additives Included
Be-11	Test 8	GB	46.2	40	0.865	13.41	D	30wt% Urea-HCl at 250 °F with all additives Included
Be-13	Test 9	GB	103.5	120.2	1.161	13.14	S	30wt% Urea-HCl Only CI and Intensifier Included-at 250°F
G-14	Test 10	GB	162.9	167.78	1.03	3	S	30wt% Urea-HCl- Only CI and Intensifier Included-at 250°F
G-15	Test 11	GB	126.8	165.6	1.306	29.4	S	30wt% Urea-HCl at 250 °F with all additives Included

Table 3—3 Continued.

Bandera Experiments

Table 3—4 below shows the initial and final brine permeability measurements for 2 Bandera sandstone cores and their respective percent damage permeability values were obtained for each test. Test description and outcome was also mentioned. Bandera has a lower permeability compared to both types of Grey Berea cores. Both coreflood experiments resulted in a range of permeability damage from (5-22%). 30 wt% urea-HCl with all of the additives included at 250 °F resulted in 22% damage using a flow rate of 2 cm³/min ,on the other hand, using a higher flow rate of 5 cm³/min resulted in a 4.87% damage only (no significant damage was found). The test with the lower flow rate showed 5 times more damage compared to the test performed at a higher flow rate. The following phenomenon can be attributed to the higher residence time induced by the lower flow rate resulting in more contact time between the acid and the formation. However, it is important to take into consideration that Ba-01 initially was 3 times more permeable than Ba-02. Any minor amount of Fe precipitation or silica gel residue or fine migration would magnify the permeability reduction as there is originally a lesser number of pore throats available in in Ba-02.

This can be attributed to the damage due to the urea-HCl decomposition in formulation inciting urea precipitation and/or an additive incompatibility causing wettability alterations and induced formation damage.

Core ID	Test ID	Fm	Permeability				Treatment outcome	Test Description
			Initial K	Final K	K_f/K_i	% Regain		
Ba-01	Test 1	Ban-01	12.3	11.7	0.95	4.87	Damage	30wt% Urea-HCl @ 250 °F with all additives Included
Ba-02	Test 2	Ban-02	4.5	3.5	0.78	22.2	Damage	30wt% Urea-HCl @ 250 °F with all additives Included

Table 3—4 Bandera sandstone experiments summary.

Coreflood Experiments

Section-A: 15 wt % HCl -All of the Additives Included-250°F @ 5 cm³/min-Berea Sandstone

The following coreflood experiments were done using 15 wt% HCl. These experiments acted as a control against which the urea-HCl results were compared. Each test was repeated once on Grey Berea sandstone. A temperature of 250 and 300°F was set with a flow rate of 5 cm³/min used throughout the tests. 5 wt% KCl and 5 PV of 15 wt% HCl were injected in the injection direction at RT till the temperature of 250 °F was reached and the pressure drop stabilized. The flow was then switched to brine, continuous

injection was maintained and final permeability was measured. The effluent samples resulting from the coreflood experiments were collected every quarter PV.

The pressure drop profile explains the pressure drop in psi on the x-axis versus the pore volume injected on the y-axis. By comparing the initial and final permeability, **Fig. 3—7 and 3—9**, an enhancement in the permeability was achieved despite the damage resulting from injecting HCl at that high temperature.

Viscosity and ,as a result, the pressure drop increased as the flow was switched from brine to acid injection as the acid by default has a higher viscosity compared to 5 or 2 wt% KCl. The pressure drop at the end of the graph is lower than the pressure drop at the beginning of the graph. This can be attributed to the enhancement associated with the dissolution of the cementing material in sandstone. With the dissolution of the cementing material, the viscosity decreased and the pressure drop declined signifying a permeability enhancement. Moreover, the pressure drop elevation was due to the release of CO₂ owing to the reaction of the treatment fluid with the carbonates, accordingly, a back pressure of 1200 psi was applied to keep the gas in solution. However, when the salt concentration increased, the solubility of CO₂ in water diminished and some gas was released increasing the pressure as displayed in **Figs. 3—8. Table 3—5** summarizes the 15 wt% HCl experimental conditions.

From ICP analysis **Fig. 3—11**, no precipitate was observed in the effluent samples signifying no fines migration. However, high iron content was observed in the core effluent samples. That is attributed to the dissolution of chlorite and illite clays in the sandstone by HCl.

It can be observed that the stimulation at 300°F is higher than at 250°F as more carbonates are dissolved at higher temperatures. ICP results confirm that. The Ca^{2+} and Mg^{2+} curve is broader at 300°F compared to 250°F. This signifies more carbonates dissolution by the acid and, thereby, more stimulation. The high Fe^{2+} concentration can be attributed to the illite and chlorite attack by HCl. Al^{3+} , on the other hand, is present due to the dissolution of kaolinite and feldspars. Minute quantities of Si^{4+} are observed due to the physical dissolution of silica with HCl. **Table 3—6** and **3—7** show the properties of the Grey Berea core used in the 15 wt% HCl experiments.

Test ID	Initial Brine K	Final Brine K	Treatment Conditions	Test Description
Be-05	85.3	99.4	Injecting 5 wt% KCl at 5 cm ³ /min at 75° F Injecting 5 PV HCl at 5 cm ³ /min at 250° F	15 wt% HCl plus all the additives included at 250 °F– K _i and K _f were measured in the injection direction
Be-06	93.2	112.1	Injecting 5 wt% KCl at 5 cm ³ /min at 75° F Injecting 5 PV HCl at 5 cm ³ /min at 300° F	15 wt% HCl plus all the additives included at 300 °F – K _i and K _f were measured in the injection direction

Table 3—5 Summarizing 15 wt% HCl experimental conditions.

K _i , md	K _f , md	Increase,%	Q, cm ³ /min	Φ, %
85.20	99.40	16.67	5	15.80

Table 3—6 Berea-05 rock, flow, and % stimulation/damage properties.

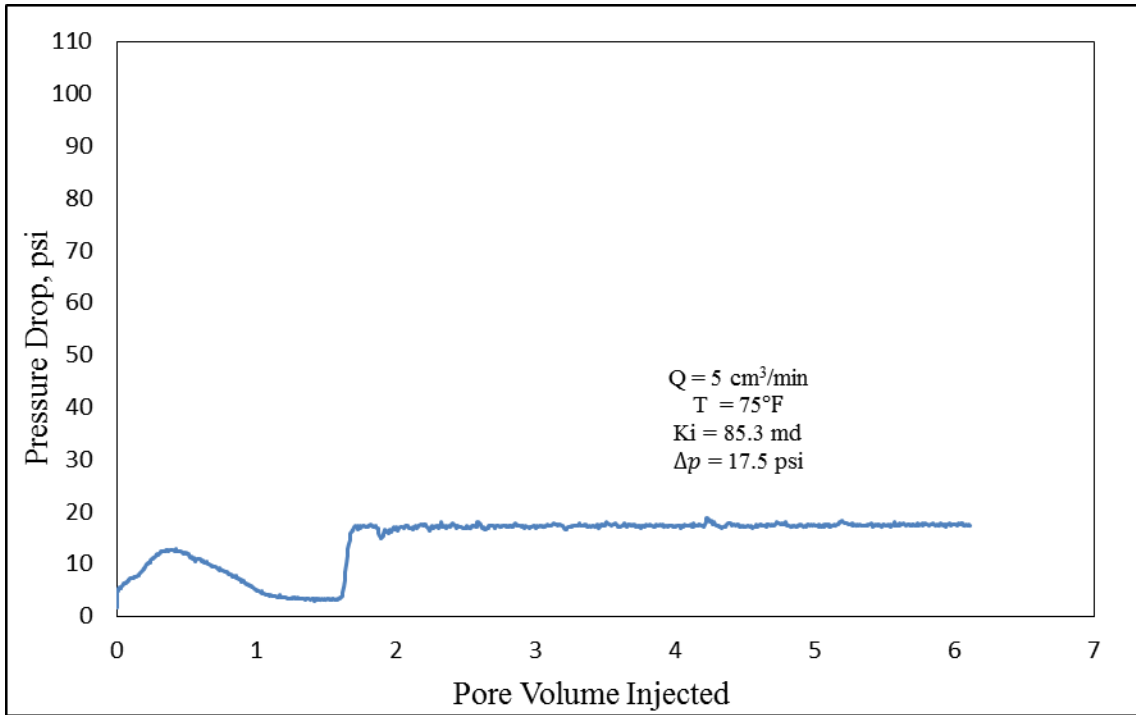


Fig. 3—7 Initial permeability of Berea-05 core at 75 °F.

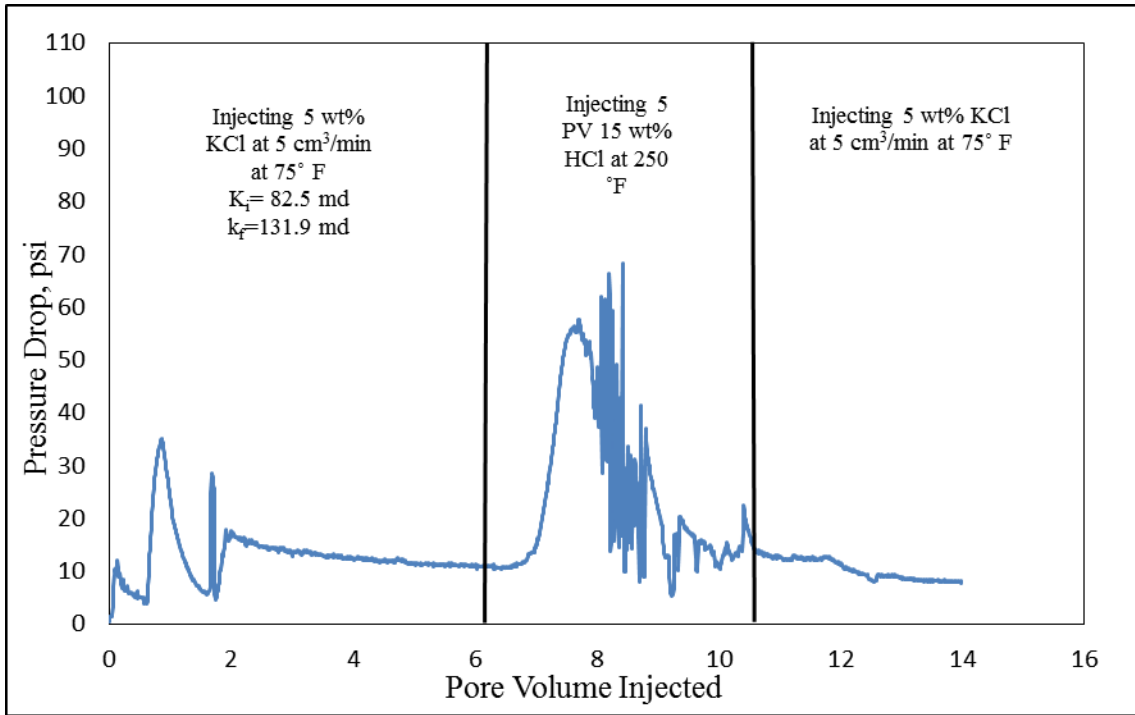


Fig. 3—8 Pressure drop profile of Berea-05 during HCl injection at 250° F.

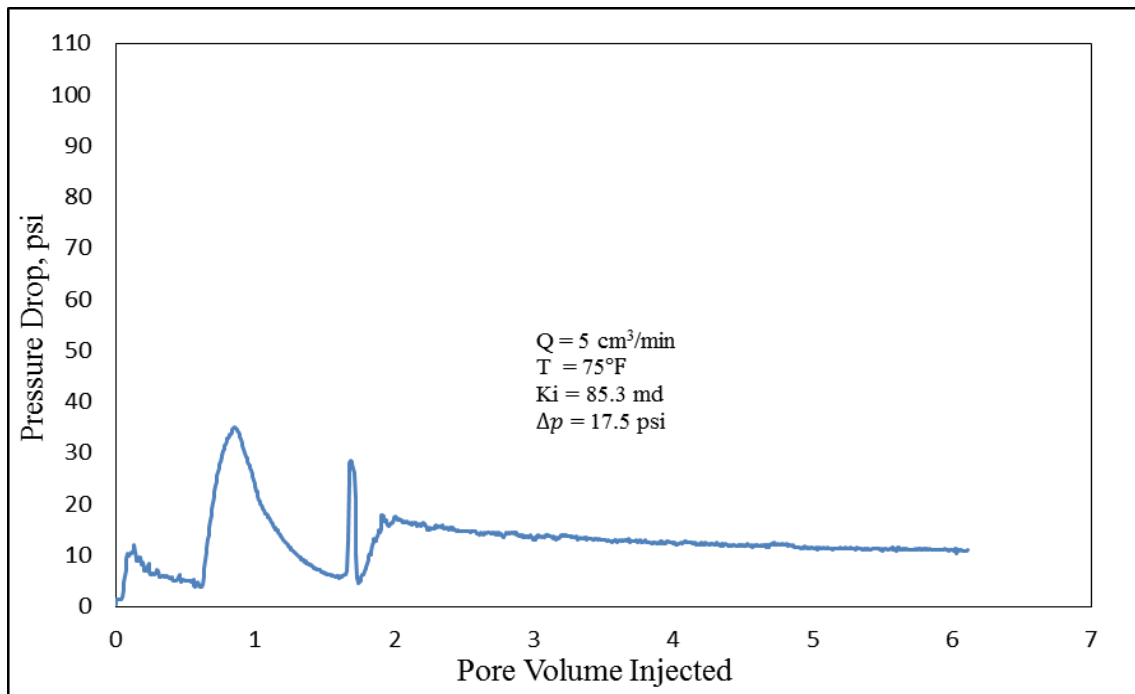


Fig. 3—9 Final permeability of Berea-05 core at 75°F.

It is evident from the pH versus PV graph shown in **Fig. 3—10** that the pH of the effluent samples containing 5 wt% KCl brine started from approximately 8. The pH sharply declined as the 5 PV of the treatment fluid was injected to reach a pH of 0. This signified that the effluent samples contained live acid and not all of the acid was spent dissolving the carbonates in the core. Subsequently, the pH rose as the core was flushed with brine.

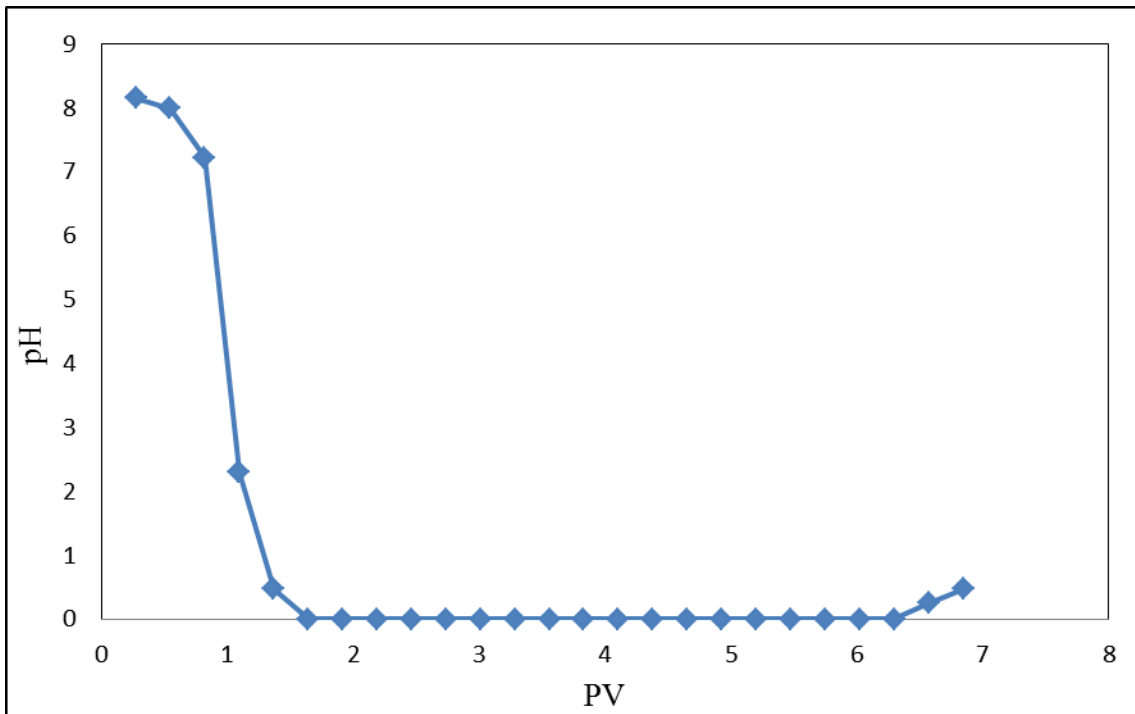


Fig. 3—10 pH of effluent samples from Berea-05 core at 75°F.

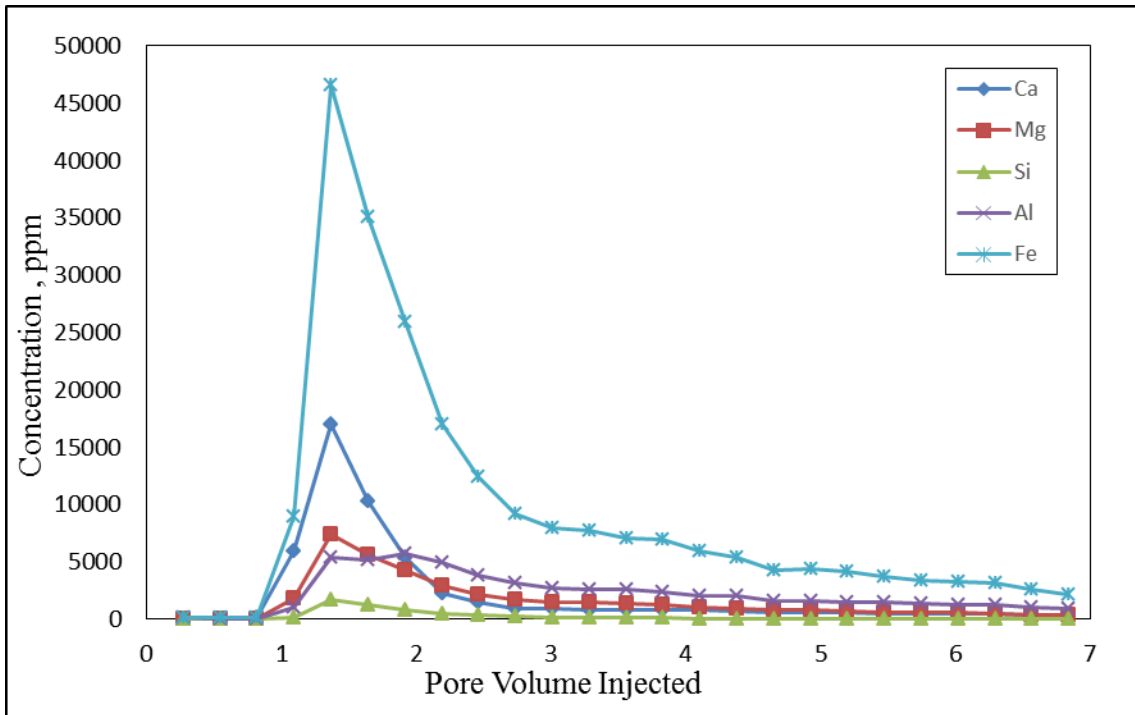


Fig. 3—11 ICP analysis for 30wt%Urea-HCl with Berea-05 core.

K_i , md	K_f , md	Increase, %	Q , cm^3/min	Φ , %
93.2	112.1	20.28	5	12.6

Table 3—7 Berea-06 rock, flow, and % stimulation/damage properties.

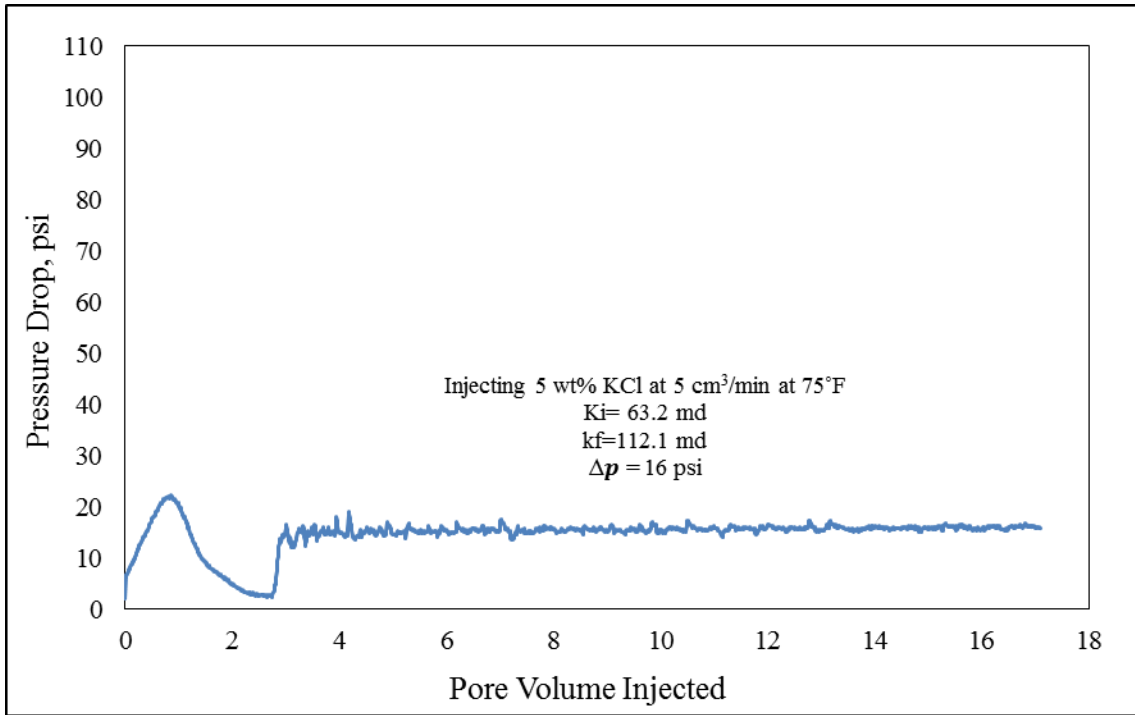


Fig. 3—12 Initial permeability of Berea-06 core at 75°F.

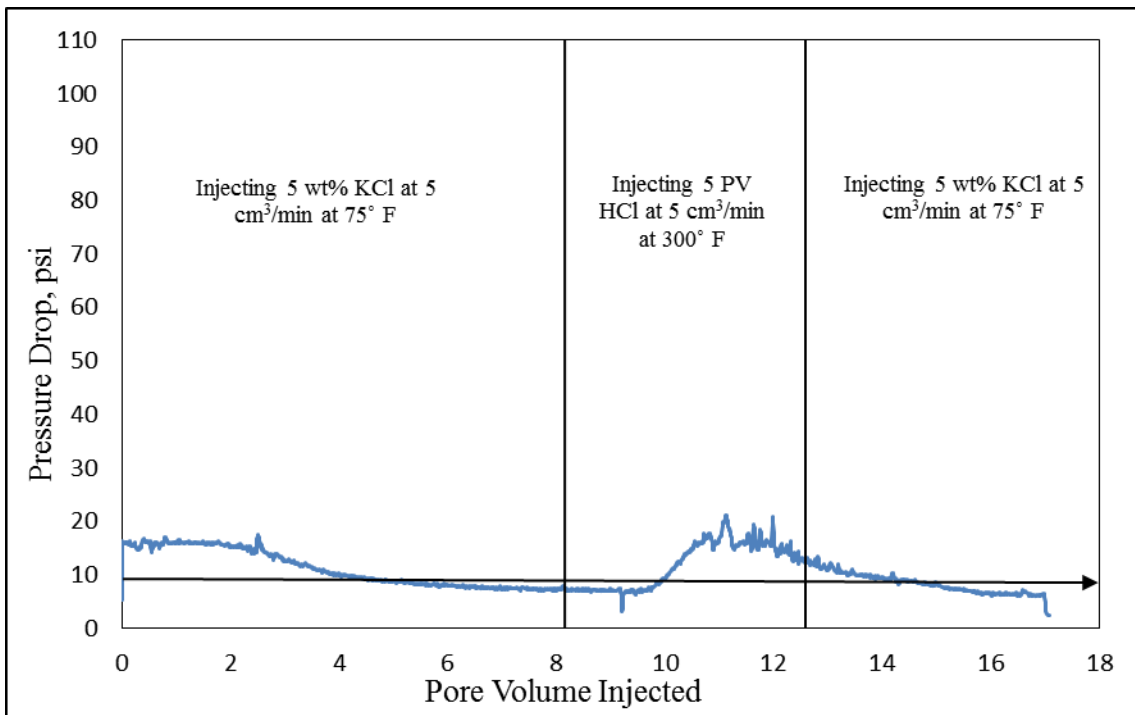


Fig. 3—13 Pressure drop profile during urea-HCl injection at 300 °F.

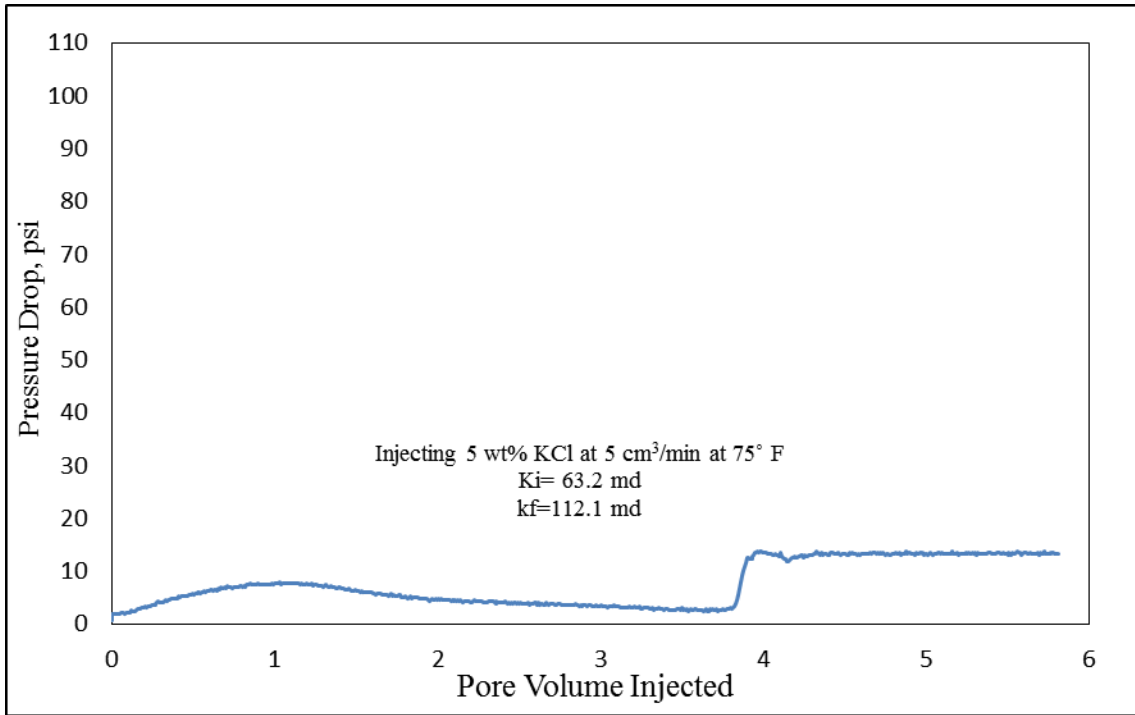


Fig. 3—14 Final permeability of Berea-06 core at 75 °F.

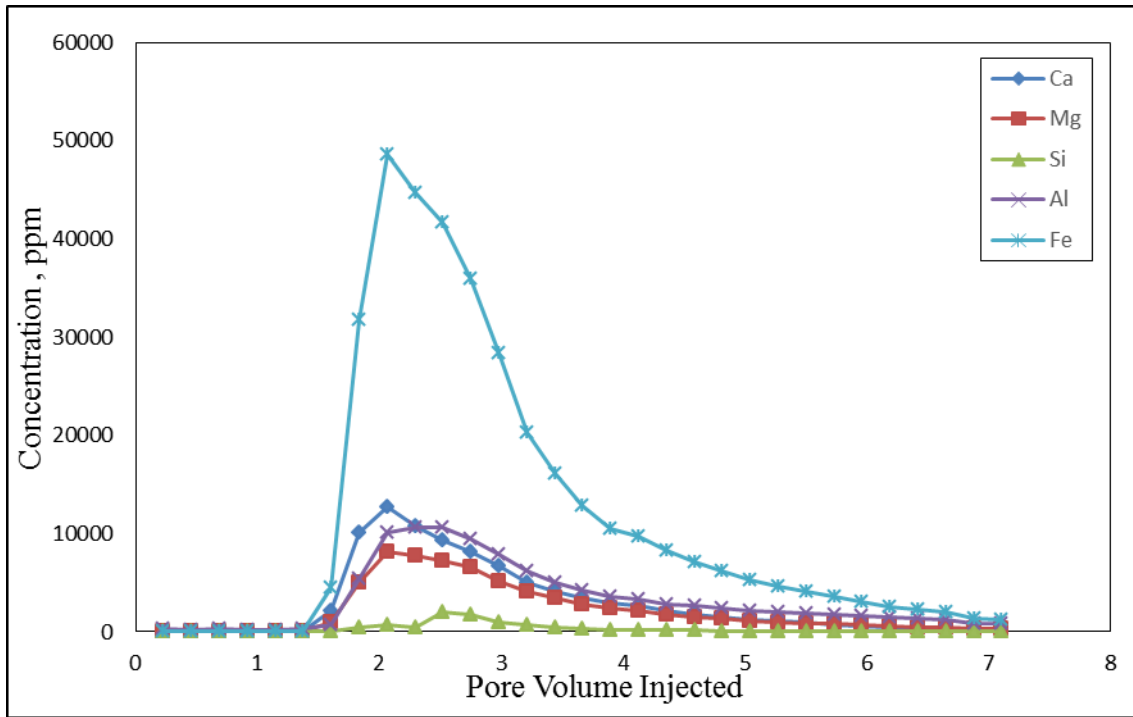


Fig. 3—15 ICP analysis for 15 wt% HCl with Berea-06 core.

Section-B: 30 wt% Urea-HCl -All of the Additives Included @ 5 cm³/min-Berea

Sandstone

For the following experiments at 250 °F, each test was repeated twice on Grey Berea sandstone. A temperature of 250°F was set with a flow rate of 5 cm³/min used throughout the tests. 5 wt% KCl and 5 PV of treatment fluid was injected in the injection direction. The effluent samples resulting from the coreflood experiments were collected every quarter PV.

Grey Berea with (5% kaolinite, 2% chlorite, 1% illite, and 3% carbonates) showed damage after its treatment using an additive package, including the six types of additives mentioned earlier, given by a local company. The damage can be attributed to a multitude of factors. This damage might be a collection of one or more factors depending on the dominant mechanism(s). Formation damage could be induced by fines migration or precipitation of silicate gel inside the core since flowing HCl in the cores containing illite and chlorite encouraged the pressure drop to elevate due to the migration of clay reaction products, formation of reaction product and/or viscosity increase, illite and chlorite (having a high surface area) are attacked by HCl, the aluminum layer is removed. This in turn weakens the clay structure making it more susceptible to fluid flow effects.

Another potential reason might be due to some acid-additive incompatibility with the core that potentially alters its wettability or urea-HCl decomposition at 250 °F as revealed by the GCMS results. This urea-HCl decomposition could have incited precipitations inside the core or other secondary and tertiary reaction depositions

reducing its permeability. According to literature, the product distribution is temperature dependent and considering the working temperature at which the coreflood system is running impacts ammonia production. That is to say, the temperature ought to be as low as possible, otherwise, the formation of other unwanted by-products could be problematic (Fang and DaCosta 2003).

Moreover, urea dissociated from the acid formulation leaving some regular HCl, could have decomposed clays such as illite and chlorite, consequently, inducing formation damage.

The reproducibility of the coreflood was achieved by repeating Be-02 test with Be-09 (24.28 and 28.53 % damage respectively) under similar experimental conditions as shown in **Table 3—8**. While, Be-10 was the repeat of Be-11 (35.03 and 13.41 % damage respectively). It is noteworthy to say that the percentage of damage in the second set of experiments (Be-10 and Be-11) was higher and lower respectively than the first set of experiments (Be-02 and Be-09). The following can be attributed to two causes, however, further experimentation and investigations are required to confirm the higher (35.03%) and lower (13.41%) damage respectively compared to the first set of experiments (Be-02 and Be-09). This could be the effect of using a lower flow rate of 1 cm³/min versus 5 cm³/min of the latter. The lower flow rate contributed to a higher residence time of the acid contacting the formation inducing the damage. On the other hand, the higher flow rate could have exceeded the critical velocity of the clay particles inducing clay dislocation, as a result, fines migration and subsequent formation damage took place.

By comparing ICP results **Fig. 3—21** and **3—25**, it can be seen that the high iron content in the core effluent is attributed to the dissolution of chlorite which results in leaving amorphous silica rich residue that damages the formation. It can be noticed accordingly that the pressure drop at the end of the coreflood experiment is greater than the pressure drop at the beginning of the pressure drop profile. Finally, the spikes in the pressure drop profile **Fig. 3—2** are a result of the fines migration caused by injecting HCl in an illite- rich formation. Table 3—8 summarizes the 30 wt% Urea/ HCl experimental conditions.

The damage highlighted from the ICP results in some cores may be due to fines migration due to the formation unconsolidation after the dissolution of the cementing material (carbonate and dolomite). The maximum concentrations of Ca occurred almost after the injection of a limited PV injection of acid. However, the maximum peak for the dissolved concentrations of Fe and Al is after a larger PV of acid was injected, which shows that acid first reacted with calcite and dolomite in the core and then with the chlorite. The aluminum sheet contacts the acid as kaolinite has 1:1 layered structure. Illite and chlorite, on the other hand, both have 2:1 layered structure, which contain the aluminum sheet in between the two silicon sheets. This arrangement makes it more challenging for acid to contact the aluminum sheet. Thus less Al was dissolved in the effluent solutions.

Test ID	Initial Brine K	Final Brine K	Treatment Conditions	Test Description
Be-02	73.3	55.5	5 cm ³ /min for brine and acid injection throughout the test	30 wt% urea-HCl plus all the additives 250°F –K measured at 75°F
Be-09	34.7	24.8	5 cm ³ /min for brine and acid injection throughout the test	30 wt% urea-HCl plus all the additives at 250°F –K measured at 75°F
Be-10	49.1	31.9	3 cm ³ /min for brine injection and 1 cm ³ /min for acid injection	30 wt% urea-HCl plus all the additives – K measured at 250°F
Be-11	46.2	40	3 cm ³ /min for brine injection and 1 cm ³ /min for acid injection	30 wt% urea-HCl plus all the additives –K measured at 250°F
Be-03	80.2	-	5 cm ³ /min for brine and acid injection throughout the test	30 wt% urea-HCl plus all the additives 250°F –K measured at 75°F

Table 3—8 Summarizing 30 wt% Urea/ HCl experimental conditions.

K _i ,md	K _f , md	Decrease,%	Q, cm ³ /min	Φ, %
73.3	55.5	24.28	5	18.6

Table 3—9 Berea-02 rock, flow, and % stimulation/damage properties (Urea-HCl plus additives).

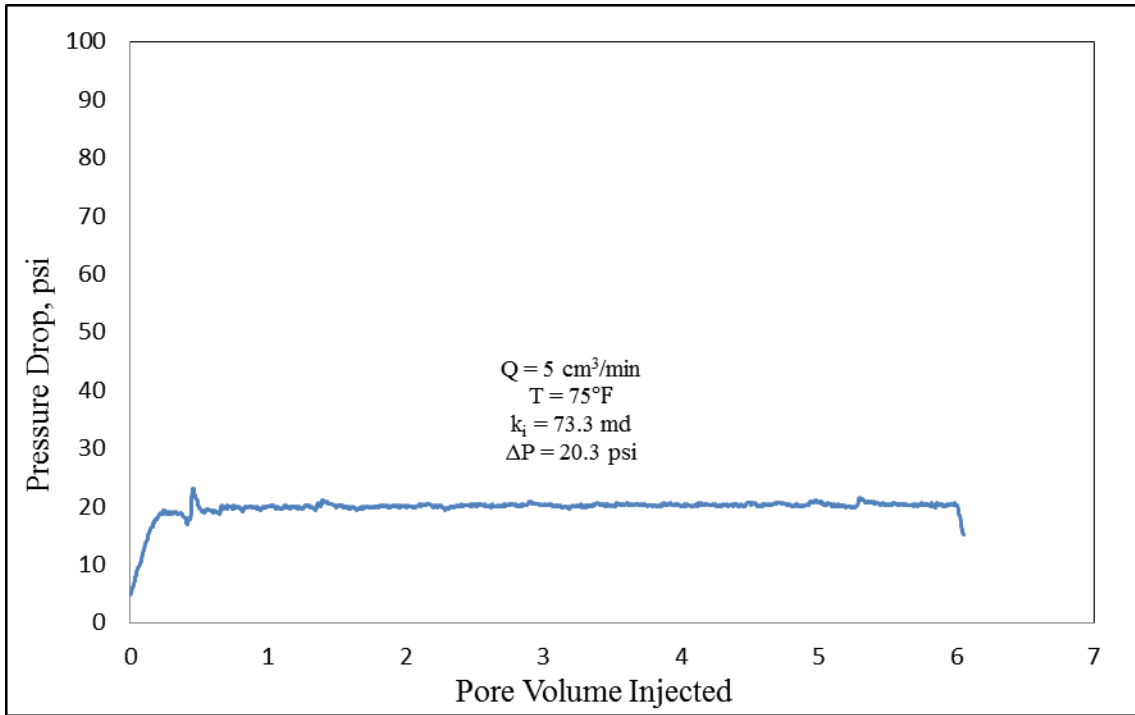


Fig. 3—16 Initial permeability of Berea-02 core at 75 °F.

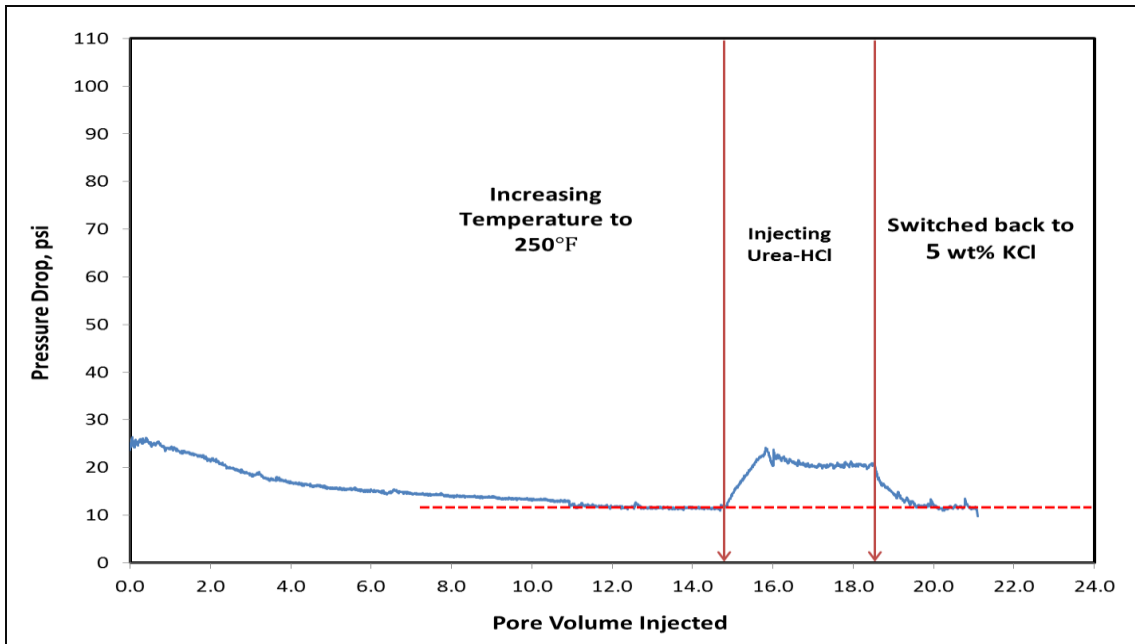


Fig. 3—17 Pressure drop curve of Berea-02 during urea-HCl injection at 250°F.

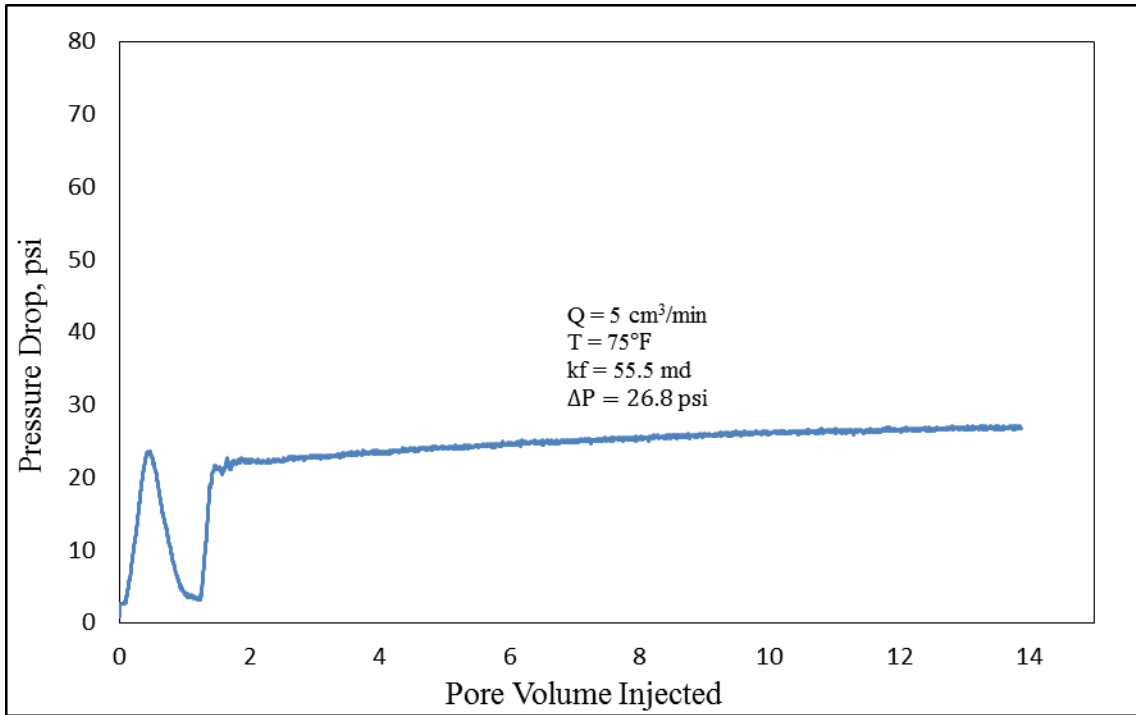


Fig. 3—18 Final permeability of Berea-02 core at 75 °F.

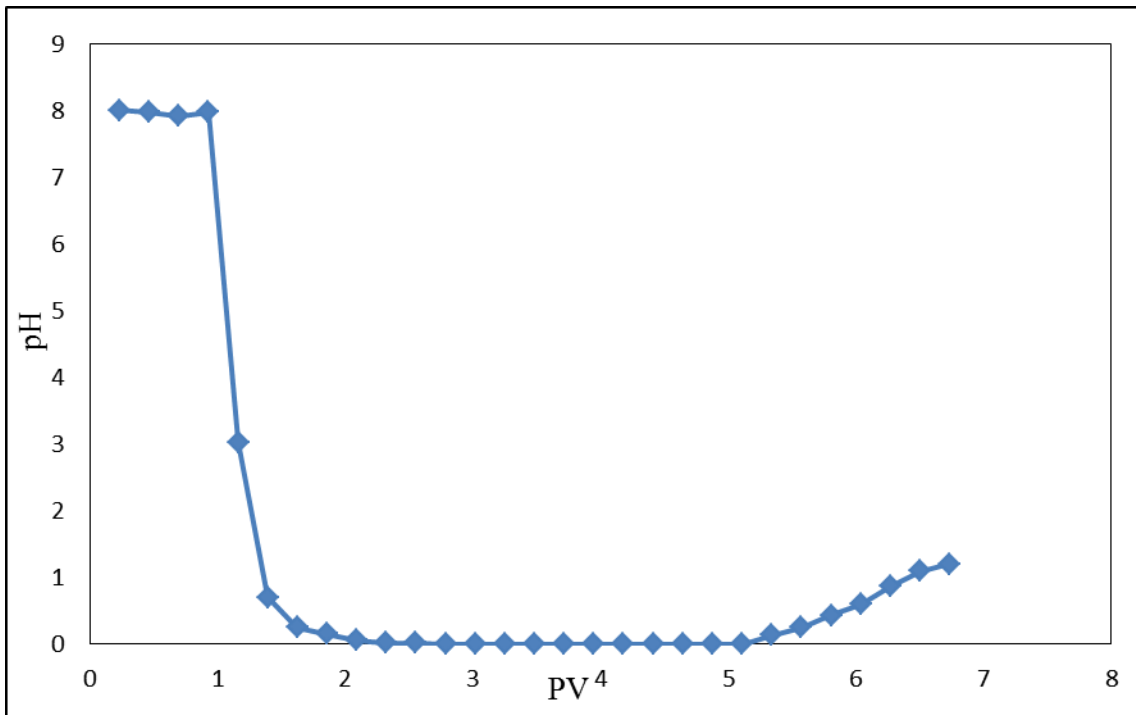


Fig. 3—19 pH of effluent samples from Berea-02 core.

The density of effluent samples from Berea-02 core at 75°F is plotted as shown in **Fig. 3—3**. The density of brine pumped is around 1.025 g/cm³, then as the 5 PV of treatment fluid is injected, the density starts to suddenly increase as the acid dissolves more Ca, Mg, Al, and Fe. As the acid becomes spent and less available H⁺ ions attack the carbonates, less cation dissolution occurs and as a result a gradual decrease in density is observed. As soon as the flow is switched back to brine, the density returns back to its original value.

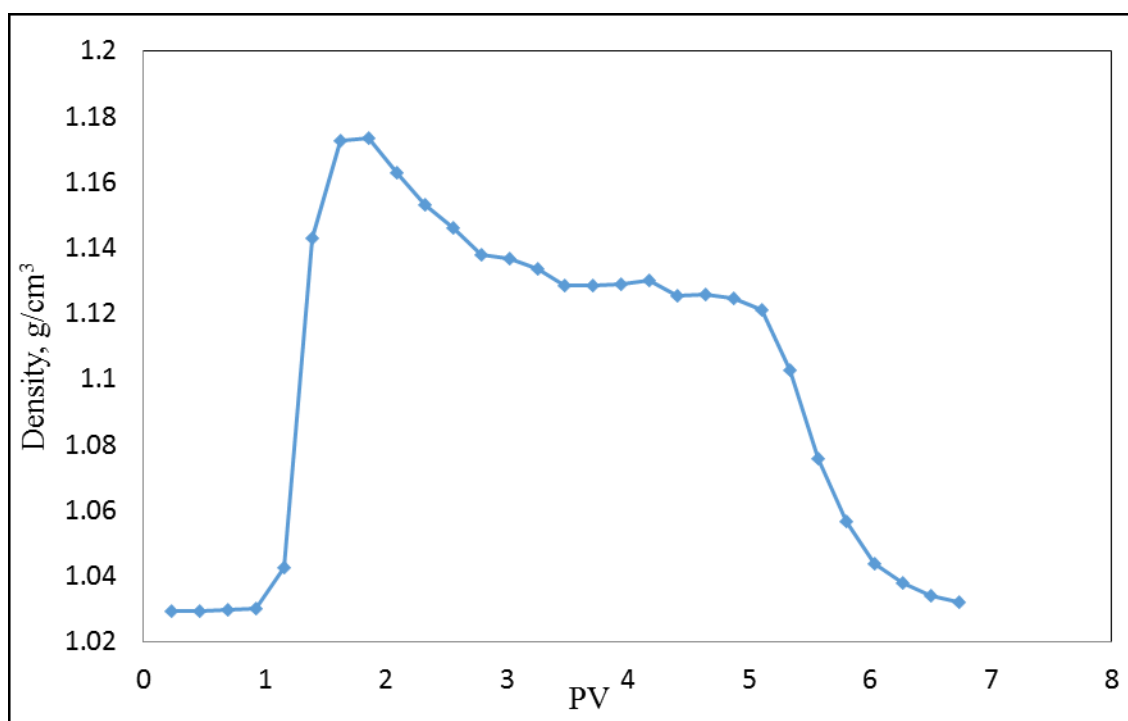


Fig. 3—20 Density of effluent samples from Berea-02 core at 75°F.

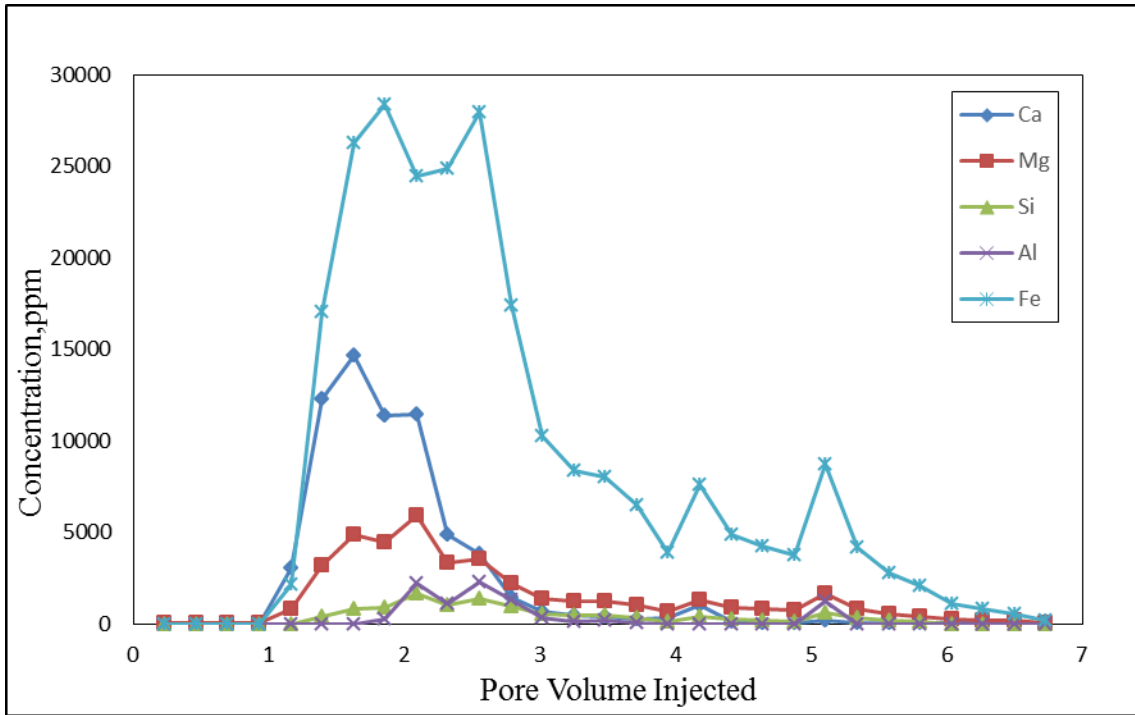


Fig. 3—21 ICP analysis for 30 wt% urea-HCl with Berea-02 core.

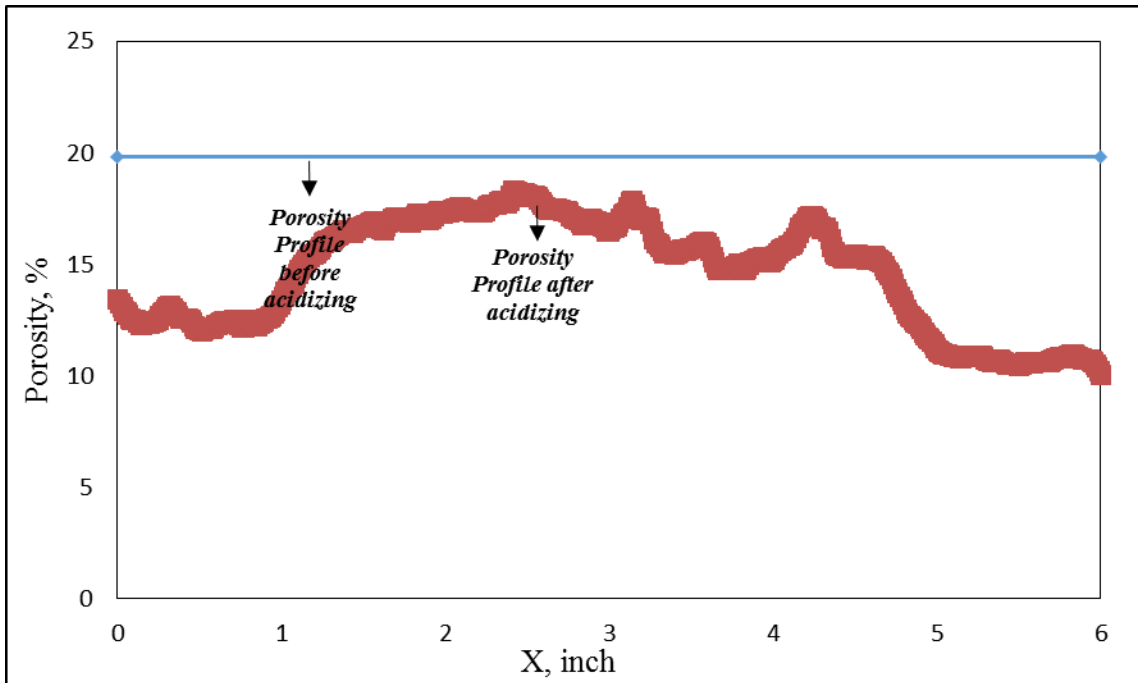


Fig. 3—22 Porosity profile before and after 30 wt% urea-HCl treatment for Berea-02.

K_i , md	K_f , md	Decrease, %	Q , cm ³ /min	Φ , %
34.70	24.80	28.53	5	12.80

Table 3—10 Berea-09 rock, flow, and % stimulation/damage properties.

The pressure drop at the end of the following pressure drop profile displayed in **Fig. 3—23** is greater than the pressure drop at the beginning of the graph. This can be attributed to the damage associated with urea-HCl or additive decomposition precipitating inside the core.

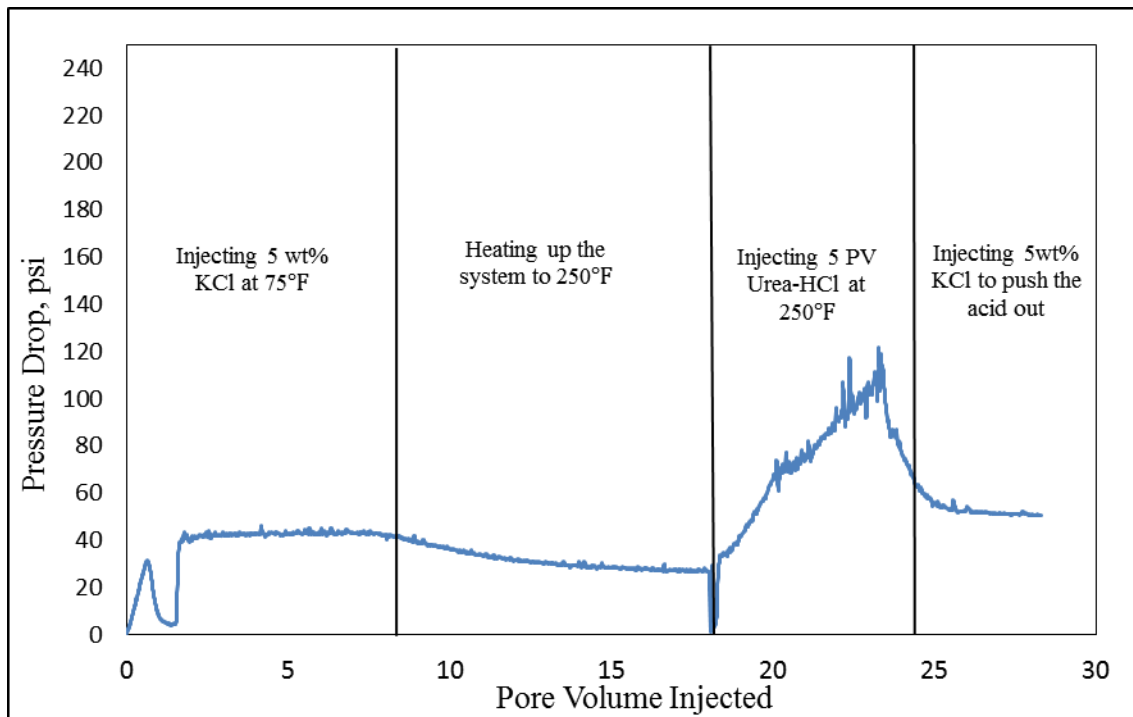


Fig. 3—23 Pressure drop profile during 30 wt% urea-HCl injection at 250 °F for Berea-09.

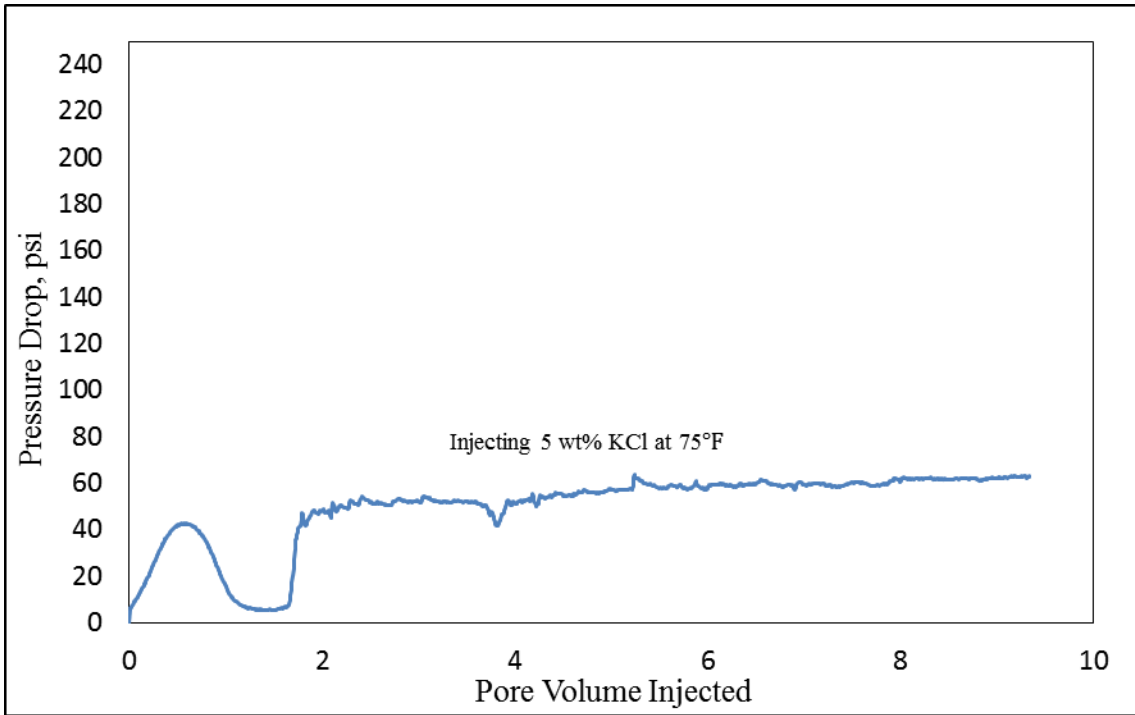


Fig. 3—24 Final permeability of Berea core-09 at 75°F.

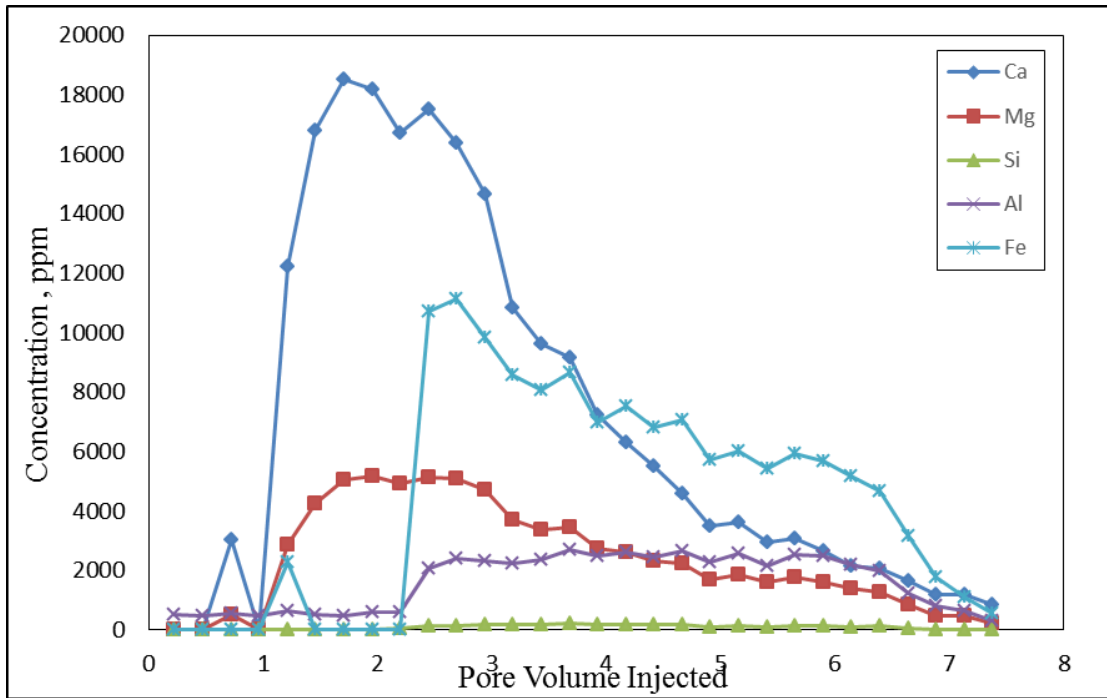


Fig. 3—25 ICP analysis for 30 wt% urea-HCl with Berea-09 core.

K_i , md	K_f , md	Decrease, %	Q , cm^3/min	Φ , %
49.10	31.90	35.03	1	18.30

Table 3—11 Berea-10 rock, flow, and % stimulation/damage properties.

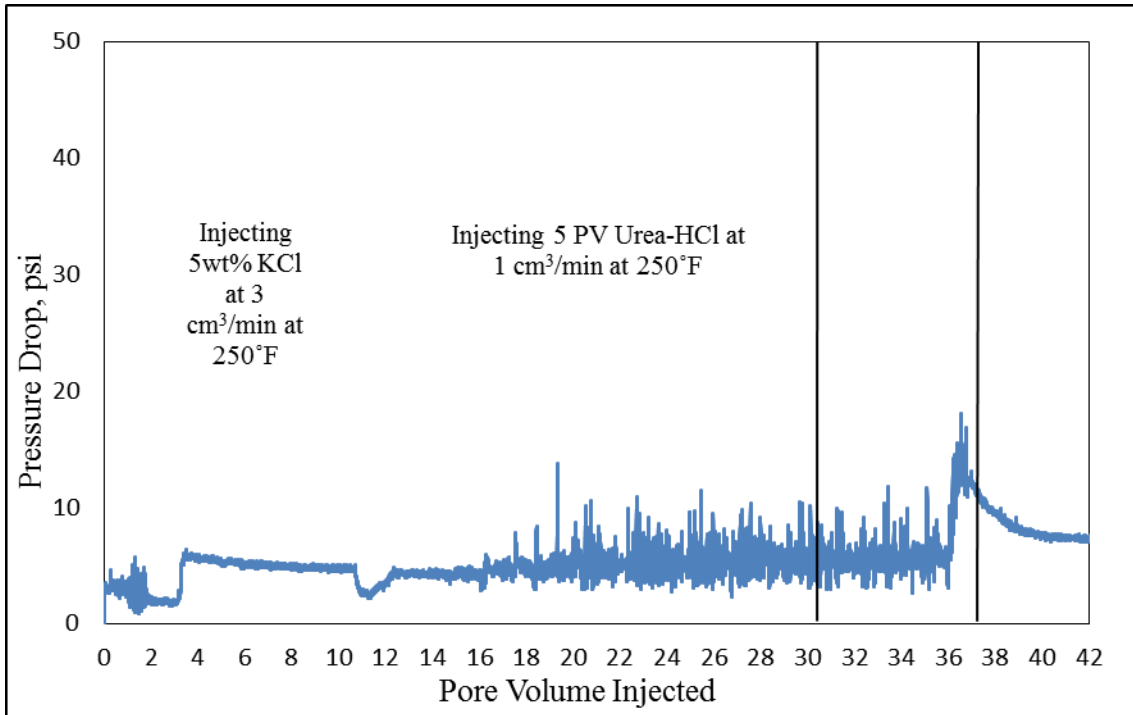


Fig. 3—26 Pressure drop profile during urea-HCl injection at 250 °F for Berea-10 core.

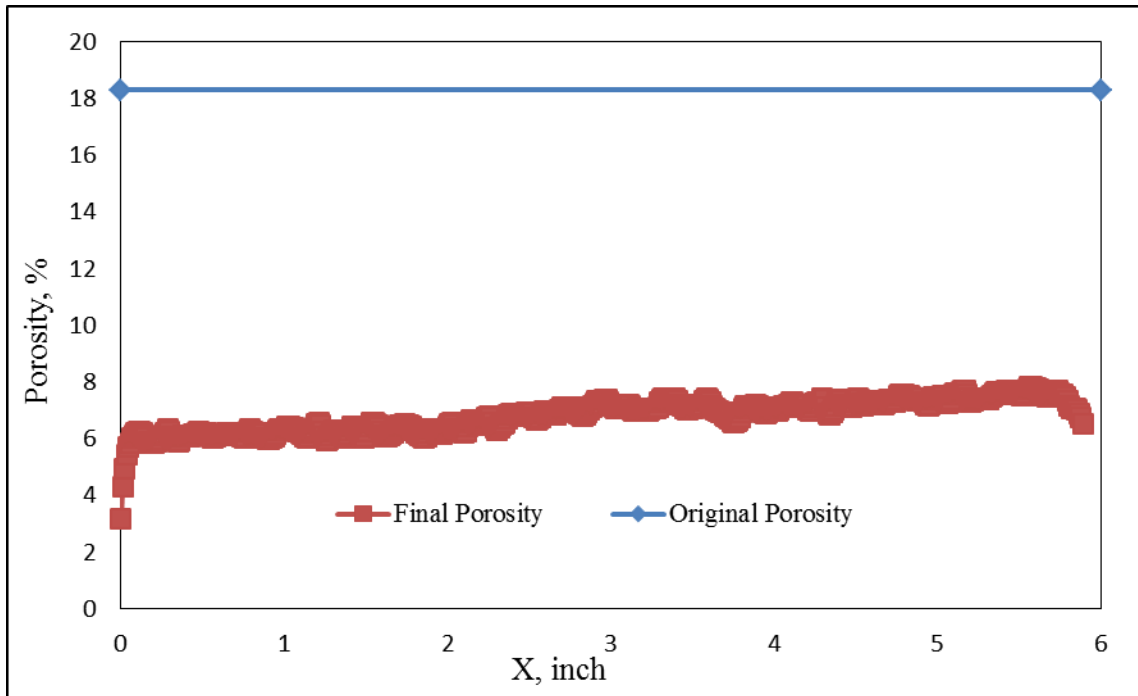


Fig. 3—27 Porosity profile before and after 30wt% urea-HCl treatment for Berea-10.

K_i , md	K_f , md	% decrease	Q , cm^3/min	Φ , %
46.20	40.0	13.41	1	11.40

Table 3—12 Berea-11 rock, flow, and % stimulation/damage properties.

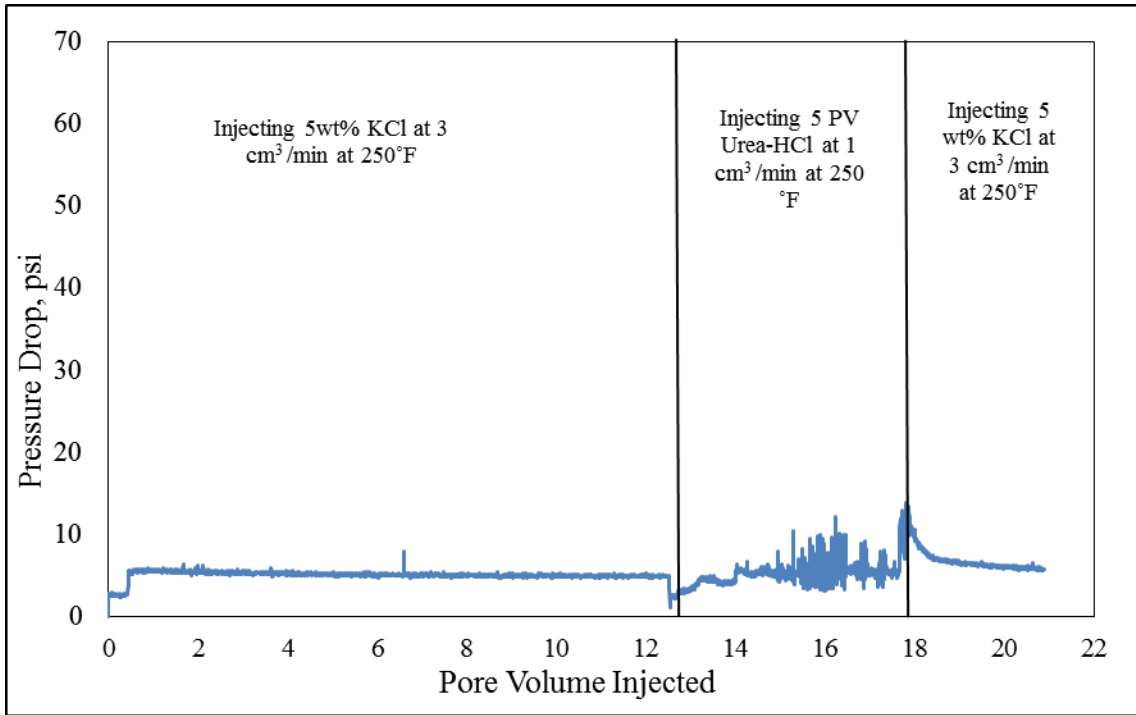


Fig. 3—28 Pressure drop profile during urea-HCl injection at 250°F for Berea-11.

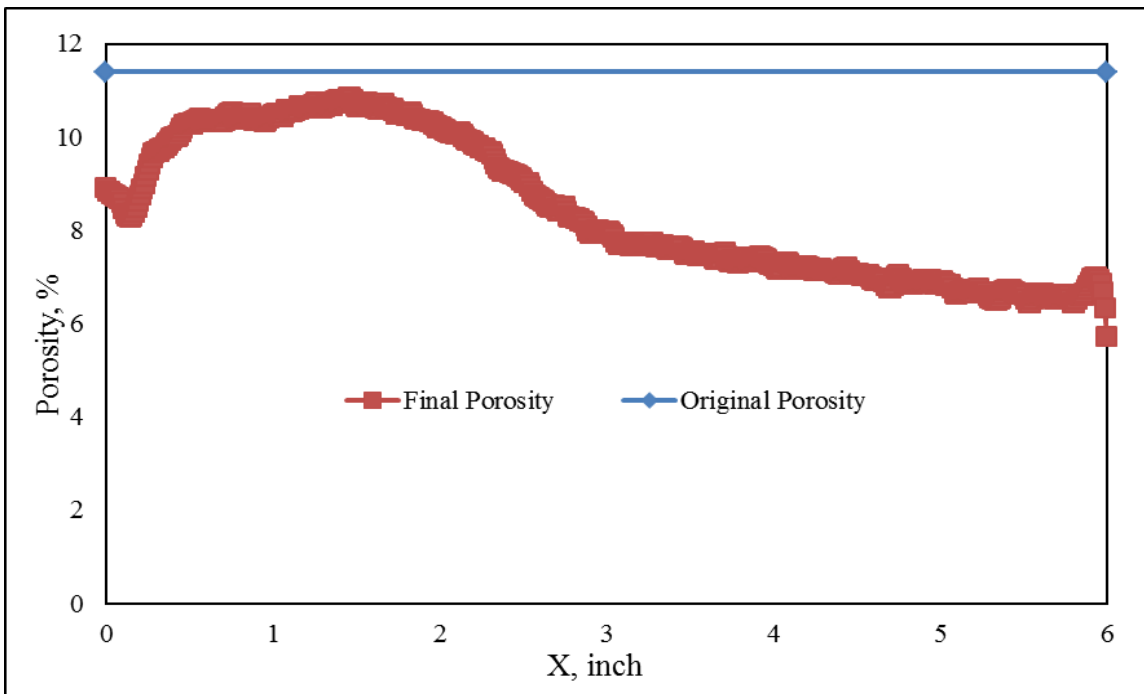


Fig. 3—29 Porosity profile before and after 30 wt% urea-HCl treatment for Berea-11.

The second set of tests was conducted at 300°F with experimental conditions of Be-03 shown in **Table 3—13**. The final permeability after the injection of almost 5 PV Urea-HCl was measured shown in **Fig. 3—32**, and it was noticed that the pressure drop across the core did not stabilize. The following is displayed in **Fig. 3—30**, which is an indication of significant damage to the core. This severe damage can be attributed to more sensitive-clay dispersion and migration and the decomposition of the insitu-generated acid mixture. To further analyze and confirm the damage and its source, a CT scan and ICP were run as shown by **Fig. 3—34** and **3—35**. Significant amounts of Fe dissolution was found due to the acid attack on illites and chlorites. Moreover, the degree of damage at 300°F was higher compared to what was achieved at 250°F.

As expected, the final porosity displayed in Fig. 3—34, shows a higher CT number. This signifies a higher density core suggesting either a lower porosity was achieved due to a higher density precipitate deposited inside the rock (density of precipitate is higher than the void spaces) such as Fe precipitation. Another reason for the damage seen could be due urea decomposition at high temperature leading to precipitations inside the core or the development of secondary and tertiary reactions of chlorinated complexes contributing to this severe loss of porosity.

K _i , md	K _f , md	Increase/Decrease, %	Q, cm ³ /min	Φ, %
80.20	-	-	5	18.70

Table 3—13 Berea-03 rock, flow, and % stimulation/damage properties.

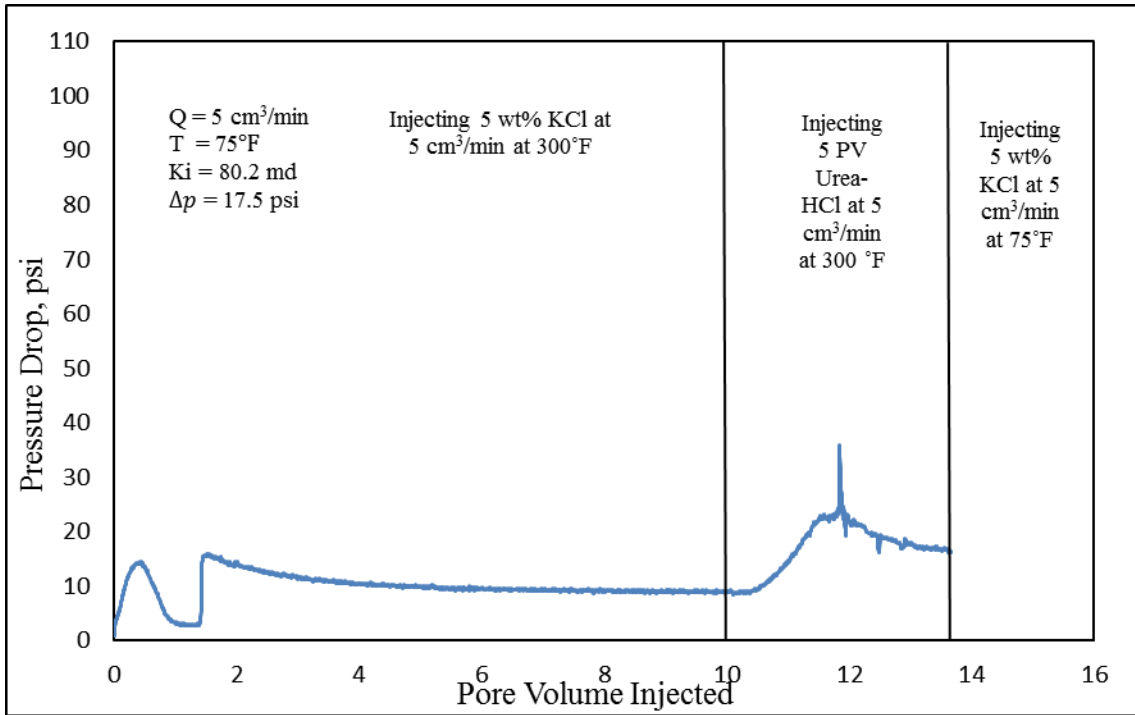


Fig. 3—30 Pressure drop curve of Berea-03 during urea-HCl injection at 250 °F.

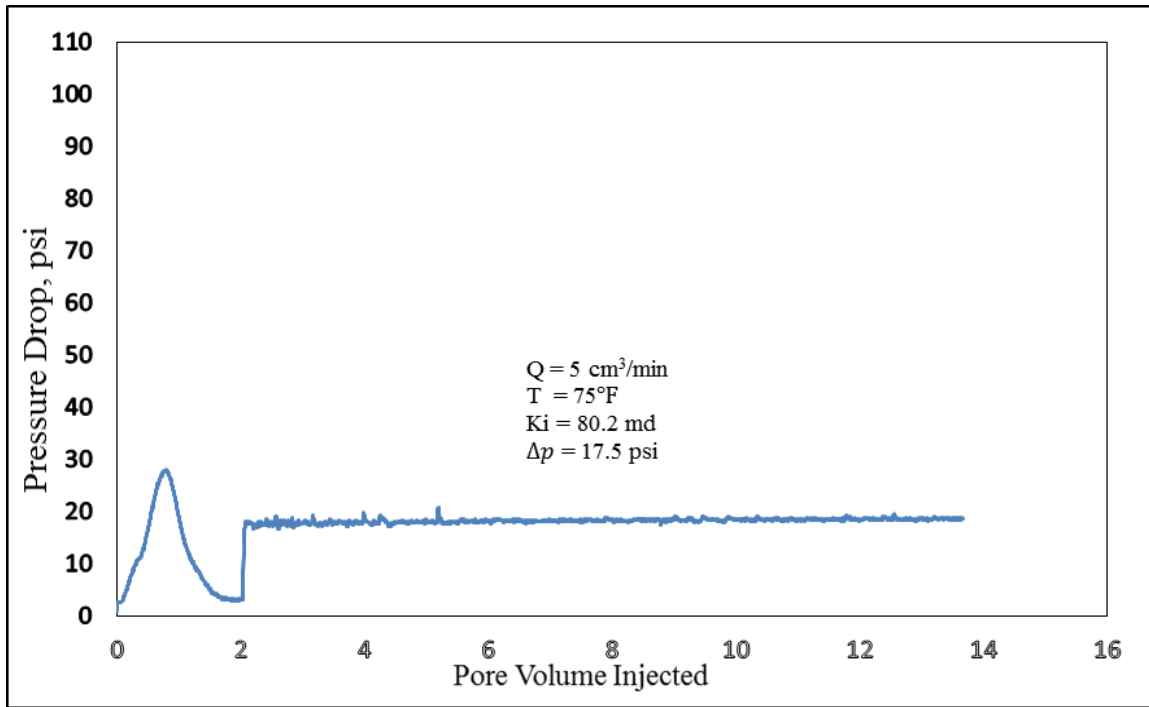


Fig. 3—31 Initial permeability of Berea-03 core at 75 °F.

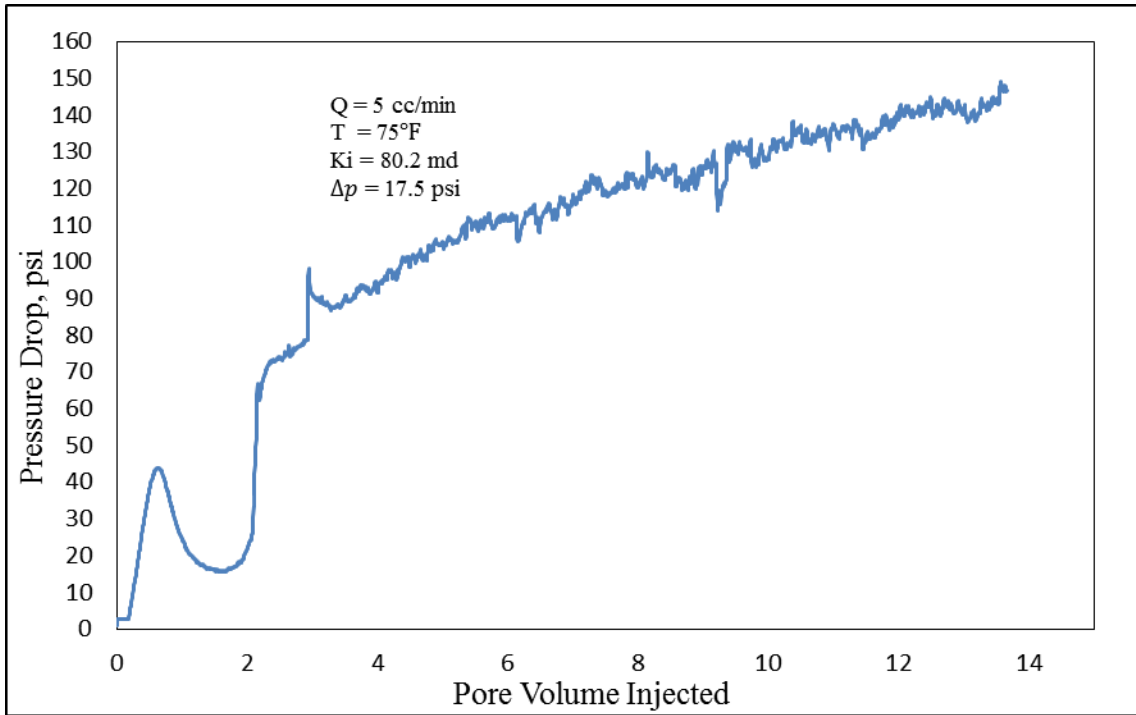


Fig. 3—32 Final permeability of Berea-03 core at 75 °F.

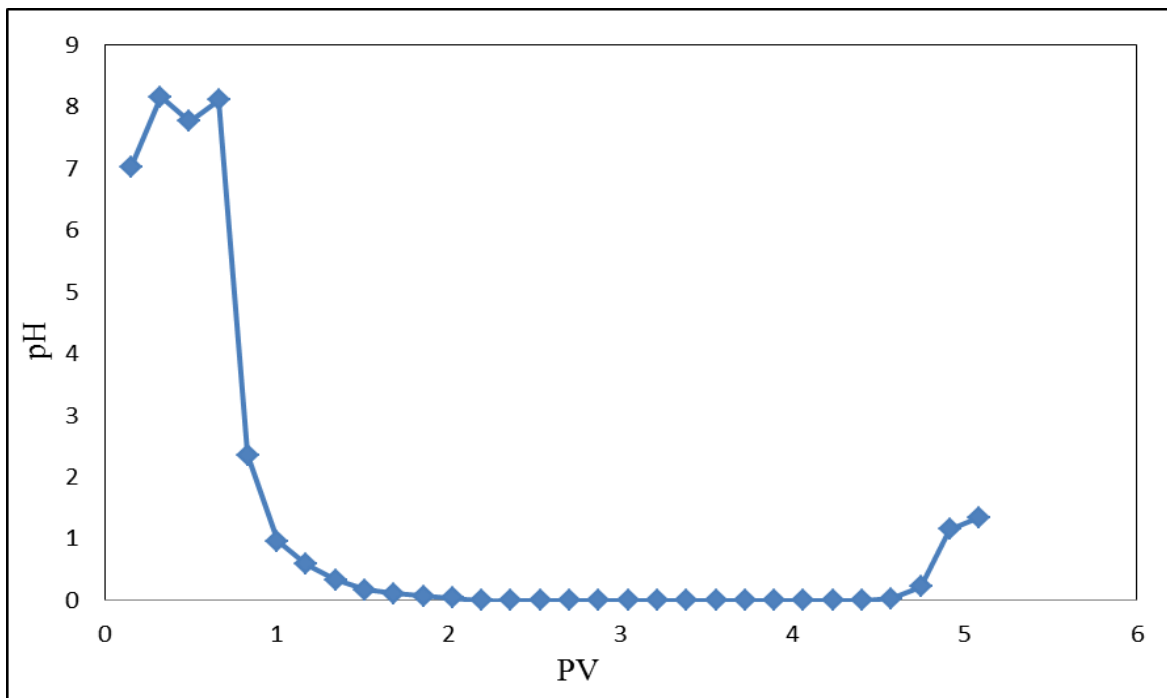


Fig. 3—33 pH of effluent samples from Berea-03 core at 75°F.

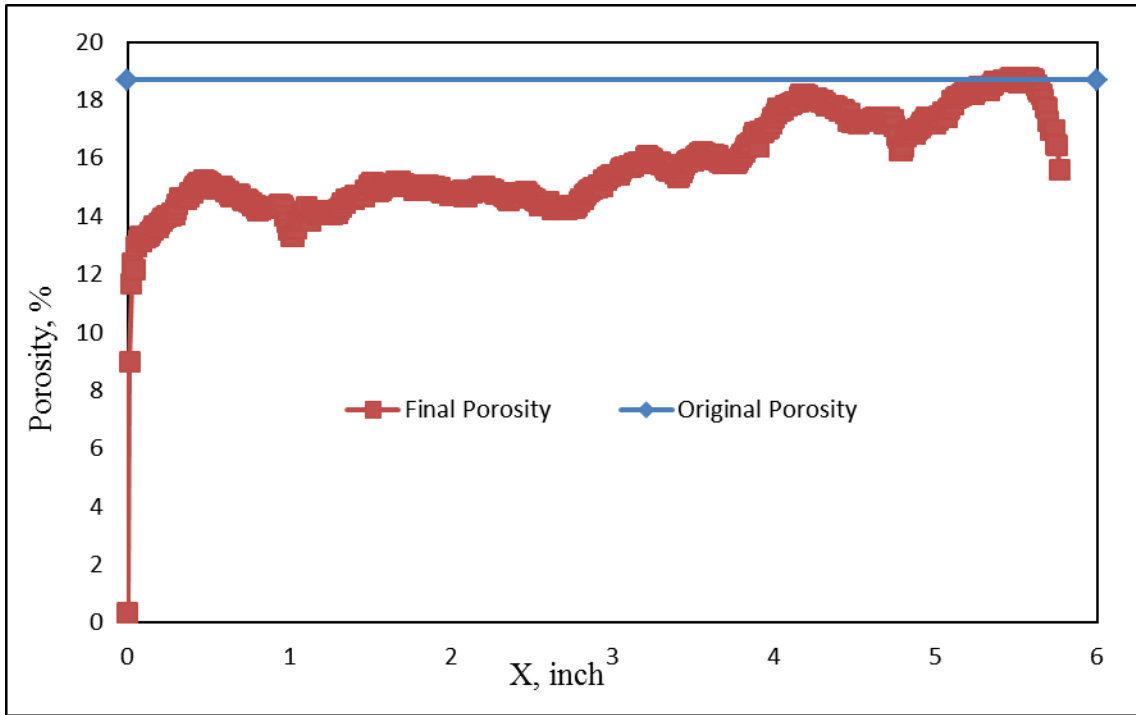


Fig. 3—34 Porosity profile for the before and after treatment for Berea-03 core.

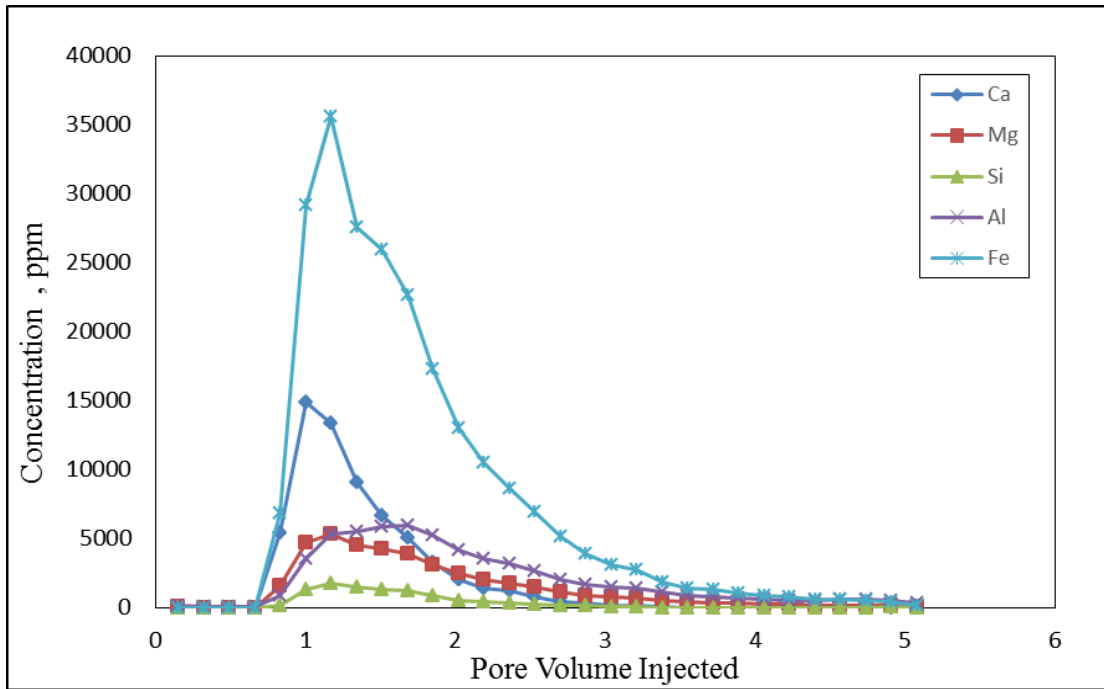


Fig. 3—35 ICP analysis for 30wt% Urea-HCl for Berea-03 core.

**Section-C: 30 wt% Urea-HCl -Only CI and Intensifier Included-250°F @ 5
cm³/min- Berea Sandstone**

For the following experiments shown in **Table 3—14** and **3—15**, each test was repeated twice on Grey Berea sandstone. A temperature of 250°F was set with a flow rate of 5 cm³/min used throughout the tests. 5 wt% KCl and 5 PV of treatment fluid were injected in the injection direction. The effluent samples resulting from the coreflood experiments were collected every quarter PV.

As previously mentioned, the urea in the novel insitu-generated system after hydrolysis could have contacted the kaolinite mineral present in the sandstone core. In other words, it is possible that the urea in the urea-HCl formulation binded with the kaolinite present in sandstones (as urea starts to slightly decompose at 110°C). The timing of the experiment (the time it takes to inject 5 PV of acid into the core) provided enough contact time between urea and kaolinite. The following proposition mimics the dynamic intercalation technique where urea molecules diffuse into the kaolinite crystal layers and delaminates it forming urea-kaolinite complex (UKC). The reaction temperature of 250°F (121.1°C) used in the coreflood shown in **Fig. 3—4** could have promoted the fast movement of urea molecules and, as a result, increased the contact and collision probability between urea molecules and kaolinite. The retardation effect that urea offers is sufficient to replace further retarding agents. This achieves cost savings and a more environmentally friendly approach compared to acid retarders that are difficult to handle and dispose of. Moreover, the addition of any enough material will dilute the acid to a lower concentration, as a result, reducing its activity and efficiency.

The decrease in the CT number seen in **Fig. 3–41** typically suggests a lower density. This might indicate an increase in the core porosity after the treatment (i.e., the core was stimulated) or through the dissolution of a heavy material.

K_i , md	K_f , md	Increase, %	Q , cm ³ /min	Φ , %
49.40	54.60	10.53	5	11.50

Table 3—14 Berea-08 rock, flow, and % stimulation/damage properties.

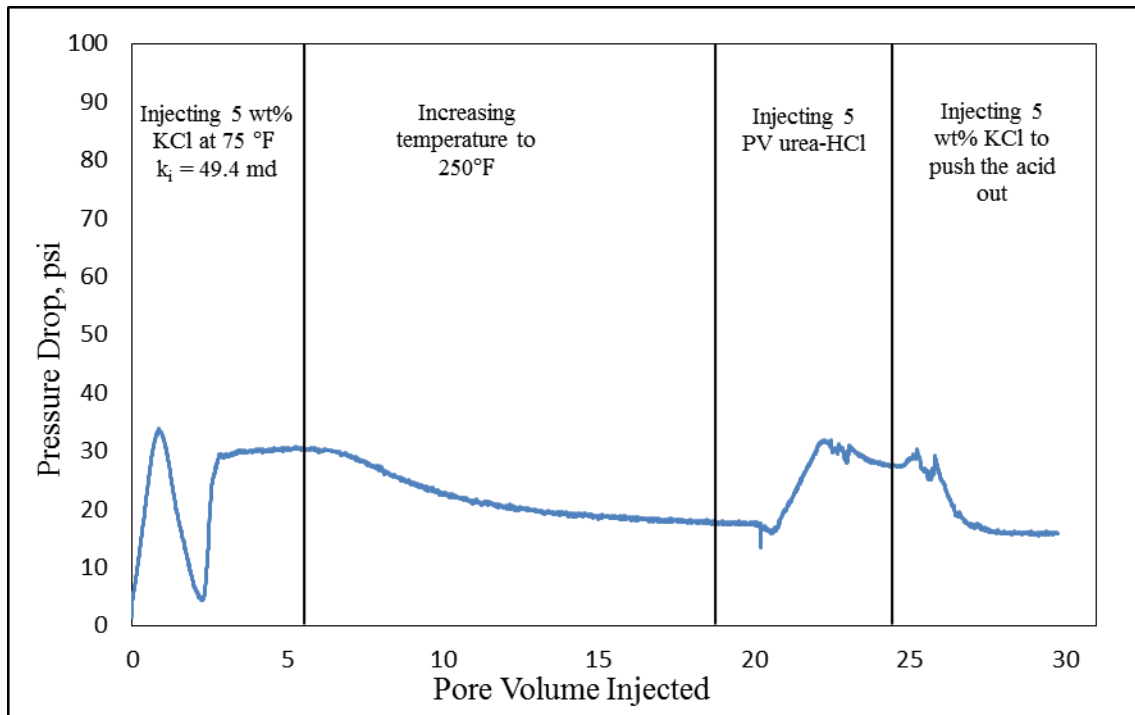


Fig. 3—36 Pressure drop curve during urea-HCl injection at 250°F Berea-08.

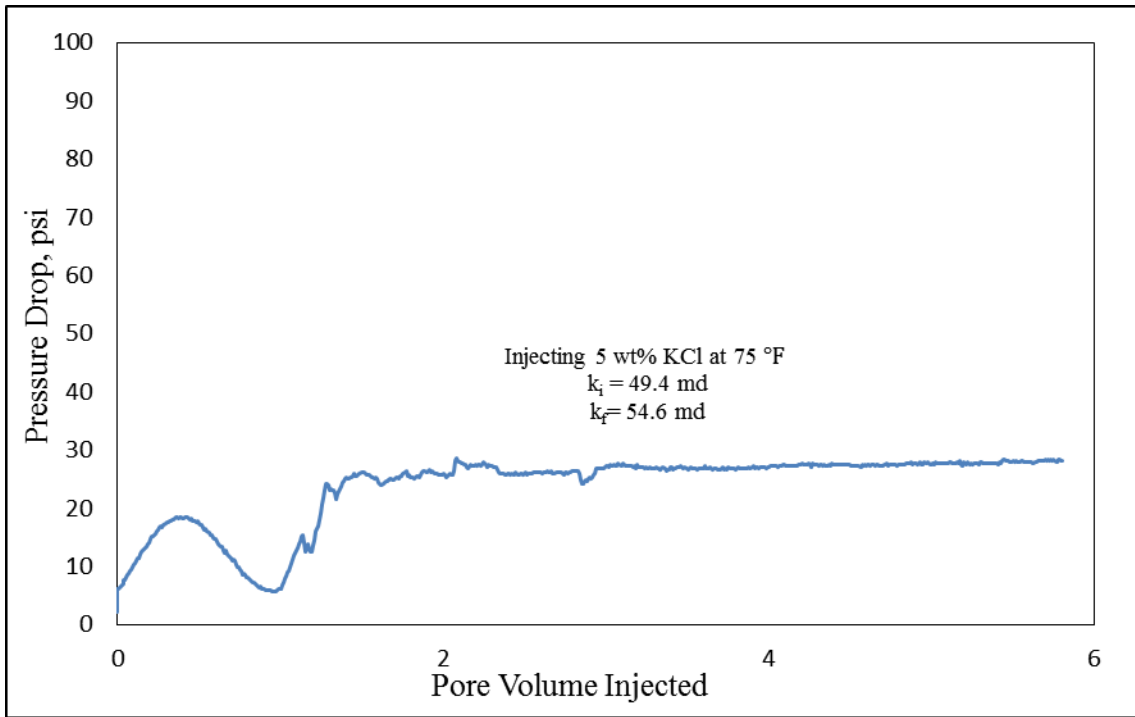


Fig. 3—37 Final permeability of Berea core-08 at 75° F.

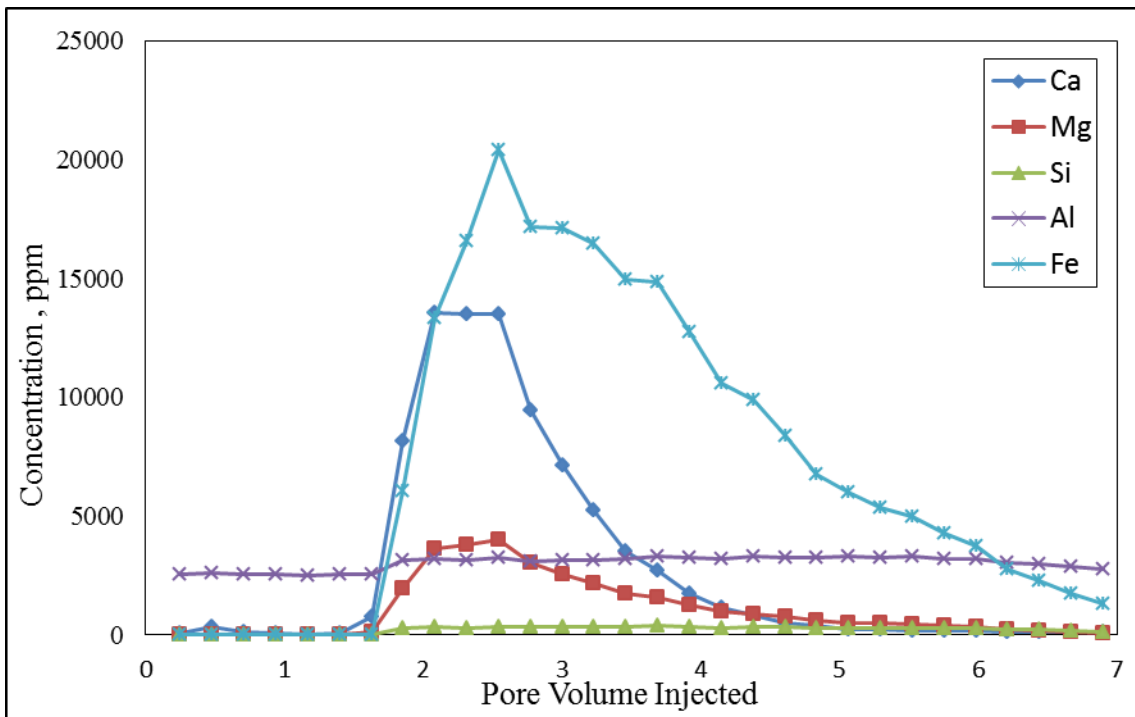


Fig. 3—38 ICP analysis for 30 wt %Urea-HCl with Berea-08 core.

K_i , md	K_f , md	Increase, %	Q , cm^3/min	Φ , %
103.50	120.20	13.14	5	16.90

Table 3—15 Berea-13 rock, flow, and % stimulation/damage properties.

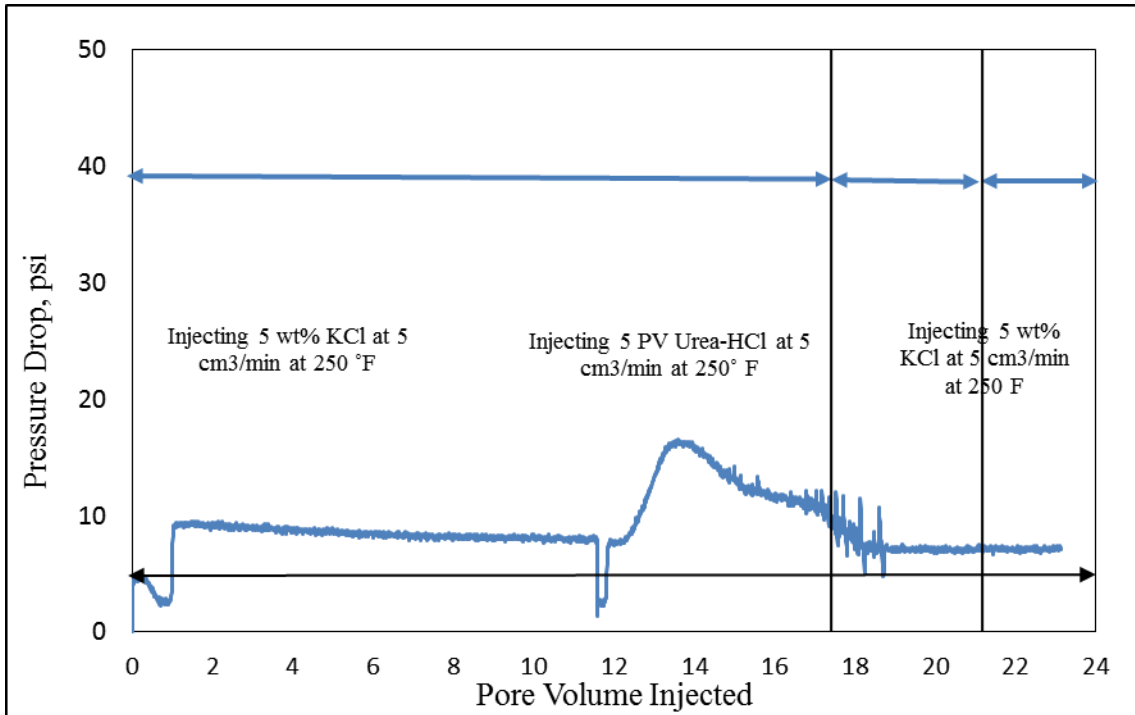


Fig. 3—39 Pressure drop curve during urea-HCl injection at 250 °F for Berea-13.

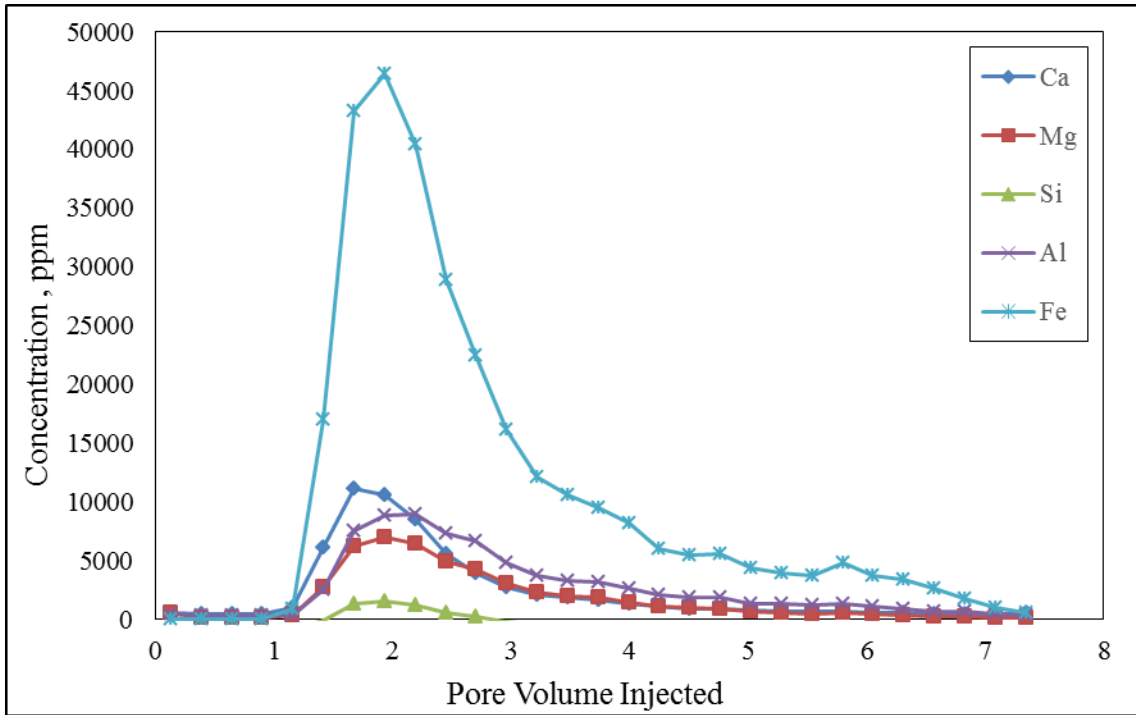


Fig. 3—40 ICP analysis for 30 wt % urea-HCl with Berea-13 core.

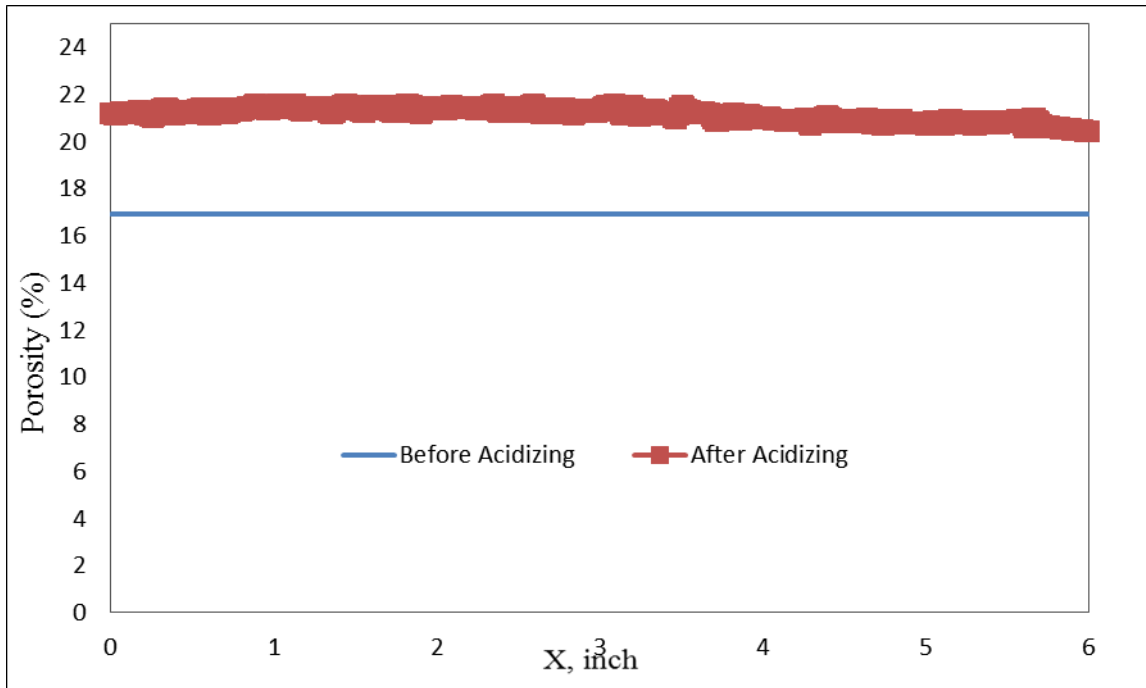


Fig. 3—41 Porosity profile before and after 30 wt% urea-HCl treatment-only CI and intensifier Included for Berea-13.

Section-D: 30 wt% Urea-HCl -Only CI and Intensifier Included-250°F @ 2 and 5 cm³/min- Bandera Sandstone

For the following experiments, each test was repeated twice on Bandera sandstone. A temperature of 250°F was set with a flow rate of 2 cm³/min was used with Ba-02 test and 5 cm³/min used with Ba-01 test. 5 wt% KCl and 5 PV of treatment fluid were injected in the injection direction. The effluent samples resulting from the coreflood experiments were collected every quarter PV. The treatment fluid did not cause any noticeable damage to the Bandera core at 250 °F. The concentrations of iron in all the effluent samples were high (≈ 25000 ppm) and above. There was some precipitation at the bottom of some of the effluent samples after treating the Bandera core.

To further analyze and confirm the damage and its source, ICP shown in **Fig. 3—45 and 3—50** were run. From CT scan and ICP analysis, it can be deduced that HCl first reacted with carbonate and dolomite and subsequently reacted with chlorite. That explains the peak for Ca and Mg being at a lower pore volume than for the Al and Fe. Al is dissolved from clays and feldspars whereas Fe is dissolved from illite and chlorite. The following could be due to the effect of using a lower flow rate of 2 cm³/min versus 5 cm³/min of the latter. The lower flow rate could have increased the resident time of the acid contacting the rock causing more clay decomposition and as a result further damage.

Bandera with (3% kaolinite, 1% chlorite, 10% illite, and 16% dolomite) was damaged but not with the same extent as Grey Berea sandstone. In Bandera sandstone, two counter reacting mechanisms come to play. HCl mobilizes illite whereas HCl

dissolves the high amount of dolomite present in the core. Depending on whichever reaction is dominant, stimulation or damage will occur.

K_i , md	K_f , md	Decrease, %	Q , cm^3/min	Φ , %
12.30	11.70	4.87	5	14.0

Table 3—16 Bandera-01 rock, flow, and % stimulation/damage properties.

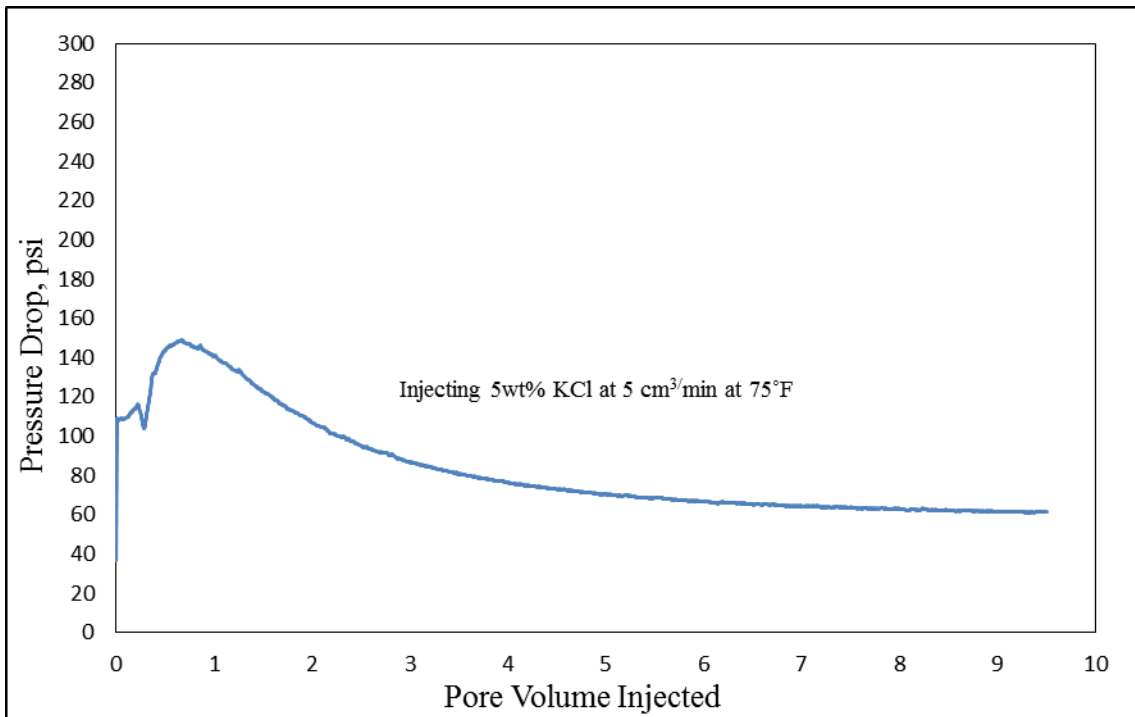


Fig. 3—42 Initial permeability of Bandera-01 core at 75°F.

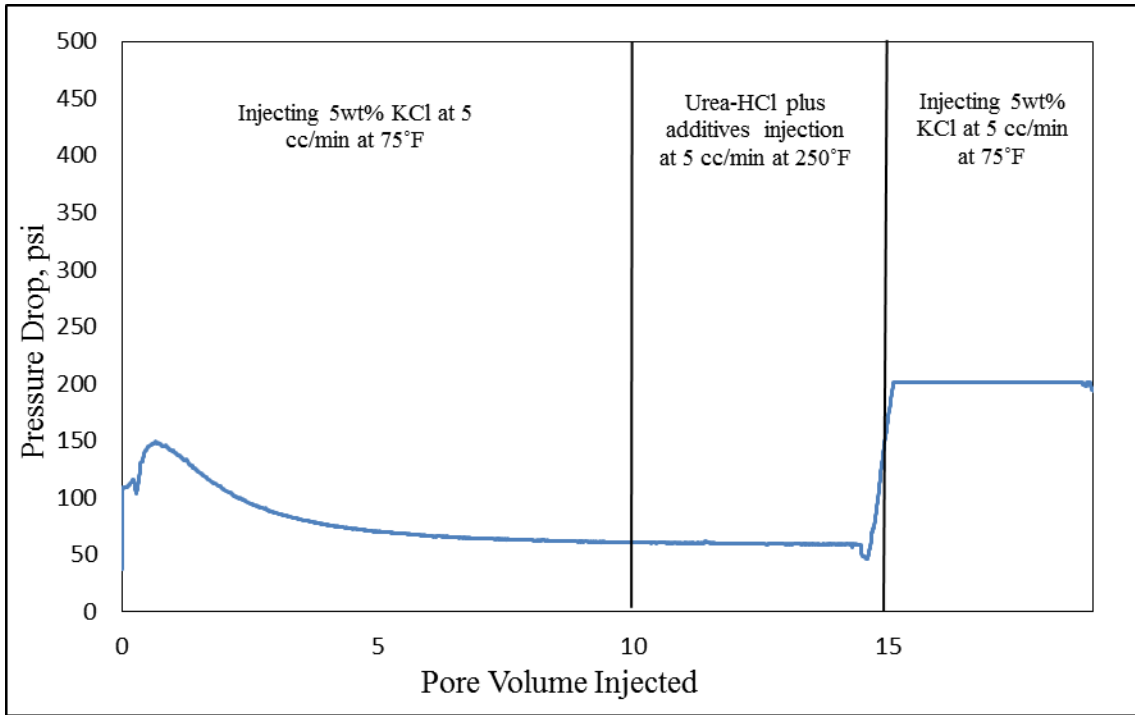


Fig. 3—43 Pressure drop profile during urea-HCl injection at 250 °F.

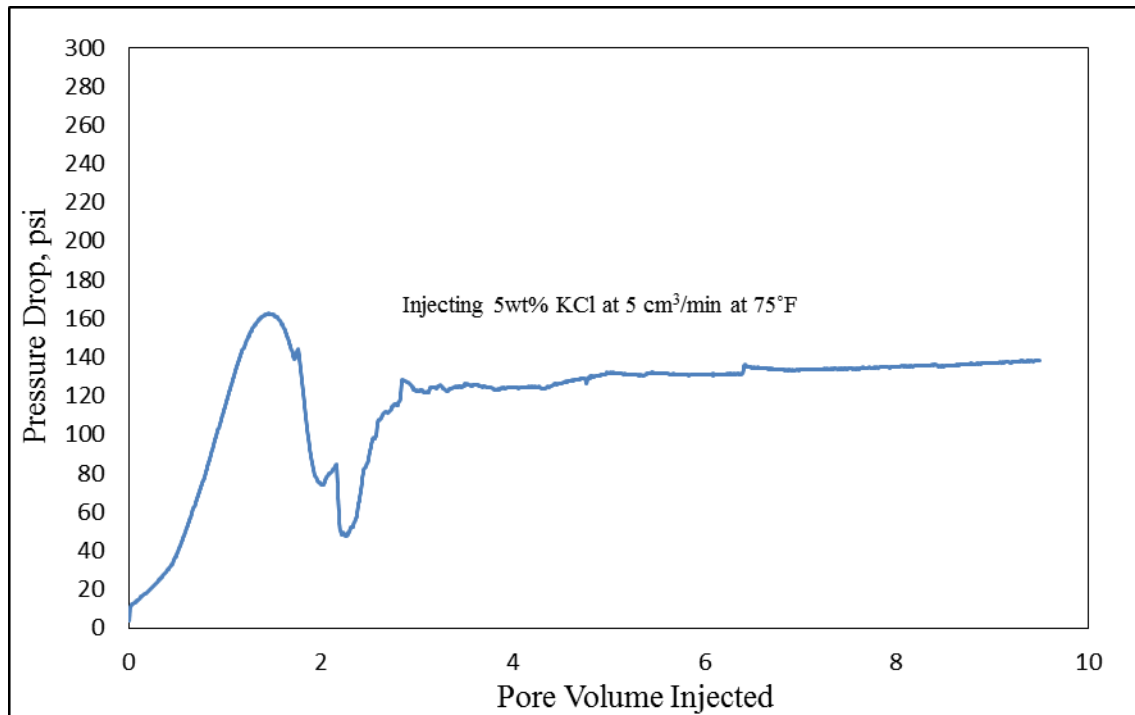


Fig. 3—44 Final permeability of Bandera-01 core at 75°F

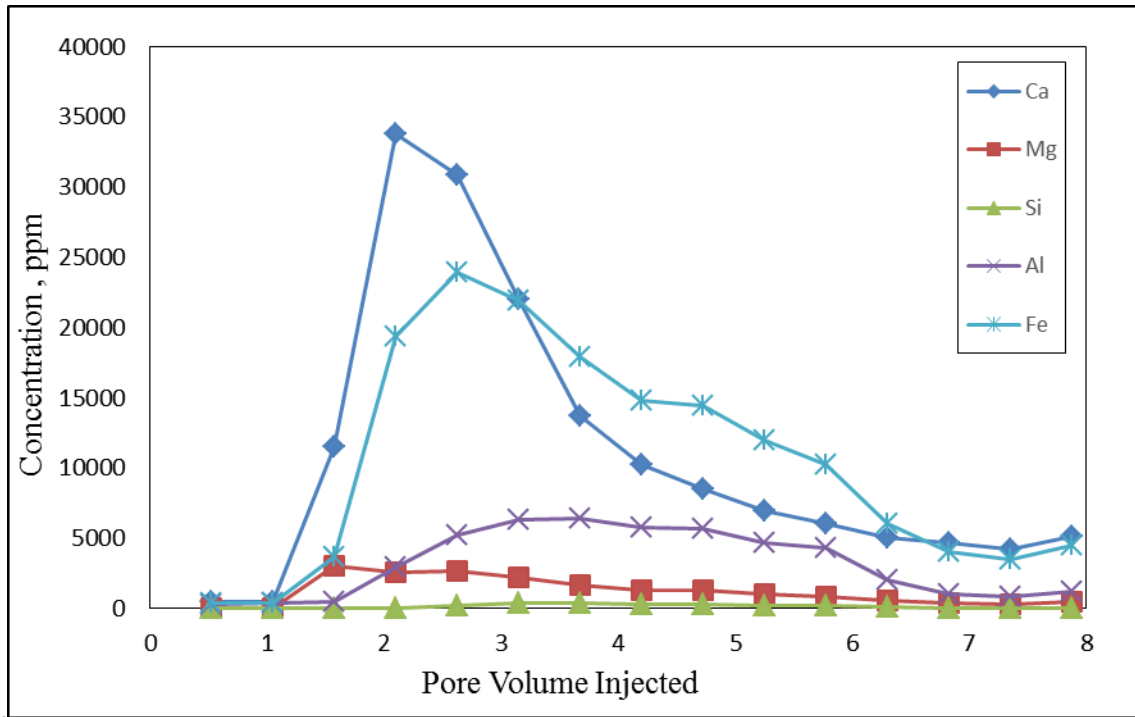


Fig. 3—45 ICP analysis for 30wt%Urea-HCl with Bandera-01 core.

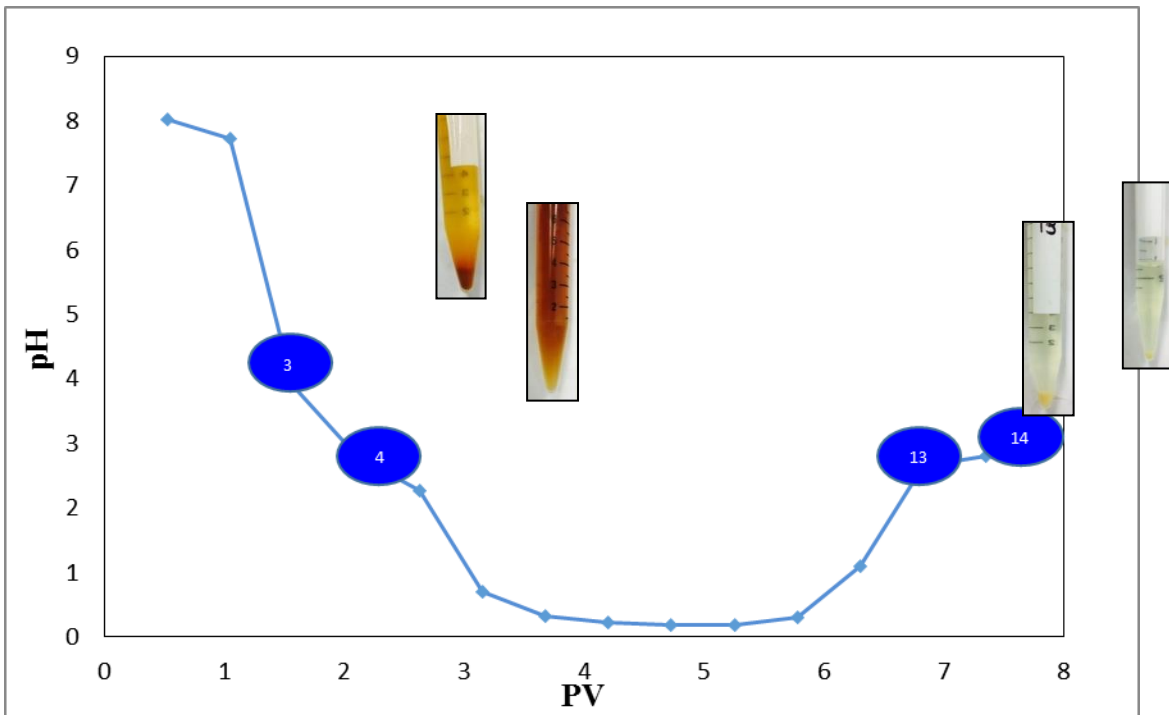


Fig. 3—46 pH of effluent samples from Bandera-01 core.

K_i , md	K_f , md	Decrease, %	Q , cm^3/min	Φ , %
4.50	3.50	22.22	2	19.80

Table 3—17 Bandera-02 rock, flow, and % stimulation/damage properties.

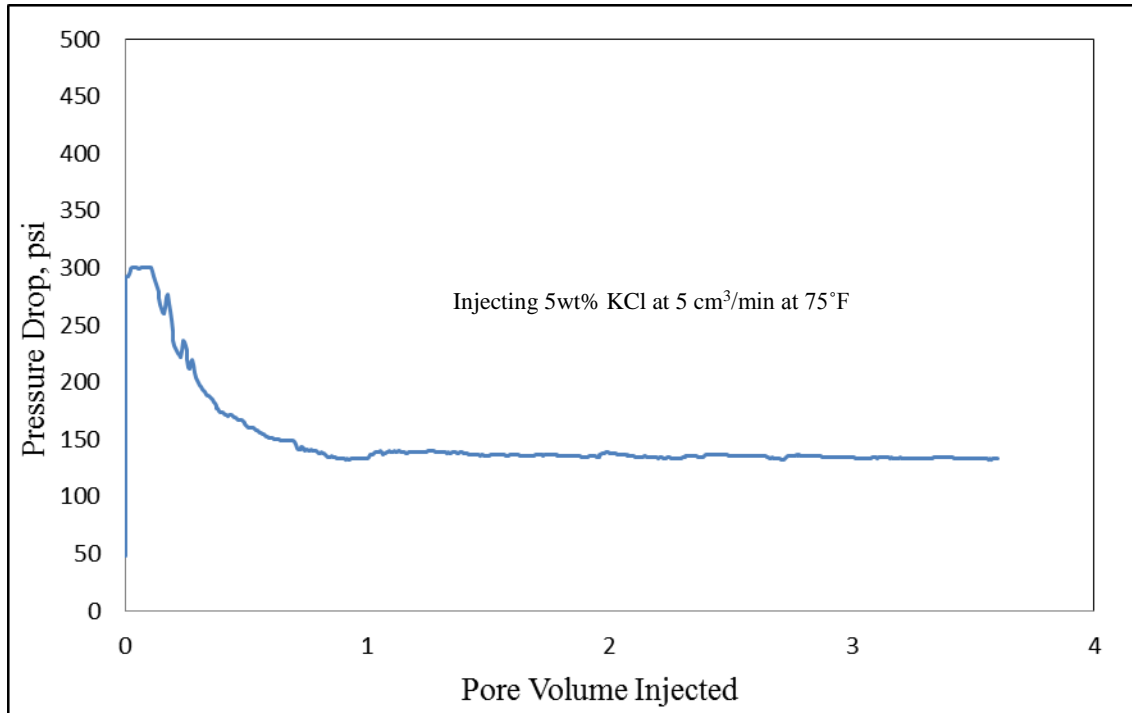


Fig. 3—47 Initial permeability of Bandera-02 core at 75°F.

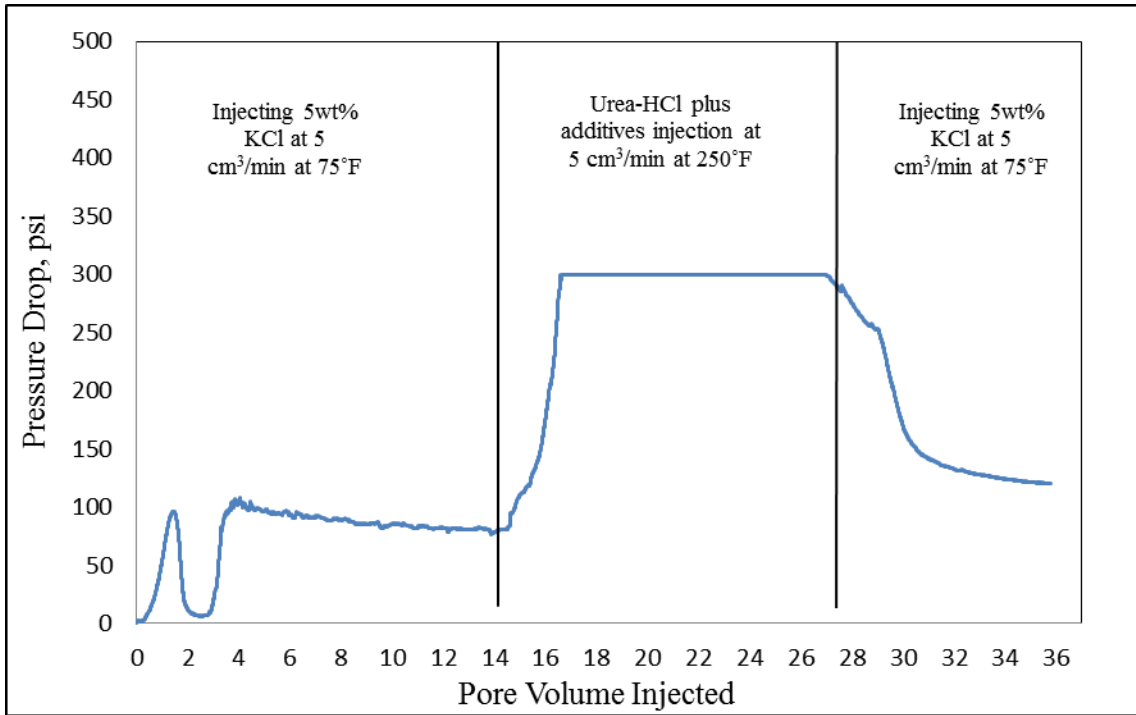


Fig. 3—48 Pressure drop curve of Bandera-02 core during urea-HCl injection at 250°F.

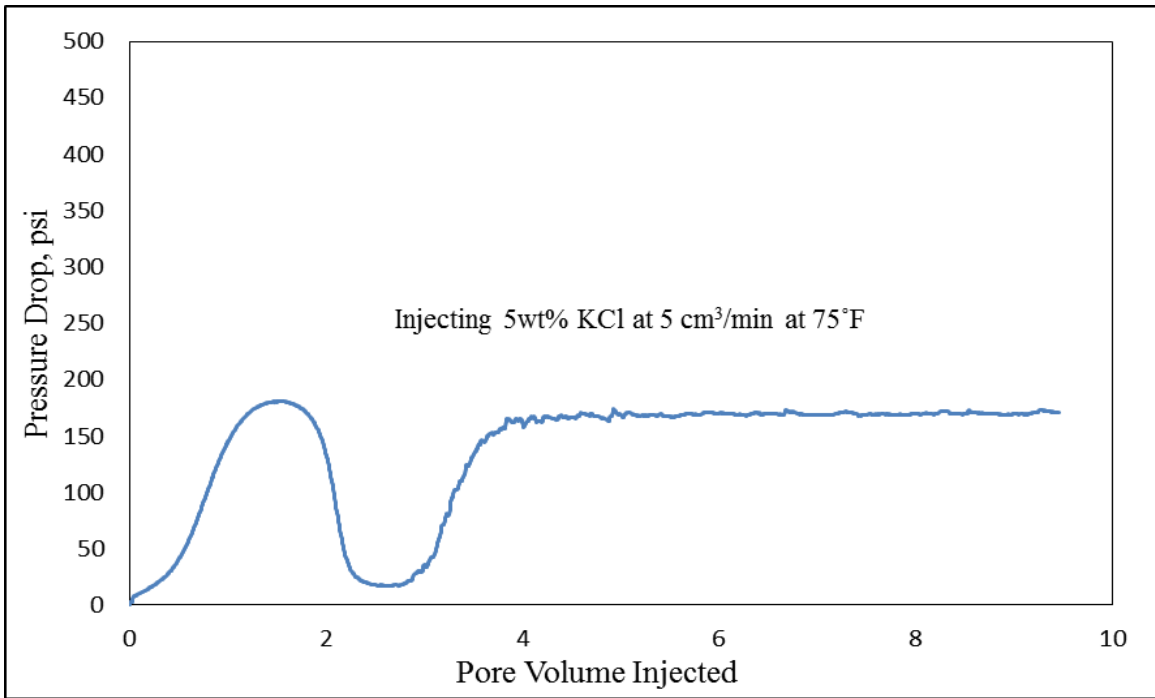


Fig. 3—49 Final permeability of Bandera-02 core at 75°F.

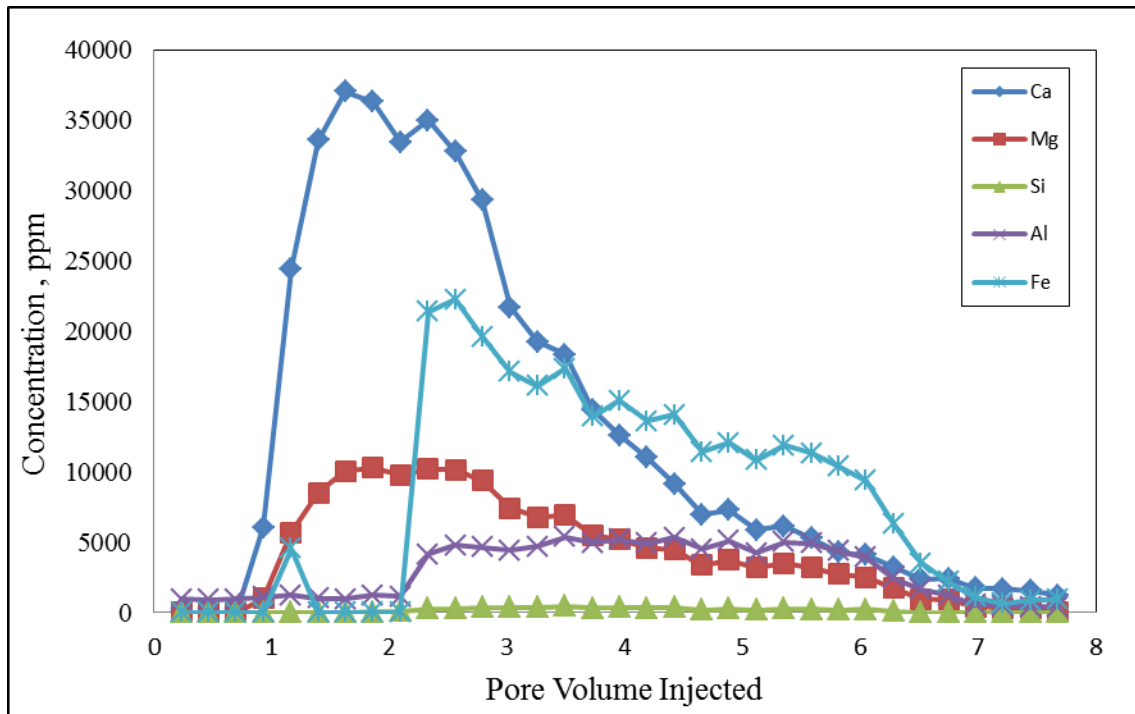


Fig. 3—50 ICP analysis for 30 wt% urea-HCl with Bandera-02 core.

Section-E: 30 wt% Urea-HCl - 250°F @ 1cm³/min- Berea Sandstone with Different Mineralogy

For the following experiments, each test was repeated once on Grey Berea sandstone with different mineralogy shown by the XRD analysis shown previously. A temperature of 250°F was set with a flow rate of 1 cm³/min for the injection of 5 PV of the treatment fluid while 2 wt% KCl was injected at 3 cm³/min through the attached core sample until a steady state pressure drop across the core sample is reached, shown in **Fig. 3—5**. Initial and regained permeability were measured in the production direction, and acid was pumped in the injection direction. Darcy's law was used to calculate the initial and

regained (final) permeability of the core sample. The effluent samples resulting from the coreflood experiments were collected every quarter PV.

By comparing the initial and final permeability displayed in **Figs. 3—51 and 3—53** an enhancement in the permeability (with varying degrees) was achieved despite the damage resulting from injecting HCl at a high temperature. From the ICP analysis displayed in **Fig. 3—6 and 3—58**, high iron content was detected in the core effluent from the dissolution of chlorite and illite. Despite the damaging mechanisms, the permeability enhancement proves that dissolving the carbonate content (dolomite in this case), is possibly the main mechanism causing the permeability enhancement. The second suggested mechanism is the urea-kaolinite intercalation mechanism forming UKC which could be a supporting reason in the stimulation outcome.

G-14: 30 wt% Urea-HCl-Only CI and Intensifier Included on Berea Sandstone with different mineralogy

K _i , md	K _f , md	Increase,%	Q, cm ³ /min	Φ, %
162.90	167.78	3	1	14.70

Table 3—18 Berea-G-14 rock, flow, and % stimulation/damage properties.

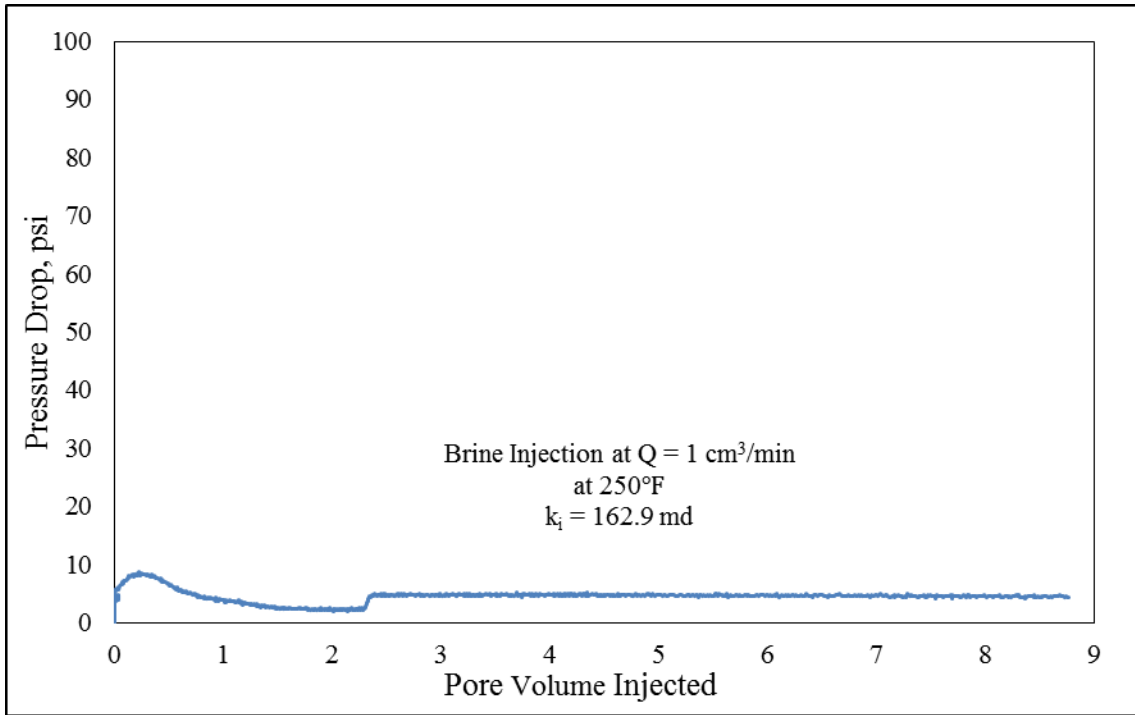


Fig. 3—51 Initial permeability of Berea-G-14 core at 250°F.

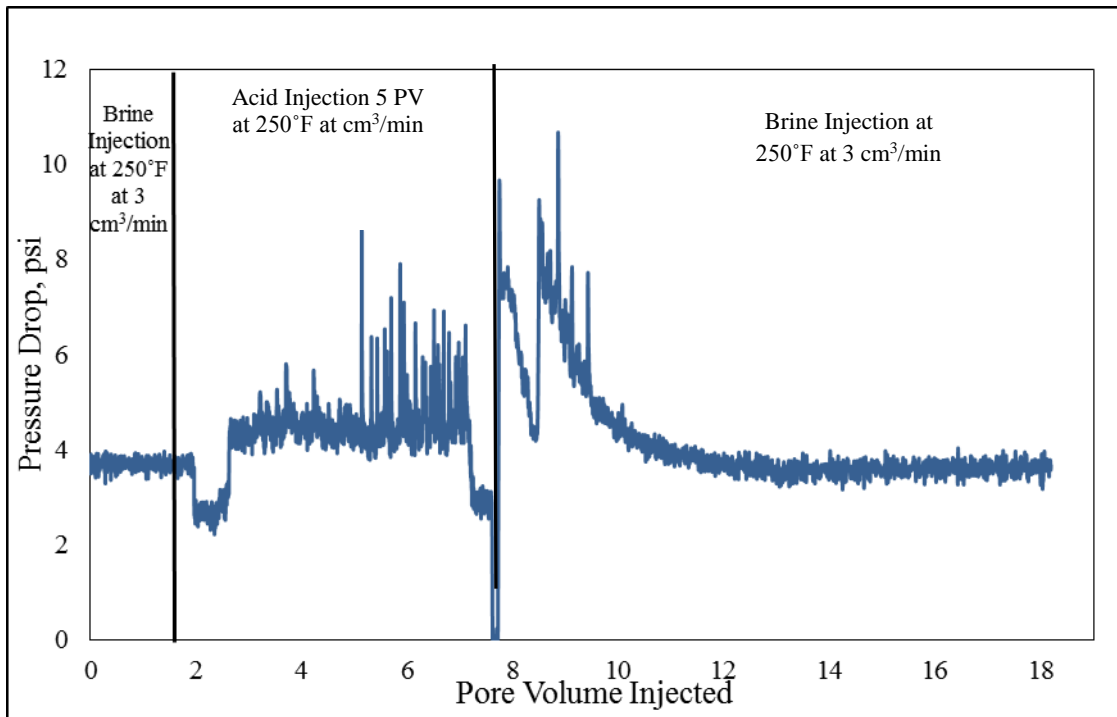


Fig. 3—52 Pressure drop profile of Berea-G-14 core during urea-HCl injection at 250°F.

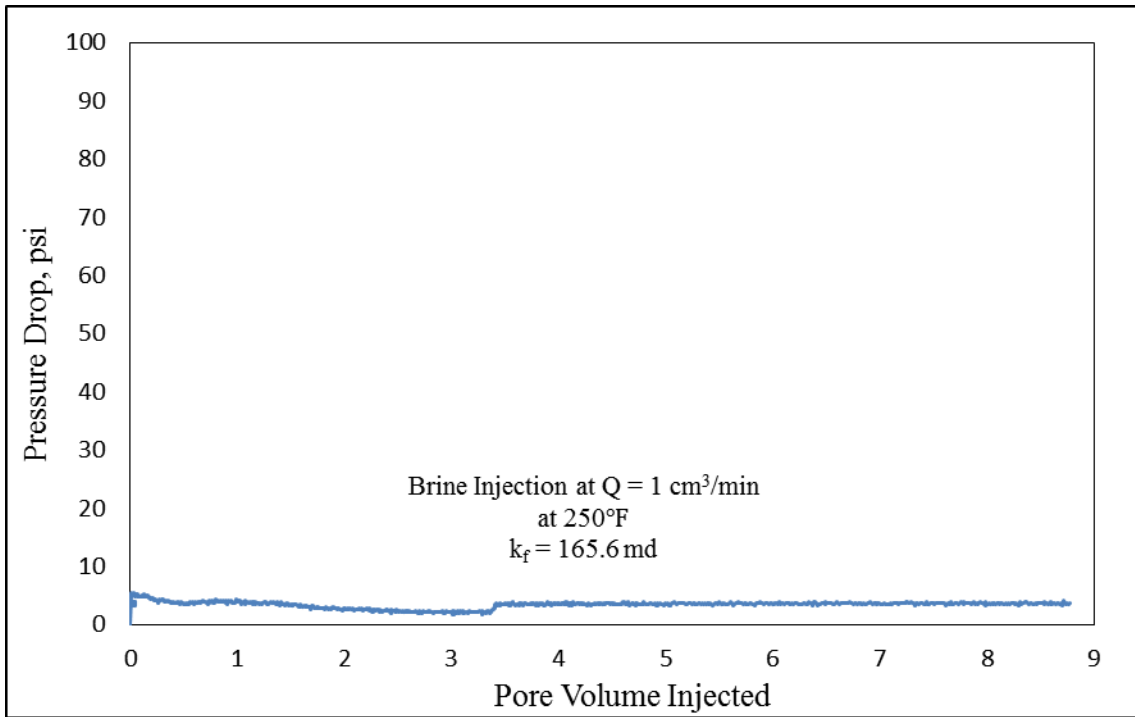


Fig. 3—53 Final permeability of Berea-G-14 core at 250°F.

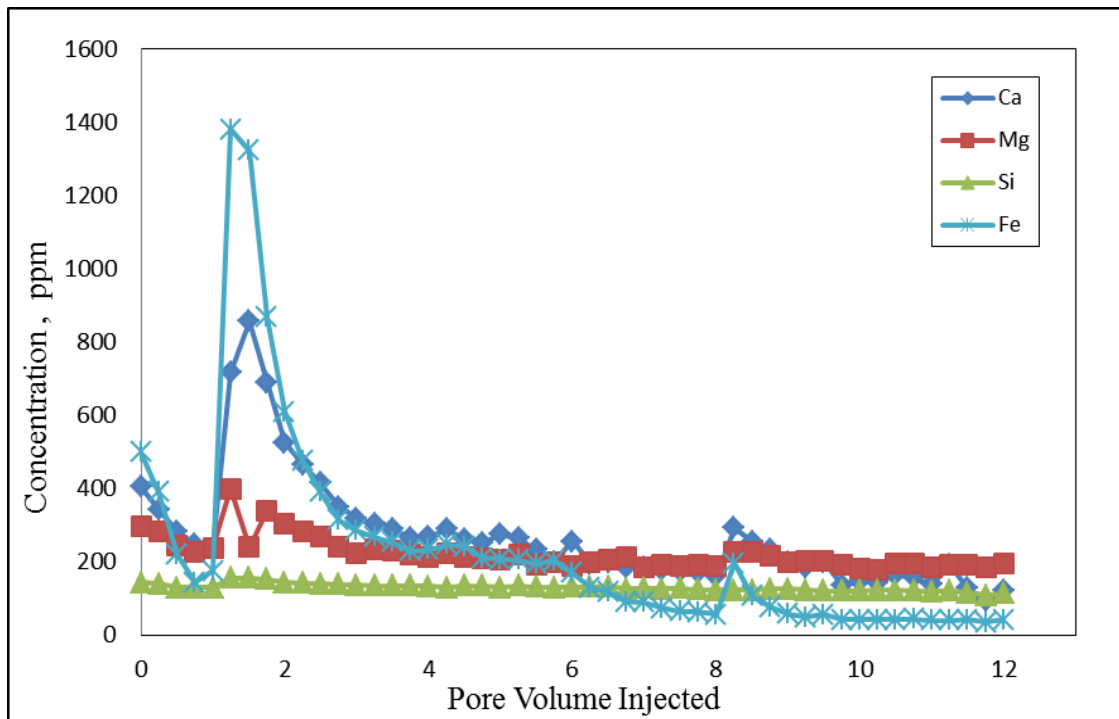


Fig. 3—54 ICP analysis for 30 wt% urea-HCl with Berea-G-14 core.

G-15: 30 wt% Urea-HCl-All of the Additives Included on Berea Sandstone with different mineralogy

K_i , md	K_f , md	Increase,%	Q , cm^3/min	Φ , %
126.8	165.6	30	1	14.7

Table 3—18 Berea-G-15 rock, flow, and % stimulation/damage properties.

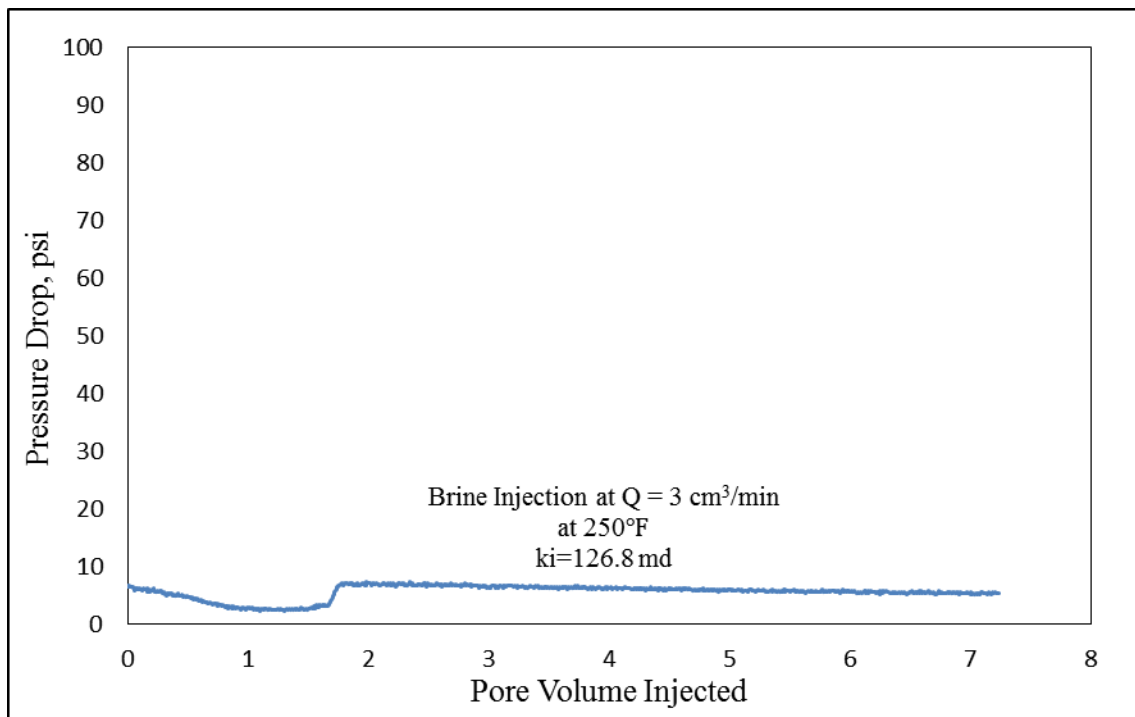


Fig. 3—55 Initial permeability of Berea-G-15 core at 250°F.

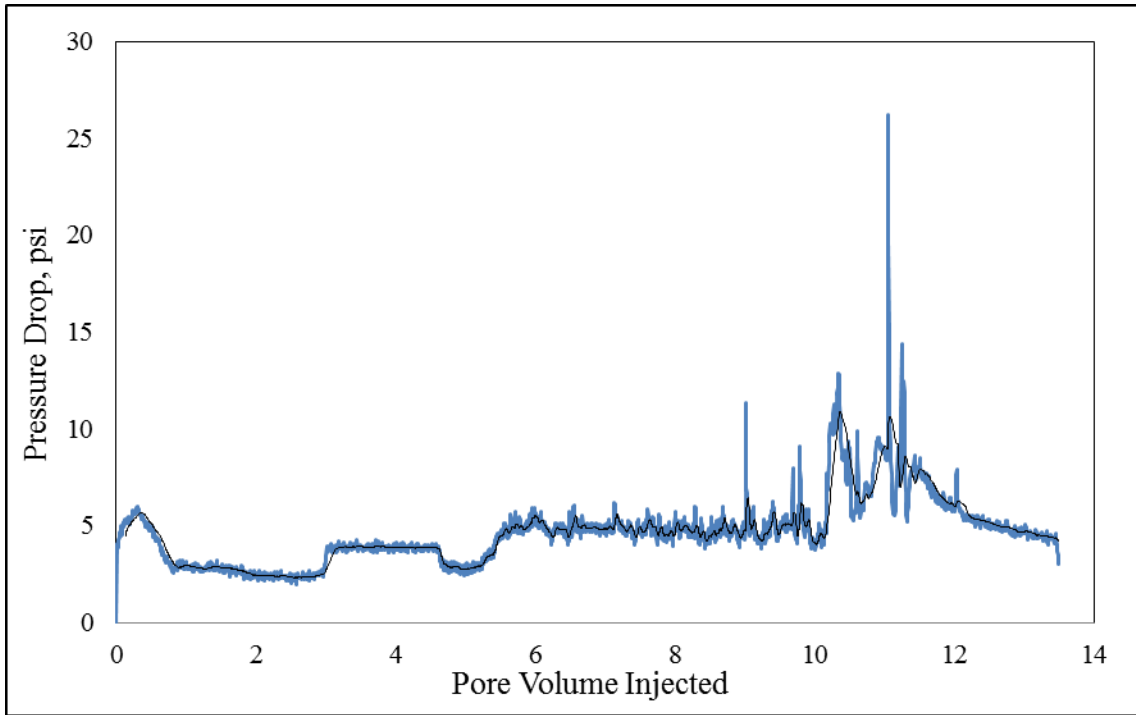


Fig. 3—56 Pressure drop curve of Berea-G-15 core during urea-HCl injection at 250 °F.

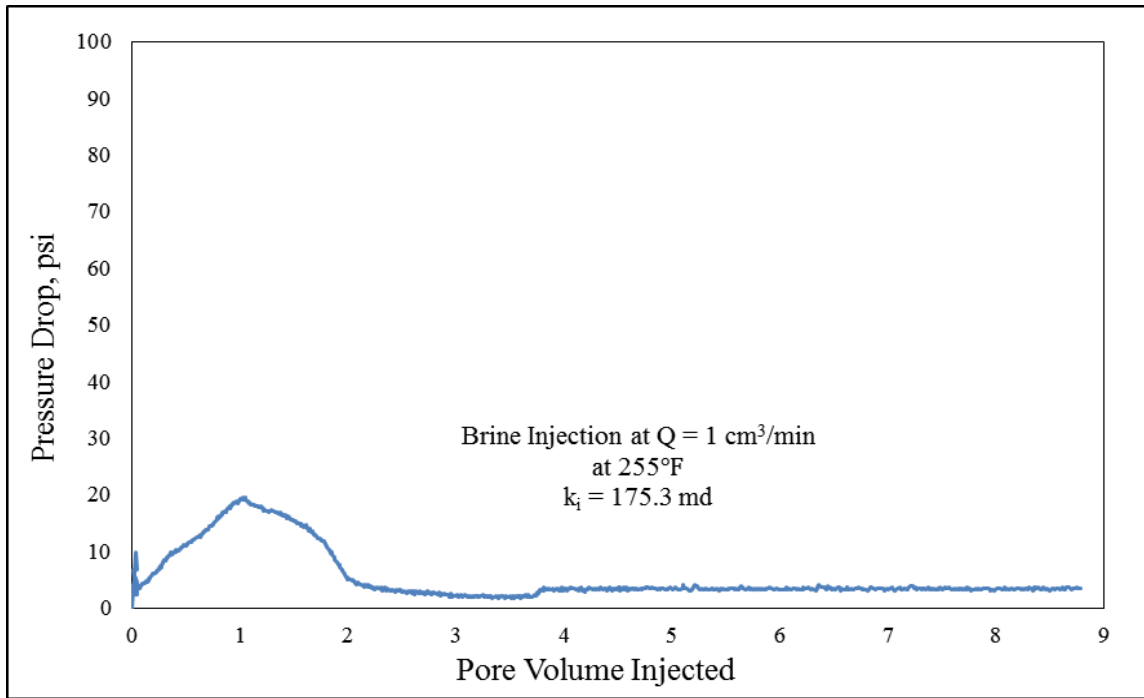


Fig. 3—57 Final permeability of Berea-G-15 core at 75°F.

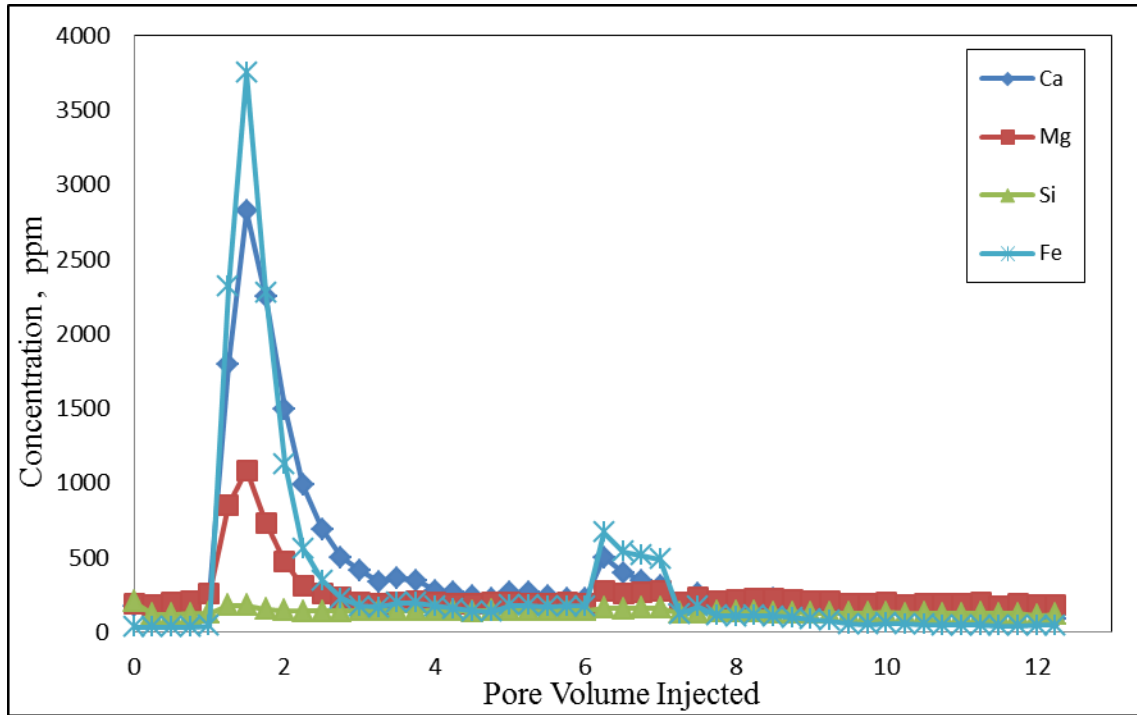


Fig. 3—58 ICP analysis for 30 wt% Urea-HCl with Berea-G-15 core.

It is evident from the density versus PV graph shown in **Fig. 3—8** , that the density originally started with the 2 wt% KCl then it gradually increased throughout the 5 PV of acid injection. The density increased as the acid dissolved more cations such as Ca^{2+} , Mg^{2+} , Fe^{2+} , and Al^{3+} . The density again decreased from the peak of 1.08 g/cm^3 as the brine was flowed back.

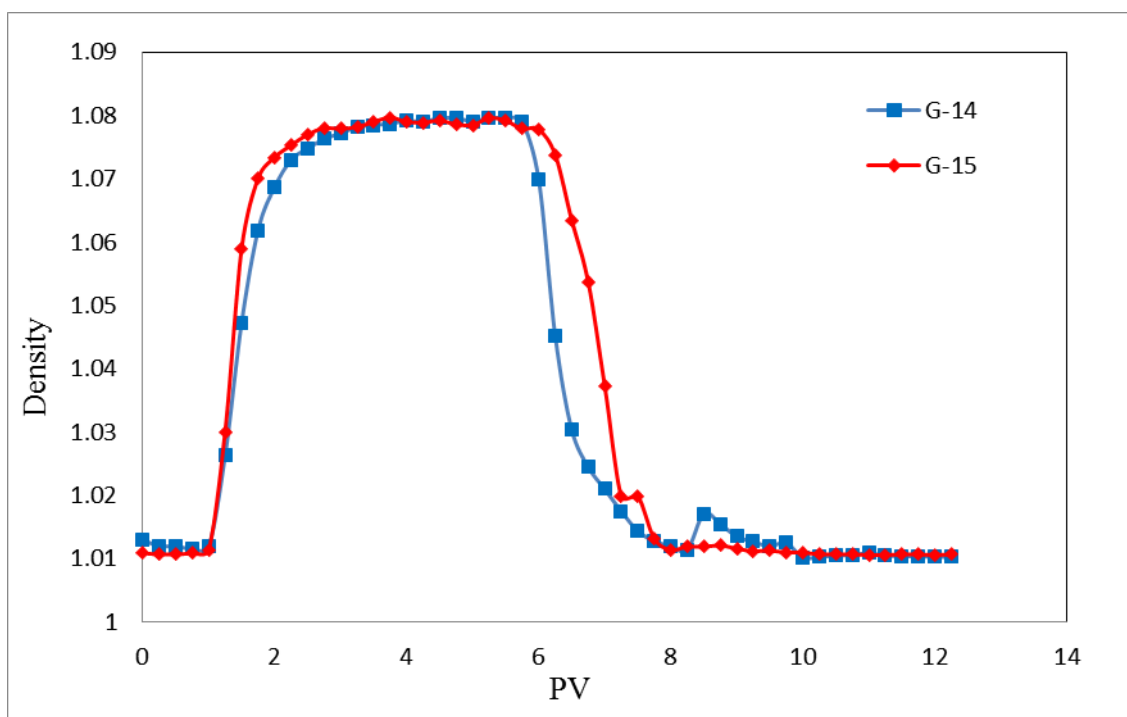


Fig. 3—59 Density of 2 sets of effluent samples from Berea-G-15 and G-14 core at 75°F.

The addition of the full additive package on the 30 wt% urea-HCl was used with a different type of Grey Berea core having different mineralogy. According to the XRD results, G-14 and G-15 cores had no calcite in their mineralogy. Dolomite and clay minerals such as Kaolinite, chlorite, and illite were present.

Approximately a 30% permeability enhancement was achieved with G-15. However, using only the corrosion inhibitor and intensifier on G-14 sandstone caused a slight enhancement of permeability of 3%.

According to the pH versus PV graph shown in **Fig. 3—9**, the pH of the effluent samples starts from around 4 increasing throughout the 5 PV of the treatment fluid injected ending with a pH of 6 where all of the acid is spent ending with a brine post-

flush of 2 wt% KCl. Unlike previous Grey Berea experiments, there is no live acid remaining which indicates that all of the acid dissolved the existing minerals and clays. A suggested explanation could be the hydrolysis of urea resulting in the formation of two moles of ammonia and one of carbon dioxide, causing the pH of the mixture to increase as the reaction proceeds. Moreover, there is a possibility of having a higher kaolinite content compared to the other type of Berea sandstone. This could have encouraged more intercalation with urea forming more UKC, thus, buffering the solution.

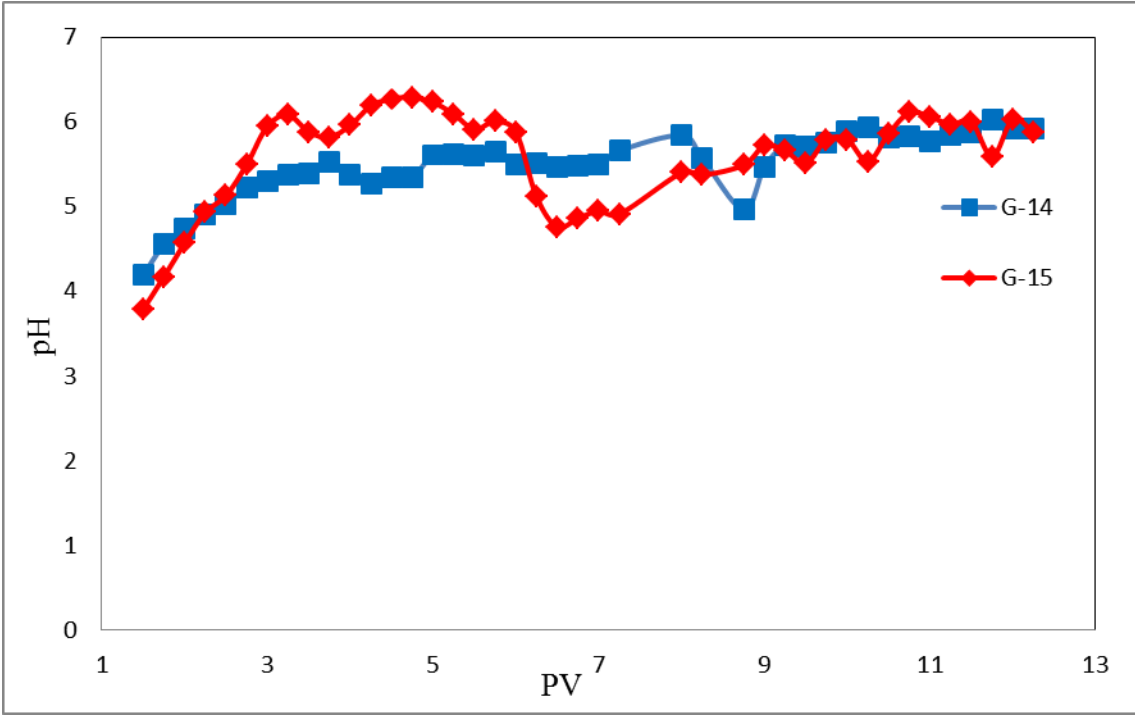


Fig. 3—60 pH of 2 sets of effluent samples from Berea-G-15 and G-14 core at 75°F.

4. CONCLUSIONS AND RECOMMENDATIONS

Clay instability and decomposition at high BHT is one of the most, critical and frequent, problems occurring during acid treatments, especially when using regular HCl in high temperature reservoirs. One of the numerous advantages presented by using the new insitu-generated system proposed in this research is the lack of need to use iron control agents at a low pH of 0. Moreover, there is no need for clay stabilizers due to the NH_4Cl insitu-generation. An added benefit is the lack of need to use acid retarders, as the urea in the formulation helps in the retardation mechanism depending on the % equivalence of HCl. In this study, different variables were changed. Based on the results obtained, the following conclusions can be drawn:

1. A stimulation K_f/K_i (% increase) ranging from 10 to 30% was achieved using urea-HCl for the stimulation of Grey Berea sandstone with different mineralogy.
2. Grey Berea with clays (5% kaolinite, 2% chlorite, 1% illite, and 3% carbonates) showed damage after treatment using the new additive package, possibly due to additive incompatibility with the rock.
3. The generated NH_4Cl from urea-HCl hydrolysis can act as a clay stabilizer and alleviate formation damage.
4. The insitu-generated acid caused stimulation for Grey Berea cores at 250°F.
5. The urea-HCl can act as a preflush before the mud acid treatment to dissolve carbonates in sandstone reservoirs.
6. The HCl in the formulation dissolves the acid soluble materials insitu at BHT.
7. As a weak base, urea has a buffering effect on the acidic system.

8. Greater stimulation was obtained with Berea sandstone compared to Bandera sandstone.
9. Pumping the urea-HCl acid solution at lower flow rates caused more damage compared to higher flow rates.
10. Pumping the urea-HCl acid solution at a temperature of 300°F caused more clay instability and decomposition and, thus, further formation damage occurred.

It is recommended that the type and order of additives should be identified and taken into consideration when the acid treatment is designed. It is also recommended to perform additive compatibility tests while designing field treatments to prevent additive precipitation and emulsions causing formation damage. An advantage of the urea present in the mixture is that it contributes to the retarded rates of reaction.

The sandstone permeability enhancement is suggested to occur with the combination of two scenarios:

1. H^+ attack to the carbonate site causing the formation of acid-soluble Ca^{2+} and Mg^{2+} salts, and
2. The intercalation of the urea in the urea-HCl mixture with the kaolinite in the sandstone cores to form a UKC.

Bandera sandstone is rich in dolomite and illite. Therefore, two counter-reacting effects come to play. At 250 °F HCl mobilizes illite and decomposes it, weakening the clay structure and causing fines migration, on the other hand, the HCl in the formula dissolves large amounts of dolomite, inducing stimulation. Depending on the dominance of each of the above-mentioned counter-reacting mechanisms, permeability enhancement or reduction will occur, thus influencing the treatment outcome.

REFERENCES

- Al-Dahlan, M.N., Nasr-El-Din, H.A., and Al-Qahtani, A.A. 2001. Evaluation of Retarded HF Acid Systems. Presented at the SPE International Symposium on Oilfield Chemistry, Houston, 13–16 February. SPE-65032-MS. <http://dx.doi.org/10.2118/65032-MS>.
- Al-Harbi, B.G., Al-Dahlan, M.N., Al-Khalidi, M.H. et al. 2013. Evaluation of Organic Hydrofluoric Acid Mixtures for Sandstone Acidizing. Presented at the International Petroleum Technology Conference, Beijing, China, 26–28 March. IPTC-16967-MS. <http://dx.doi.org/10.2523/16967-MS>
- Amaefule, J.O., Kersey, D.G., Norman, D.L. Et Al. 1988. Advances in Formation Damage Assessment and Control Strategies. Presented at the Annual Technical Meeting of the Petroleum Society of CIM, Calgary, Alberta, 12–16 June. PETSOC-88-39-65. <http://dx.doi.org/10.2118/88-39-65>.
- Apelblat, A. 1993. Solubilities of Organic Salts of Magnesium, Calcium, and Iron in Water. *The Journal of Chemical Thermodynamics* **25** (12): 1443–5. <http://dx.doi:10.1006/Jcht.1993.1145>.
- Averill, B. And Eldredge, P. 2012. General Chemistry: Principles, Patterns, and Applications. In. 978-1-4533-3122-4. The Saylor Foundation.
- Bartko, K.M., Newhouse, D.P., Andersen, C.A. et al. 1995. The Use of CT Scanning in the Investigation of Acid Damage to Sandstone Core. Presented at the Annual Technical Conference and Exhibition, Dallas, Texas, 22–25 October. SPE-30457-MS. <http://dx.doi.org/10.2118/30457-MS>.
- Buijse, M., Boer, P.D., Breukel, B. et al. 2004. Organic Acids in Carbonate Acidizing. *SPE Prod & Oper* **19** (3): 128–134. SPE-82211-PA. <http://dx.doi.org/10.2118/82211-PA>.
- Buijse, M., De Boer, P., Breukel, B. et al. 2003. Organic Acids in Carbonate Acidizing. Presented at the SPE European Formation Damage Conference, The Hague, Netherlands, 13–14 May. SPE-82211-MS. <http://dx.doi:10.2118/82211-MS>.

- Chatelain, J.C., Silberberg, I.H., and Schechter, R.S. 1976. Thermodynamic Limitations in Organic-Acid/Carbonate Systems. *SPE J* **16** (4): 189–195. SPE-5647-PA. <http://dx.doi.org/10.2118/5647-PA>.
- Chiu, T.J., Caudell, E.A., and Wu, F. L. 1993. Development of an Expert System to Assist With Complex Fluid Design. *SPE Computer Applications* **5** (1): 18-20. SPE-024416. <http://dx.doi.org/spe-024416>.
- Civan, F. 2000. Reservoir Formation Damage: Fundamentals, Modeling, Assessment, and Mitigation. Houston: Gulf Publishing Company.
- Coulter, G. And Jennings Jr, A. 1997. A Contemporary Approach to Matrix Acidizing. Presented at the SPE Annual Technical Conference and Exhibition, San Antonio, Texas, 5–8 October. SPE-38594-MS. <http://dx.doi.org/10.2118/38594-MS>.
- Coulter, G.R. and Jennings, A.R., Jr. 1999. A Contemporary Approach to Matrix Acidizing. *SPE Production & Operations* **14** (2): 144-149. SPE-056279. <http://dx.doi.org/SPE-056279>.
- Crowe, C.W., MCGowan, G.R. and Baranet, S.E. 1990. Investigation of Retarded Acids Provides Better Understanding of their Effectiveness and Potential Benefits. *SPE Prod Eng* **5** (02): 166–70. SPE-18222-PA. <http://dx.doi:10.2118/18222-PA>.
- Dean, E. and Stark, D. 1920. A Convenient Method for the Determination of Water in Petroleum and Other Organic Emulsions. *Industrial & Engineering Chemistry* **12** (5): 486-90.
- Dill, R.W. And Keeney, B.R. 1978. Optimizing HCl-Formic Acid Mixtures for High Temperature Stimulation. Presented at the SPE Annual Fall Technical Conference And Exhibition, Houston, Texas, 1–3 October. SPE-7567-MS. <http://dx.doi:10.2118/7567-MS>.
- Economides, M.J., Nolte, K.G., Ahmed, U. et al. 2000. *Reservoir Stimulation*: Wiley Chichester.

- Estiu, G. And Merz, K.M. 2004. The Hydrolysis of Urea and the Proficiency of Urease. *Journal of the American Chemical Society* **126** (22): 6932–44. <http://dx.doi.org/10.1021/Ja049327g>.
- Fang, H.L. And Dacosta, H.F. 2003. Urea Thermolysis and NO X Reduction With and Without SCR Catalysts. *Applied Catalysis B: Environmental* **46** (1): 17–34. [http://dx.doi.org/10.1016/S0926-3373\(03\)00177-2](http://dx.doi.org/10.1016/S0926-3373(03)00177-2).
- Fredd, C.N. 1998. The Influence of Transport and Reaction on Wormhole Formation in Carbonate Porous Media: A Study of Alternative Stimulation Fluids. Ph.D. Thesis, University Of Michigan, Ann Arbor, MI.
- Fredd, C.N. and Fogler, H.S. 1998. Alternative Stimulation Fluids and their Impact on Carbonate Acidizing. *SPE Journal*. **3** (1): 34–41. SPE-31074-PA. <http://dx.doi.org/10.2118/31074-PA>.
- Frenier, W.W., Fredd, C.N., and Chang, F. 2001. Hydroxyaminocarboxylic Acids Produce Superior Formulations for Matrix Stimulation of Carbonates. Presented at the SPE European Formation Damage Conference, The Hague, The Netherlands, 21-22 May. SPE-68924-MS. <http://dx.doi:10.2118/68924-MS>.
- Gdanski, R. 1998. Kinetics of Tertiary Reactions of Hydrofluoric Acid on Aluminosilicates. *SPE Prod & Fac* **13** (02): 75–80. SPE-31076-PA. <http://dx.doi.org/10.2118/31076-PA>.
- Gdanski, R. 1999. Kinetics of the Secondary Reaction of HF on Aluminosilicates. *SPE Prod & Fac* **14** (04): 260–8. SPE- 59094-PA. <http://dx.doi.org/10.2118/59094-PA>.
- Gdanski, R.D. 1998. Kinetics of the Tertiary Reactions of Hydrofluoric Acid on Alumino-Silicates. *SPE Prod & Fac* **13** (2): 75–80. SPE-31076-PA. <http://dx.doi.org/10.2118/31076-PA>.
- Geology.uprm.edu. Terrigenous Sediments and Rocks. <http://Geology.Uprm.Edu/Morelock/Terrigenous.htm> (Accessed 22 August).

- Gidley, J., Brezovec, E. and King, G. 1996. An Improved Method for Acidizing Oil Wells in Sandstone Formations. *SPE Prod & Fac* **11** (01): 4–10. SPE-26580-PA. <http://dx.doi:10.2118/26580-PA>.
- Godfrey, P., Brown, R., Hunter, A. 1997. The Shape of Urea. *Journal of Molecular Structure*. **413–414**: 405–414. [http://dx.doi:10.1016/S0022-2860\(97\)00176-2](http://dx.doi:10.1016/S0022-2860(97)00176-2).
- Harris, F. 1961. Applications of Acetic Acid to Well Completion, Stimulation and Reconditioning. *J Pet Technol* **13** (07): 637–9. SPE-63-PA. <http://dx.doi:10.2118/63-PA>.
- Hibbeler, J., and O'driscoll, K. 1996. Sandstone Matrix Acidizing Featuring Bj Sandstone Acid. In, Ed. Bob Hall Boles, S.M.J.La Follette, R.et al.
- Hill, A.D. and Rossen, W. 1994. Fluid Placement and Diversion in Matrix Acidizing. Presented at the University of Tulsa Centennial Petroleum Engineering Symposium, Tulsa, Oklahoma, 29–31 August. SPE-27982-MS. <http://dx.doi:10.2118/27982-MS>.
- Huang, T., Mcelfresh, P.M. and Gabrysch, A.D. 2003. Carbonate Matrix Acidizing Fluids at High Temperatures: Acetic Acid, Chelating Agents or Long-Chain Carboxylic Acids? Presented at the SPE European Formation Damage Conference, The Hague, Netherlands, 13–14 May. SPE-82268-MS. <http://dx.doi:10.2118/82268-MS>.
- Huang, T., Ostensen, L. and Hill, A. 2000. Carbonate Matrix Acidizing With Acetic Acid. Presented at the SPE International Symposium on Formation Damage Control, Lafayette, Louisiana, 23–24 February. SPE-58715-MS. <http://dx.doi:10.2118/58715-MS>.
- Imperial College London. Urea. 23 March 2015, http://www.Ch.Ic.Ac.Uk/Rzepa/Mim/Environmental/Html/Urea_Text.Htm (Accessed 21 July 2015).
- Izgec, O., Demiral, B., Bertin, H. et al. 2005. CO₂ Injection in Carbonates. Presented at the SPE Western Regional Meeting, Irvine, California, 30 March-1 April. SPE-93773-PA. <http://dx.doi.org/10.2118/93773-MS>.

- Jiang, L., Lecerf, B., Jones, T.G. et al. 2013. Aqueous Solution and Method for Use Thereof. U.S. Patent No.20150037234.
- Kalfayan, L. And Metcalf, A. 2000. Successful Sandstone Acid Design Case Histories: Exceptions to Conventional Wisdom. Presented at the SPE Annual Technical Conference And Exhibition, Dallas, Texas, 1–4 October. SPE-63178-MS. <http://dx.doi.org/10.2118/63178-MS>.
- Kieke, M., Schoppelrei, J. And Brill, T. 1996. Spectroscopy of Hydrothermal Reactions. 1. The CO₂-H₂O System and Kinetics of Urea Decomposition in an FTIR Spectroscopy Flow Reactor Cell Operable To 725 K And 335 Bar. *The Journal of Physical Chemistry* **100** (18): 7455–62. <http://dx.doi:10.1021/Jp950964q>.
- King, G.E. 1986. Acidizing Concepts-Matrix Vs. Fracture Acidizing. *J Pet Technol* **38** (05): 507–8. SPE-15279-PA. <http://dx.doi:10.2118/15279-PA>.
- Laidler, K. and Hoare, J. 1950. The Molecular Kinetics of the Urea-Urease System. III. Heats and Entropies of Complex Formation and Reaction. *Journal of the American Chemical Society* **72** (6): 2489–94. <http://dx.doi:10.1021/Ja01162a038>.
- Lepage, J.N., De Wolf, C., Bemelaar, J. Et Al. 2009. An Environmentally Friendly Stimulation Fluid for High-Temperature Applications. Presented at the SPE International Symposium on Oilfield Chemistry, The Woodlands. Texas, 20–22 April. SPE-121709-MS. <http://dx.doi.org/10.2118/121709-MS>.
- Letaief, S., Elbokl, T.A. and Detellier, C. 2006. Reactivity of Ionic Liquids With Kaolinite: Melt Intercalation of Ethyl Pyridinium Chloride in a Urea-Kaolinite Pre-Intercalate. *Journal of Colloid And Interface Science* **302** (1): 254–8. <http://dx.doi:10.1016/J.Jcis.2006.06.008>.
- Li, L., Nasr-El-Din, H.A., Chang, F.F. et al. 2008. Reaction of Simple Organic Acids and Chelating Agents With Calcite. Presented at the International Petroleum Technology Conference, Kuala Lumpur, Malaysia, 3–5 December. IPTC-12886-MS. <http://dx.doi.org/10.2523/12886-MS>.

- Mahmoud, M., Nasr-El-Din, H. and Dewolf, C. 2011. Removing Formation Damage and Stimulation Of Deep Illitic-Sandstone Reservoirs Using Green Fluids. Presented at the SPE Annual Technical Conference and Exhibition, Denver, Colorado, USA, 30 October–2 November. SPE-147395-MS. <http://dx.doi.org/10.2118/147395-MS>.
- Mcleod, H.O., Jr. and Norman, W.D. 2000. *Sandstone Acidizing in Reservoir Stimulation*, 3rd Edition Ed. Economides, M.J. and Nolte, K.G., Chichester, UK: John Wiley And Sons.
- Mcleod, H.O., Ledlow, L.B., and Till, M.V. 1983. The Planning, Execution, and Evaluation of Acid Treatments in Sandstone Formations. Paper Presented at the SPE Annual Technical Conference and Exhibition, San Francisco, California. 5-8 October. SPE SPE-011931. <http://dx.doi.org/10.2118/11931-MS>.
- Mcleod, H.O. 1984. Matrix Acidizing. *Journal of Petroleum Technology* **36** (12): 2055-2069. SPE-13752-PA. <http://dx.doi.org/10.2118/SPE-13752-PA>.
- Mcleod, H.O. 1989. Significant Factors for Successful Matrix Acidizing. Presented at the SPE Centennial Symposium at New Mexico Tech, Socorro, New Mexico, 16–19 October. SPE-20155-MS. <http://dx.doi.org/10.2118/20155-MS>.
- Nasr-El-Din, H. and Zhou, L. 2013. Interactions of Sandstone Acid Systems With Aluminosilicates. Presented at the SPE International Symposium on Oilfield Chemistry. The Woodlands, Texas, 8-10 April. SPE-164050-MS. <http://dx.doi.org/10.2118/164050-MS>.
- Nasr-El-Din, H., Lynn, J. and Taylor, K. 2001. Lab Testing and Field Application of a Large-Scale Acetic Acid-Based Treatment in a Newly Developed Carbonate Reservoir. Presented at the SPE International Symposium On Oilfield Chemistry, Houston, Texas, 13–16 February. SPE-65036-MS. <http://dx.doi.org/10.2118/65036-MS>.
- Nasr-El-Din, H.A., Hopkins, J.A., Shuchart, C.E., and Wilkinson, T. Aluminum Scaling and Formation Damage due to Regular Mud Acid Treatment. Presented at the 1998 International Symposium on Formation Damage Control Held in Lafayette, LA, 18–19 February. SPE-39483-MS. <http://dx.doi.org/10.2118/39483-MS>.

- Nitters, G., Roodhart, L., Jongma, H. et al. 2000. Structured Approach to Advanced Candidate Selection and Treatment Design of Stimulation Treatments. Presented at the SPE Annual Technical Conference and Exhibition, Dallas, Texas, 1–4 October. SPE-63179-MS. <http://dx.doi:10.2118/63179-MS>.
- Perrin, D. 1981. Dissociation Constants of Organic Bases in Aqueous Solution. Butterworths, London, UK.
- Sargent, R., Alender, J., and Moss, T. 1997. Method for Using Urea Hydrochloride. U.S. Patent No. 5672279.
- Schaber, P.M., Colson, J., Higgins, S. et al. 2004. Thermal Decomposition (Pyrolysis) of Urea in an Open Reaction Vessel. *Thermochimica Acta* **424** (1): 131–42. <http://dx.doi:10.1016/J.Tca.2004.05.018>.
- Schauhoff, S. and Kissel, C. 2000. New Corrosion Inhibitors for High Temperature Applications. *Materials and Corrosion* **51** (3): 141-6.
- Schechter, R.S. 1992a. Acid Additives. In *Oil Well Stimulation*. Chap. 18, 528 – 547. New York City: Prentice Hall.
- Schechter, R.S. 1992b. Rates of Acid Reactions with Reservoir Minerals. In *Oil Well Stimulation*. Chap. 14, 403–423. New York City: Prentice Hall.
- Shaughnessy, C.M. and Kunze, K.R. 1981. Understanding Sandstone Acidizing Leads to Improved Field Practices. *Journal of Petroleum Technology* **33** (7): 1196-1202. SPE-009388-PA. <http://dx.doi.org/10.2118/SPE-009388-PA>.
- Shaw, W.H. and Bordeaux, J.J. 1955. The Decomposition of Urea in Aqueous Media. *Journal of the American Chemical Society* **77** (18): 4729–33. <http://dx.doi:10.1021/Ja01623a011>.
- Shuchart, C.E. and Gdanski, R.D. 1996. Improved Success in Acid Stimulation With a New Organic-HF System. Presented at European Petroleum Conference, Milan, Italy, 22–24 October. SPE-36907-MS. <http://dx.doi:10.2118/36907-MS>.

- Simon, D. and Anderson, M. 1990. Stability of Clay Minerals in Acid. Presented at the SPE Formation Damage Control Symposium, Lafayette, Louisiana, 22–23 February. SPE-19422-MS. <http://dx.doi.org/10.2118/19422-MS>.
- Smith, C. And Hendrickson, A. 1965. Hydrofluoric Acid Stimulation of Sandstone Reservoirs. *J Pet Technol* **17** (02): 215–22. SPE-980-PA. <http://dx.doi.org/10.2118/980-PA>.
- Smith, C., Crowe, C. and Wieland, D. 1970. Fracture Acidizing In High Temperature Limestone. Presented at the SPE Deep Drilling and Production Symposium, Monahans, Texas, 26 March. SPE-2859-MS. <http://dx.doi.org/10.2118/2859-MS>.
- Smith, C.F., Crowe, C.W., and Wieland, D.R. 1970. Fracture Acidizing in High Temperature Limestone Original Edition. Presented at the SPE Annual Meeting, Houston, Texas, 4–7 October. SPE-3008-MS. <http://dx.doi.org/10.2118/3008-MS>.
- Thomas, R., Nasr-El-Din, H., Mehta, S. et al. 2002. The Impact of HCl to HF Ratio on Hydrated Silica Formation During the Acidizing of a High Temperature Sandstone Gas Reservoir in Saudi Arabia. Presented at the SPE Annual Technical Conference and Exhibition, San Antonio, Texas, 29 September–2 October. SPE-77370-MS. <http://dx.doi.org/10.2118/77370-MS>.
- Tuttle, R. 1987. Corrosion in Oil and Gas Production. *Journal of Petroleum Technology* **39** (07): 756-62. SPE-17004-PA. <http://dx.doi.org/SPE-17004-PA>.
- Van Domelen, M.S. and Jennings Jr, A.R. 1995. Alternate Acid Blends for HPHT Applications. Presented at the Offshore Europe, Aberdeen, United Kingdom, 5-8 September. SPE-30419-MS. <http://dx.doi.org/10.2118/30419-MS>.
- Walker, J. And Wood, J.K. 1903. Hydrolysis of Urea Hydrochloride. *Journal of the Chemical Society, Transactions* **83**: 484–91. <http://dx.doi.org/10.1039/ct9038300484>.
- Walker, M.L., Dill, W.R., Besler, M.R. et. al 1991. Iron Control In West Texas Sour-Gas Wells Provides Sustained Production Increases. *J Pet Technol* **43** (05): 603–7. SPE-20122-PA. <http://dx.doi.org/10.2118/20122-PA>.

- Walsh, M.P., Lake, L.W. and Schechter, R.S. 1982. A Description of Chemical Precipitation Mechanisms and their Role in Formation Damage during Stimulation by Hydrofluoric Acid. *J Pet Technol* **34** (09): 2, 097–2,112. SPE-10625-PA. <http://dx.doi.org/10.2118/10625-PA>.
- Warner, R.C. 1942. The Kinetics of the Hydrolysis of Urea and of Arginine. *Journal of Biological Chemistry* **142** (2): 705–23. <http://dx.doi.org/142/2/705>.
- Werner, E.A. 1918. The Mechanism of the Decomposition of Urea when Heated in Solution With Alkalis and With Acids Respectively. The Hydrolysis of Metallic Cyanates. *Journal of the Chemical Society, Transactions* **113** (13): 84-99.
- Werner, E.A. 1920. The Mechanism of the Synthesis of Urea from Ammonium Carbamate. The Preparation of Certain Mixed Tri-Substituted Carbamates and Dithiocarbamates. *Journal of the Chemical Society, Transactions* **117** (11): 1046-53.
- Wheland, G.W. 1956. *Resonance in Organic Chemistry*. *Journal of the American Pharmaceutical Association* **45** (03):192. <http://dx.doi.org/10.1002/Jps.3030450324>.
- Wöhler, F. 1829. On the Decomposition of Urea and Uric Acid at High Temperature. *Ann.Phys.Chem* **15**: 619–30.
- Wöhler, F. 2006. Ueber Künstliche Bildung Des Harnstoffs. *Annalen Der Physik Und Chemie*. **87** (2): 253–256. <http://dx.doi:10.1002/Andp.18280870206>.
- Yan, C., Chen, J., Zhang, C. et al. 2005. Kaolinite-Urea Intercalation Composites. *American Ceramic Society Bulletin* **84** (12): 9301–5.
- Yang, F., Nasr-El-Din, H.A. and Al-Harbi, B.M. 2012. Acidizing Sandstone Reservoirs Using HF and Formic Acids. Presented at the SPE International Symposium and Exhibition on Formation Damage Control, Lafayette, Louisiana, USA, 15–17 February. SPE-150899-MS. <http://dx.doi.org/10.2118/150899-MS>.